

SHOT NOISE
AND ELECTRICAL CONDUCTION
IN MESOSCOPIC SYSTEMS

PROEFSCHRIFT

TER VERKRIJGING VAN DE GRAAD VAN DOCTOR
AAN DE RIJKSUNIVERSITEIT TE LEIDEN,
OP GEZAG VAN DE RECTOR MAGNIFICUS DR. L. LEERTOUWER,
HOGLERAAR IN DE FACULTEIT DER GODGELEERDHEID,
VOLGENS BESLUIT VAN HET COLLEGE VAN DEKANEN
TE VERDEDIGEN OP WOENSDAG 21 JUNI 1995
TE KLOKKE 14:15 UUR

DOOR

MARC JOHAN MARTIJN DE JONG
GEBOREN TE HERTEN IN 1969

Promotiecommissie:

- Promotor: Prof. dr. C. W. J. Beenakker
Referenten: Prof. dr. M. Büttiker (Université de Genève)
Prof. dr. H. van Houten
Overige leden: Prof. dr. J. Amesz
Prof. dr. ir. G. E. W. Bauer (Technische Universiteit Delft)
Prof. dr. J. M. J. van Leeuwen
Prof. dr. L. W. Molenkamp (Rheinisch-Westfälische
Technische Hochschule Aachen)
Prof. dr. ir. W. van Saarloos

Shot noise and electrical conduction in mesoscopic systems/

Marc Johan Martijn de Jong -

Thesis Leiden University - with summary in Dutch -

printed by Copynomie Veldhoven - ISBN 90-74445-19-5

Subject headings:

Shot noise/ fluctuations/ mesoscopic systems/ electrical conductance

© Philips Electronics N. V. 1995

All rights are reserved. Reproduction in whole or in part is prohibited without the written consent of the copyright owner.

Het onderzoek beschreven in dit proefschrift is uitgevoerd aan het Philips Natuurkundig Laboratorium als onderdeel van het wetenschappelijke programma van de Stichting voor Fundamenteel Onderzoek der Materie (FOM) en de Nederlandse Organisatie voor Wetenschappelijk Onderzoek (NWO).

The research described in this thesis has been carried out at the Philips Research Laboratories as part of the scientific program of the Foundation for Fundamental Research on Matter (FOM) and the Netherlands Organization for Scientific Research (NWO).

Table of contents with extremely faint text and page numbers, likely bleed-through from the reverse side of the page.

Aan mijn vader en moeder

Present address M. J. M. de Jong:
Philips Research Laboratories
Box WB-12
Prof. Holstlaan 4
5656 AA Eindhoven
The Netherlands
Phone: +31-40-742069
Fax: +31-40-743365
E-mail: jongmjm@prl.philips.nl

Contents

1	Introduction	1
1.1	Shot noise in mesoscopic conductors	2
1.1.1	Current fluctuations	2
1.1.2	Classical shot noise	3
1.1.3	Quantum transport	5
1.1.4	Shot noise in a quantum point-contact	11
1.1.5	Shot noise in a diffusive conductor	12
1.1.6	Experimental results	16
1.2	This thesis	18
	References	28
2	Mesoscopic fluctuations in the shot-noise power of metals	33
2.1	Introduction	33
2.2	Average and variance of the shot-noise power	35
2.3	Effect of inelastic scattering	37
2A	Appendix: Moment expansion and solution	39
	References	46
3	Doubled shot noise in disordered normal-metal–superconductor junctions	47
	References	54
4	Andreev reflection in ferromagnet–superconductor junctions	55
	References	63
5	Transition from Sharvin to Drude resistance in high-mobility wires	65
5.1	Introduction	65
5.2	Integro-differential equation for the transmission probability	66
5.3	Numerical solution	69
5.4	Three-dimensional wire	71

5.5	Comparison with experiment	73
5A	Appendix: Boltzmann approach	73
	References	76
6	Semiclassical theory of shot-noise suppression	77
6.1	Introduction	77
6.2	Boltzmann-Langevin equation	79
6.3	Impurity scattering	83
6.4	Barrier scattering	88
6.5	Inelastic and electron-electron scattering	94
6.6	Conclusions and discussion	102
6A	Appendix: Thermal noise	103
6B	Appendix: Noise at arbitrary cross section	105
6C	Appendix: Nonisotropic scattering	107
	References	108
7	Hydrodynamic electron flow in high-mobility wires	111
7.1	Introduction	111
7.2	Experimental observation of Knudsen and Gurzhi transport regimes	116
7.3	Boltzmann equation	121
7.4	Theoretical results	124
7.5	Comparison between experiment and theory	132
7.6	Discussion and conclusions	135
7A	Appendix	137
7B	Appendix	138
	References	140
	Summary	143
	Samenvatting	145
	List of publications	149
	Curriculum vitae	151
	Acknowledgements	152

Chapter 1

Introduction

Mesoscopic physics is the branch of physics dedicated to the investigation of the novel phenomena that arise in small electronic devices. Pushed by the industry's ever increasing effort to miniaturize and integrate electronic circuits, this branch has grown in the last decade from a very promising niche to a substantial part of solid-state physics. The mesoscopic world is situated in between the microscopic world of atoms and molecules and the macroscopic world of our day-to-day experience. Here, the laws of classical mechanics can no longer fully describe the phenomena observed. However, a complete quantum mechanical theory, extrapolated from the microscopic world, becomes impractical because of the relatively large numbers of particles. For a successful description the physicist is required to combine concepts from quantum mechanics, statistical physics, and electronics. It is this interdisciplinary aspect that has made this new field so attractive to many. The intense scientific activity in this area has forced a reconsideration of established concepts and has provided deeper insights in many physical phenomena occurring in macroscopic systems. For an overview of the field we refer the reader to the many reviews that have appeared, e.g. Refs. [1–4].

The theoretical investigations described in this thesis concern electrical conduction in mesoscopic systems, with an emphasis on the current fluctuations known as "shot noise." The first Section of this introductory Chapter provides some background on shot noise in mesoscopic systems. The second Section continues with an overview of the topics treated in this thesis.

1.1 Shot noise in mesoscopic conductors

1.1.1 Current fluctuations

Even under constant operation conditions the current $I(t)$ through a conductor may fluctuate in time. The noise, i.e. the deviations $\Delta I(t) \equiv I(t) - \bar{I}$ from the average \bar{I} , is usually characterized by its power spectrum P at frequency ω . This is defined as the Fourier transform of the current correlation function [5, 6]

$$P(\omega) \equiv 2 \int_{-\infty}^{\infty} dt e^{i\omega t} \langle \Delta I(t+t_0) \Delta I(t_0) \rangle, \quad (1.1)$$

where $\langle \dots \rangle$ denotes an ensemble average (or equivalently an average over the initial time t_0). Basically, we can distinguish between equilibrium and non-equilibrium fluctuations.

Equilibrium fluctuations are present even in the absence of an applied voltage. The first type is thermal or Johnson-Nyquist noise [7] due to the random motion of the charge carriers. It has a white (ω -independent) noise spectrum and its intensity is proportional to the conductance G ,

$$P = 4k_B T G, \quad (1.2)$$

where T is the temperature. Equation (1.2) is an example of the fluctuation-dissipation theorem [8]. For very high frequencies, $\hbar\omega \gtrsim k_B T$, Eq. (1.2) no longer applies, because zero-point fluctuations should be included. For arbitrary frequency the spectrum is given by [8]

$$P(\omega) = 4G \left[\frac{1}{2} \hbar\omega + \frac{\hbar\omega}{\exp(\hbar\omega/k_B T) - 1} \right]. \quad (1.3)$$

Thermal noise does not give any information about the conductor, beyond that contained in the conductance.

The second type of equilibrium fluctuations is due to time-dependent fluctuations in the resistance. The current I fluctuates proportionally to these resistance fluctuations, so that $P \propto I^2$. The noise spectrum depends on the physical processes which underlie the resistance fluctuations. In many cases $P \propto \omega^{-1}$ over a wide frequency range. (For a recent review on this so called $1/f$ noise, see Ref. [9].) Often, these physical processes are thermally activated, so that the intensity of the resistance fluctuations becomes smaller at decreasing temperatures.

Shot noise is a non-equilibrium fluctuation, which is generated rather than probed by the current. It is caused by the discreteness of the charge of the carriers. Thus, the current is not a continuous flow, but consists of discrete

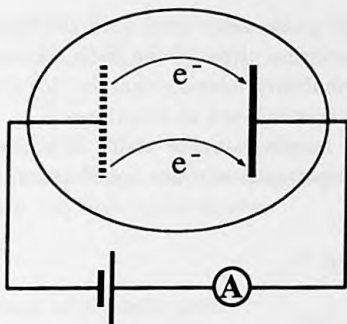


Figure 1.1: Schematic drawing of a thermionic vacuum diode. At a high enough applied voltage electrons will jump from cathode to anode.

charge pulses in time. Shot noise has a white spectrum and is linearly proportional to the magnitude of the current. The time-dependent fluctuations are maximal if the current pulses are independent, as in a Poisson process. Then the shot-noise power takes its full value

$$P = 2e|\bar{I}| \equiv P_{\text{Poisson}}. \quad (1.4)$$

Full shot noise is present in, for example, Schottky barrier diodes and p-n junctions [5].

1.1.2 Classical shot noise

Already in 1918 Schottky [10] found out that in ideal vacuum tubes in which all spurious noise sources had been eliminated, one would still encounter two types of noise described by him as the "Wärmeeffekt" and the "Schroteffekt." Below, we briefly discuss the latter, shot noise in a thermionic vacuum diode. If the applied voltage between the electrodes inside a vacuum tube is high enough, electrons will jump from the heated cathode to the anode, see Fig. 1.1. In a temperature-limited diode, the magnitude of the current is completely determined by the cathode temperature. The applied voltage is high enough to eliminate accumulation of space charge between the electrodes. In this case the electrons are emitted independently and at random, so that the statistics of the emission times can be described by a Poisson distribution. Let us see how Eq. (1.4) can be derived, which is an elementary exercise in statistics.

The total current through the diode is written as the sum of individual current pulses, identical in shape and shifted in time

$$I(t) = \sum_k j(t - t_k), \quad (1.5)$$

where $j(t)$ is the current pulse associated with the transfer of one electron at $t = 0$, and t_k is the emission time of the k -th electron. Let us now define $p_\theta^n(t_1, \dots, t_n)$ as the probability density that in the time interval $[-\theta/2, \theta/2]$ exactly n electrons are transmitted at the times t_1, \dots, t_n . (The width of the time interval θ is much larger than the width of a one-electron current pulse τ .) Since the electron-transmission times are Poisson distributed we have [11]

$$p_\theta^n(t_1, \dots, t_n) = \pi_\theta^n \theta^{-n}, \quad (1.6a)$$

$$\pi_\theta^n = \frac{(\lambda\theta)^n \exp(-\lambda\theta)}{n!}, \quad (1.6b)$$

where λ denotes the average number of electrons emitted per unit time. The time-averaged current is thus $\bar{I} = e\lambda$.

Knowing the distribution of the current pulses from Eq. (1.6) we can determine the ensemble-averaged current at a time $t \in [-\theta/2 + \tau, \theta/2 - \tau]$

$$\begin{aligned} \langle I(t) \rangle &= \sum_{n=0}^{\infty} \int_{-\theta/2}^{\theta/2} dt_1 \cdots dt_n p_\theta^n(t_1, \dots, t_n) \sum_{k=1}^n j(t - t_k) \\ &= \sum_{n=0}^{\infty} \pi_\theta^n \frac{n}{\theta} \int_{-\theta/2}^{\theta/2} dt' j(t - t') = e\lambda, \end{aligned} \quad (1.7)$$

where we have used $\sum_n n \pi_\theta^n = \lambda\theta$. As expected, $\bar{I} = \langle I(t) \rangle$.

We now determine the shot-noise power. The current-correlation function is given by

$$\begin{aligned} \langle \Delta I(t) \Delta I(0) \rangle &= \sum_{n=0}^{\infty} \int_{-\theta/2}^{\theta/2} dt_1 \cdots dt_n p_\theta^n(t_1, \dots, t_n) \\ &\quad \times \left[\sum_{k=1}^n j(t - t_k) - \bar{I} \right] \left[\sum_{l=1}^n j(-t_l) - \bar{I} \right] \\ &= \sum_{n=0}^{\infty} \pi_\theta^n \left[\frac{n}{\theta} \int_{-\theta/2}^{\theta/2} dt' j(t - t') j(-t') \right. \\ &\quad \left. + \frac{n(n-1)e^2}{\theta^2} - \frac{2ne^2\lambda}{\theta} + e^2\lambda^2 \right] \end{aligned}$$

$$= \lambda \int_{-\theta/2}^{\theta/2} dt' j(t-t')j(-t'), \quad (1.8)$$

using $\sum_n n(n-1)\pi_\theta^n = (\lambda\theta)^2$. This result confirms that each current pulse is only correlated with itself, which was our starting assumption. From Eqs. (1.1) and (1.8) we obtain the shot-noise power

$$P(\omega) = 2\lambda|J(\omega)|^2, \quad (1.9)$$

with the Fourier transform of a single pulse

$$J(\omega) \equiv \int_{-\infty}^{\infty} dt e^{i\omega t} j(t). \quad (1.10)$$

(We may replace $\theta/2$ by ∞ because $\theta \gg \tau$ and $j(t) = 0$ if $|t| > \tau$.) Indeed, for frequencies $\omega \ll \tau^{-1}$ we find $J(\omega) = e$, so that Eq. (1.9) reduces to the Poisson noise Eq. (1.4). For higher frequencies ($\omega > \tau^{-1}$) the shot noise vanishes.

1.1.3 Quantum transport

In his 1957 paper [12] Landauer discussed the problem of electrical conduction as a scattering problem. This has become a crucial concept in mesoscopic physics [1, 2]. The conductor is modeled as a scattering region which is connected to electron reservoirs. The electrons inside each reservoir are assumed to be in equilibrium. Incoming states, occupied according to the distribution function of a reservoir, are scattered into outgoing states. The conductance is then fully determined by the transmission matrix of electrons at the Fermi level. The two-terminal Landauer formula [1, 13] and its multi-terminal generalization [14–17] constitute a general framework, known as the Landauer-Büttiker formalism, for the calculation of the conductance of a phase-coherent sample. A scattering theory of the noise properties of mesoscopic conductors was derived in Refs. [18–23]. The basic result is a relationship between the shot-noise power and the transmission matrix at the Fermi level, analogous to the Landauer formula for the conductance. Here we present the derivation of this result, following closely Büttiker's work [22].

We consider the two-terminal geometry of Fig. 1.2. The perfect leads act as wave guides which transport the non-interacting electrons ballistically between the reservoirs and the arbitrary scattering region. Inside lead a ($= 1, 2$) the electron flux at energy ε is carried by modes, indexed $m = 1, \dots, N_a$,

$$\phi_{am}^{\pm}(\mathbf{r}, \varepsilon) \equiv \frac{e^{\pm ik_m x}}{\sqrt{\theta_{am}}} \chi_{am}(y), \quad (1.11)$$

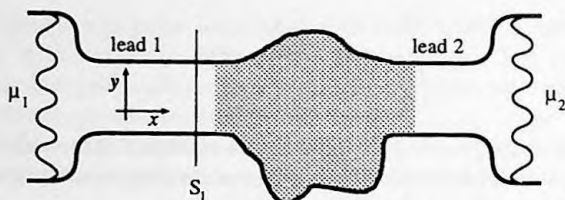


Figure 1.2: The conductor consists of a scattering region (shaded) connected by perfect leads to two electron reservoirs. A cross section in lead 1 and its coordinates are indicated.

where $\mathbf{r} \equiv (x, y)$ with x the coordinate along and y the coordinate perpendicular to lead a . The mode is thus decomposed into a transverse (χ) and a longitudinal wave function (e^{ikx}). The factor $1/\sqrt{\theta_{am}}$ ensures that all modes are normalized to carry unit flux. For example, for a 2-dimensional hard-wall lead of width W in the absence of a magnetic field one would have

$$\chi_m(y) = \sqrt{2/W} \sin \frac{m\pi y}{W}, \quad (1.12a)$$

$$\varepsilon = \frac{\hbar^2}{2M} \left[\left(\frac{m\pi}{W} \right)^2 + k_m^2 \right], \quad (1.12b)$$

$$\theta_m = \frac{\hbar k_m}{M}, \quad (1.12c)$$

where M is the effective electron mass. The form of the modes becomes more complex in the presence of a magnetic field and for other types of lateral confinement in the leads. The scattering formulation is generally applicable, for arbitrary confinement and magnetic field.

The two perfect leads are connected to the scattering region. We assume only elastic scattering so that energy is conserved. We consider a complete set of scattering states, each consisting of an incoming mode ϕ_α^+ in one lead and several reflected or transmitted outgoing modes,

$$\psi_\alpha(\varepsilon) = \phi_\alpha^+(\varepsilon) + \sum_\beta s_{\beta\alpha}(\varepsilon) \phi_\beta^-(\varepsilon). \quad (1.13)$$

The indices $\alpha \equiv (a, m)$ and $\beta \equiv (b, n)$ denote lead ($a, b = 1, 2$) as well as mode ($m, n = 1 \dots N$) number. (For simplicity the number N of modes at energy ε is taken to be equal for lead 1 and 2.) The reflection and transmission amplitudes are elements of the $2N \times 2N$ scattering matrix $S(\varepsilon)$, which has the block form

$$S = \begin{pmatrix} s_{11} & s_{12} \\ s_{21} & s_{22} \end{pmatrix} \equiv \begin{pmatrix} r & t' \\ t & r' \end{pmatrix}, \quad (1.14)$$



Figure 1.3: Schematic representation of the transport through the conductor. Incoming states (I) are scattered into outgoing states (O).

where the $N \times N$ matrix s_{ba} contains the amplitudes from incoming modes in lead a to outgoing modes in lead b . The scattering matrix thus connects the incoming modes with the outgoing modes

$$\begin{pmatrix} O_1 \\ O_2 \end{pmatrix} = S \begin{pmatrix} I_1 \\ I_2 \end{pmatrix}, \quad (1.15)$$

where I_1, O_1, I_2, O_2 are the N -component vectors denoting the amplitudes of the incoming (I) and outgoing (O) modes in lead 1 and lead 2, see Fig. 1.3. Because of flux conservation S is a unitary matrix,

$$SS^\dagger = S^\dagger S = 1. \quad (1.16)$$

Let us now study the current in lead 1. The current operator is given by

$$\hat{I}(t) = \frac{e}{\hbar} \sum_{\alpha, \beta} \int_0^\infty d\varepsilon \int_0^\infty d\varepsilon' I_{\alpha\beta}(\varepsilon, \varepsilon') \hat{a}_\alpha^\dagger(\varepsilon) \hat{a}_\beta(\varepsilon') e^{it(\varepsilon - \varepsilon')/\hbar}, \quad (1.17)$$

where $\hat{a}_\alpha^\dagger(\varepsilon)$ [$\hat{a}_\alpha(\varepsilon)$] is the creation [annihilation] operator of scattering state $\psi_\alpha(\varepsilon)$. The matrix element $I_{\alpha\beta}(\varepsilon, \varepsilon')$ gives the value of the current at cross section S_1 in lead 1 (see Fig. 1.2) between the states $\psi_\alpha(\varepsilon)$ and $\psi_\beta(\varepsilon')$ according to

$$I_{\alpha\beta}(\varepsilon, \varepsilon') = \frac{\hbar}{2Mi} \int_{S_1} dy \{ \psi_\alpha(\mathbf{r}, \varepsilon) [\partial_x \psi_\beta(\mathbf{r}, \varepsilon')]^* - [\partial_x \psi_\alpha(\mathbf{r}, \varepsilon)] \psi_\beta^*(\mathbf{r}, \varepsilon') \}. \quad (1.18)$$

Here, $\partial_x \equiv \partial/\partial x - ieA_x(\mathbf{r})/\hbar$, with \mathbf{A} the vector potential in the lead. From the definition of the scattering states (1.13) and the fact that the modes are flux normalized one can evaluate Eq. (1.18) for equal energies,

$$I_{am, bn}(\varepsilon, \varepsilon) = \delta_{a1} \delta_{ab} \delta_{mn} - \sum_{p=1}^N s_{1p, am}(\varepsilon) s_{1p, bn}^*(\varepsilon). \quad (1.19)$$

This relation is easily checked for the case that the modes are given by Eq. (1.12), but it is generally valid [22].

The average current is given by the expectation value of Eq. (1.17). We thus need to know the expectation value of the creation and annihilation operators. Since the scattering state ψ_α is fed from reservoir a , we have

$$\langle \hat{a}_\alpha^\dagger(\varepsilon) \hat{a}_\beta(\varepsilon') \rangle = \delta_{\alpha\beta} \delta(\varepsilon - \varepsilon') f_a(\varepsilon), \quad (1.20)$$

where f_a is the distribution function in reservoir a . At an applied voltage V it is given by

$$f_1(\varepsilon) = f(\varepsilon - E_F - eV), \quad (1.21a)$$

$$f_2(\varepsilon) = f(\varepsilon - E_F), \quad (1.21b)$$

with the Fermi-Dirac distribution function $f(x) = [1 + \exp(x/k_B T)]^{-1}$. As a consequence we find

$$\begin{aligned} \langle \hat{I}(t) \rangle &= \frac{e}{h} \sum_\alpha \int_0^\infty d\varepsilon f_a(\varepsilon) I_{\alpha\alpha}(\varepsilon, \varepsilon) \\ &= \frac{e}{h} \int_0^\infty d\varepsilon \left\{ f_1(\varepsilon) \text{Tr}[1 - s_{11}^\dagger(\varepsilon) s_{11}(\varepsilon)] - f_2(\varepsilon) \text{Tr} s_{12}^\dagger(\varepsilon) s_{12}(\varepsilon) \right\}, \end{aligned} \quad (1.22)$$

where we have substituted Eq. (1.19) in the last line. From the unitarity of the scattering matrix (1.16) it is easy to show that both traces in Eq. (1.22) are equal to $\text{Tr} \mathbf{t} \mathbf{t}^\dagger$. For the linear-response conductance, $G \equiv \lim_{V \rightarrow 0} \langle I \rangle / V$, we find using Eq. (1.21)

$$G = \frac{e^2}{h} \int_0^\infty d\varepsilon \left(-\frac{\partial f}{\partial \varepsilon} \right) \text{Tr} \mathbf{t}(\varepsilon) \mathbf{t}^\dagger(\varepsilon). \quad (1.23)$$

The zero-temperature conductance is thus given by the Landauer formula

$$G = \frac{e^2}{h} \text{Tr} \mathbf{t} \mathbf{t}^\dagger = \frac{e^2}{h} \sum_{n=1}^N T_n, \quad (1.24)$$

where \mathbf{t} is taken at E_F and T_n is an eigenvalue of $\mathbf{t} \mathbf{t}^\dagger$. It follows from flux conservation (1.16) that $T_n \in [0, 1]$. The conductance is thus fully determined by the transmission eigenvalues. Knowledge of the (sometimes) complicated transmission eigenstates, each of which is a complicated superposition of incoming modes, is not required.

In order to evaluate the shot-noise power we substitute the current operators (1.17) into Eq. (1.1) and then determine the expectation value. We need to know the covariance of two pairs of a creation and an annihilation operator.

This is easily derived from the fermion commutation relations and from Eq. (1.20) (For brevity we use 1,2,3,4 instead of $\alpha, \beta, \gamma, \delta$ and $\varepsilon, \varepsilon', \varepsilon'', \varepsilon'''$.) The result is

$$\Delta_{1234} \equiv \langle \hat{a}_1^\dagger \hat{a}_2 \hat{a}_3^\dagger \hat{a}_4 \rangle - \langle \hat{a}_1^\dagger \hat{a}_2 \rangle \langle \hat{a}_3^\dagger \hat{a}_4 \rangle = \delta_{14} \delta_{23} f_1 (1 - f_2), \quad (1.25)$$

where e.g. δ_{12} stands for $\delta_{\alpha\beta} \delta(\varepsilon - \varepsilon')$. In the evaluation (1.25) we have not included the situation where all arguments of the four operators are equal. Since there is a continuum of states the measure of the resulting term is negligible in comparison to the result of Eq. (1.25) [22]. Equation (1.25) shows that there are cross correlations between different scattering states. Although this bears no effect on the average current, it is essential for the current fluctuations. For the shot-noise power we thus have

$$P(\omega) = 2 \frac{e^2}{h^2} \sum_{\alpha, \beta, \gamma, \delta} \int_{-\infty}^{\infty} dt \int_0^{\infty} d\varepsilon \int_0^{\infty} d\varepsilon' \int_0^{\infty} d\varepsilon'' \int_0^{\infty} d\varepsilon''' e^{i(\hbar\omega + \varepsilon - \varepsilon')t/\hbar} \\ \times I_{\alpha\beta}(\varepsilon, \varepsilon') I_{\gamma\delta}(\varepsilon'', \varepsilon''') \Delta_{\alpha\beta\gamma\delta}(\varepsilon, \varepsilon', \varepsilon'', \varepsilon'''). \quad (1.26)$$

Substitution of Eq. (1.25) then yields

$$P(\omega) = 2 \frac{e^2}{h} \sum_{\alpha, \beta} \int_0^{\infty} d\varepsilon \\ \times I_{\alpha\beta}(\varepsilon, \varepsilon + \hbar\omega) I_{\beta\alpha}(\varepsilon + \hbar\omega, \varepsilon) f_\alpha(\varepsilon) [1 - f_\beta(\varepsilon + \hbar\omega)]. \quad (1.27)$$

The noise power in the low-frequency limit P is found by substitution of Eq. (1.19) (for brevity we suppress the ε dependence of f and s):

$$P = 2 \frac{e^2}{h} \int_0^{\infty} d\varepsilon \left\{ [f_1(1 - f_2) + f_2(1 - f_1)] \text{Tr} s_{12}^\dagger s_{11} s_{11}^\dagger s_{12} \right. \\ \left. + f_1(1 - f_1) \text{Tr}(1 - s_{11}^\dagger s_{11})(1 - s_{11}^\dagger s_{11}) + f_2(1 - f_2) \text{Tr} s_{12}^\dagger s_{12} s_{12}^\dagger s_{12} \right\} \\ = 2 \frac{e^2}{h} \int_0^{\infty} d\varepsilon \left\{ [f_1(1 - f_2) + f_2(1 - f_1)] \text{Tr} t t^\dagger (1 - t t^\dagger) \right. \\ \left. + [f_1(1 - f_1) + f_2(1 - f_2)] \text{Tr} t t^\dagger t t^\dagger \right\}. \quad (1.28)$$

We have used the unitarity of S in the last step.

Equation (1.28) allows us to evaluate the noise for various cases. Below we will assume that eV and $k_B T$ are small enough to neglect the energy dependence of the transmission matrix, so that we can take t at the Fermi

energy E_F . Let us first determine the noise in equilibrium, i.e. for $V = 0$. Using the relation $f(1 - f) = -k_B T \partial f / \partial \varepsilon$ we find

$$P = 4k_B T \frac{e^2}{h} \text{Tr} t t^\dagger = 4k_B T \frac{e^2}{h} \sum_{n=1}^N T_n. \quad (1.29)$$

Which is indeed the Johnson-Nyquist formula (1.2). For the shot-noise power at zero temperature we obtain

$$P = 2e|V| \frac{e^2}{h} \text{Tr} t t^\dagger (1 - t t^\dagger) = 2e|V| \frac{e^2}{h} \sum_{n=1}^N T_n (1 - T_n). \quad (1.30)$$

Equation (1.30), due to Büttiker [22], is the multi-channel generalization of the single-channel formulas found earlier [18, 20, 21]. One notes, that P is again only a function of the transmission eigenvalues. From the Landauer formula for the conductance (1.24), we find that $P = P_{\text{Poisson}}$ if all transmission eigenvalues are small ($T_n \ll 1$, for all n). However, if the eigenvalues are distributed otherwise, the shot noise is suppressed below P_{Poisson} . It is clear from Eq. (1.30) that a transmission eigenstate for which $T_n = 1$ does not contribute to the shot noise. This is easily understood: At zero temperature there is a non-fluctuating incoming electron stream. If there is complete transmission, the transmitted electron stream will be noise free, too. Essentially, the non-fluctuating occupation number of the incoming states is a consequence of the electrons being fermions. In this sense, the suppression below the Poisson noise is due to the Pauli principle. On the other hand, one must realize that the noise suppression is not an exclusive property of fermions. It occurs for any incoming beam with a non-fluctuating occupation number, for example a photon number state [24]. Levitov and Lesovik have shown [25] that Eq. (1.30) follows from the fact that the electrons in each separate scattering channel are transmitted in time according to a binomial (Bernoulli) distribution. The Poisson noise is then the limiting distribution for small T_n . In the following Subsections we will discuss on the basis of Eq. (1.30) the shot noise in two mesoscopic systems, a quantum point-contact and a metallic, diffusive conductor.

The generalization of Eq. (1.30) to the non-zero voltage, non-zero temperature case is [18, 26]

$$P = 2 \frac{e^2}{h} \sum_{n=1}^N [2k_B T T_n^2 + T_n (1 - T_n) e|V| \coth(e|V|/2k_B T)]. \quad (1.31)$$

The crossover from the thermal noise (1.29) to the shot noise (1.30) depends sensitively on the transmission eigenvalues. Only if $T_n \ll 1$, for all n , one

recovers the universal crossover as known for tunnel junctions

$$P = 2e|\bar{I}| \coth(e|V|/2k_B T). \quad (1.32)$$

As a final remark, we mention that in the above derivations we have assumed the absence of spin and valley degeneracy for notational convenience. It can be easily included. For a two-fold spin degeneracy this results in the replacement of the e^2/h prefactors [such as in Eqs. (1.24) and (1.30)] by $2e^2/h$.

1.1.4 Shot noise in a quantum point-contact

A point contact is a small constriction between two pieces of conductor. If the width of the constriction is much smaller than the mean free path of the bulk material, but much greater than the Fermi wave length, the conductance is given by the Sharvin conductance [27]. This is a classical point contact. In a quantum point-contact the size of the constriction becomes comparable to the Fermi wavelength. Experimentally, a quantum point-contact can be formed in a two-dimensional electron gas in a (Al,Ga)As heterostructure [2]. The constriction is defined by means of metallic gates on top of the structure. By applying a negative voltage on these gates, the electron gas underneath them is depleted. By changing the gate voltage the width of the point contact can be varied. The conductance of such a quantum point-contact displays a stepwise increase in units of $2e^2/h$ as a function of gate voltage [28, 29]. This is caused by the discrete number of modes at the Fermi energy which fit into the constriction width. As a result a number of transmission eigenvalues is 1, the others 0. Indeed, one then finds indeed a quantized conductance from the Landauer formula (1.24).

It has been noted by Lesovik, that the shot noise should be absent in such a device [20]. This property follows from the shot-noise formula Eq. (1.30). Only in between the plateaus, when the conductance increases by $2e^2/h$, there is a transmission eigenvalues which is neither 0 nor 1, so that the shot noise should be non-vanishing. Here, we illustrate this property, using Büttiker's model of a saddle-point constriction [30]. The potential of this two-dimensional system is given by

$$V(x, y) = V_0 - \frac{1}{2}m\omega_x^2 x^2 + \frac{1}{2}m\omega_y^2 y^2, \quad (1.33)$$

where V_0 is the potential at the saddle point, and ω_x and ω_y determine the curvatures. The transmission eigenvalues at the Fermi energy are [30]

$$T_n = [1 + \exp(-2\pi\varepsilon_n/\hbar\omega_x)]^{-1}, \quad n = 1, 2, \dots, \quad (1.34)$$

where $\varepsilon_n \equiv E_F - V_0 - (n - \frac{1}{2})\hbar\omega_y$. Results for the conductance and the shot-noise power using Eqs. (1.24) and (1.30), respectively, are displayed in Fig. 1.4. Indeed, we observe that at the conductance plateaus the shot noise is completely absent.

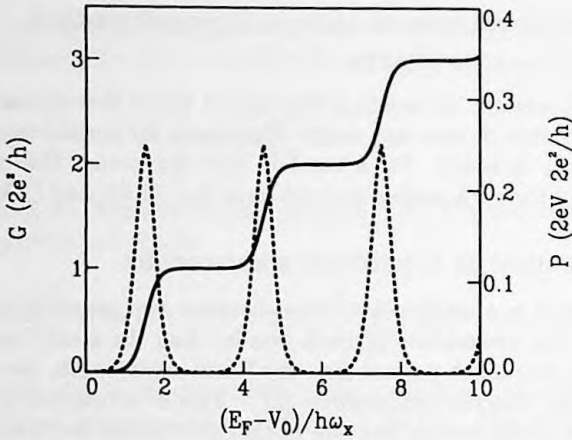


Figure 1.4: Conductance G (full line) and shot-noise power P (dotted line) versus Fermi energy of a two-dimensional quantum point-contact, according to the saddle-point model [30], with $\omega_y = 3\omega_x$.

1.1.5 Shot noise in a diffusive conductor

We now turn to transport through a diffusive conductor of length L much greater than the mean free path ℓ , in the metallic regime ($L \ll$ localization length). To compute the ensemble averages $\langle \dots \rangle$ of Eqs. (1.24) and (1.30) we need the density of transmission eigenvalues $p(T) \equiv \langle \sum_n \delta(T - T_n) \rangle$. The first moment of $p(T)$ determines the conductance,

$$\langle G \rangle = G_0 \int_0^1 dT p(T) T, \quad (1.35)$$

with $G_0 \equiv 2e^2/h$, whereas the shot-noise power contains also the second moment

$$\langle P \rangle = P_0 \int_0^1 dT p(T) T(1 - T), \quad (1.36)$$

with $P_0 \equiv 2e|V|G_0$. In the metallic regime, Ohm's law for the conductance holds to a good approximation, which implies that $\langle G \rangle \propto 1/L$, up to small corrections of order e^2/h (due to weak localization). The Drude formula gives

$$\langle G \rangle = G_0 \frac{N\bar{\ell}}{L}, \quad (1.37)$$

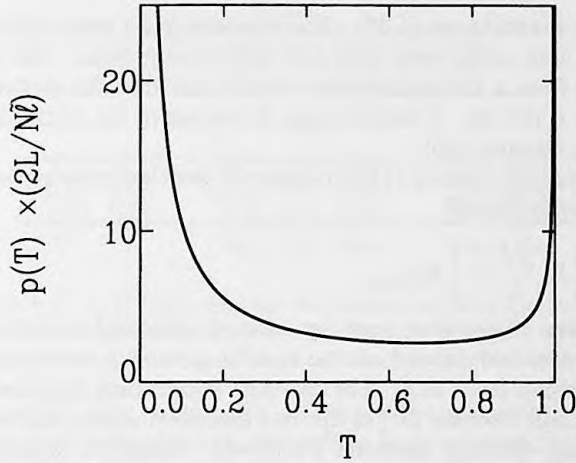


Figure 1.5: The bimodal distribution of transmission eigenvalues according to Eq. (1.39). The cutoff for $T \lesssim 4 \exp(-2L/\tilde{\ell})$ is not shown.

where $\tilde{\ell}$ equals the mean free path ℓ times a numerical coefficient

$$\tilde{\ell} = a_d \ell. \quad (1.38)$$

The precise coefficient a_d depends on the dimensionality d of the Fermi surface and on the specific kind of scattering. For isotropic impurity scattering with mean free path ℓ one has $a_2 = \pi/2$ in 2D (Fermi circle) and $a_3 = 4/3$ in 3D (Fermi sphere).

From Eqs. (1.35) and (1.37) one might surmise that for a diffusive conductor all the transmission eigenvalues are of order $\tilde{\ell}/L$, and hence much smaller than 1. This would imply the shot-noise power $P = P_{\text{Poisson}}$ of a Poisson process. However, the surmise $T_n \approx \tilde{\ell}/L$ for all n is completely incorrect for a metallic, diffusive conductor. This was first pointed out by Dorokhov [31], and later by Imry [32] and by Pendry *et al.* [33]. In reality, a fraction $\tilde{\ell}/L$ of the transmission eigenvalues is of order unity (open channels), the others being exponentially small (closed channels). The full distribution function is [31]

$$p(T) = \begin{cases} \frac{N\tilde{\ell}}{2L} \frac{1}{T\sqrt{1-T}}, & \text{if } 4e^{-2L/\tilde{\ell}} < T < 1, \\ 0, & \text{otherwise.} \end{cases} \quad (1.39)$$

The cutoff at $T \lesssim 4e^{-2L/\tilde{\ell}} \ll 1$ is such that $\int_0^1 dT p(T) = N$ and is irrelevant for the computation of $\langle G \rangle$ and $\langle P \rangle$. One easily checks that Eq. (1.39) leads

to the Drude conductance (1.37). The function $p(T)$ is plotted in Fig. 1.5. It is *bimodal* with peaks near unit and zero transmission. The distribution (1.39) follows from a scaling equation, which describes the evolution of $p(T)$ on increasing L [34, 35]. A microscopic derivation of Eq. (1.39) has recently been given by Nazarov [36].

The bimodal distribution (1.39) implies for the shot-noise power (1.36) the unexpected result [36–40]

$$\langle P \rangle = \frac{1}{3} P_0 \frac{N\bar{\ell}}{L} = \frac{1}{3} P_{\text{Poisson}}. \quad (1.40)$$

This suppression of the shot noise by a factor one-third is *universal*, in the sense that it does not depend on the specific geometry nor on any intrinsic material parameter (such as ℓ). The one-third suppression has been first found by Beenakker and Büttiker [37] in the way described above, and subsequently by others using different methods [36, 38–40]. Nagaev's derivation [38] of Eq. (1.40) is based on a semiclassical calculation, where the electron motion is treated classically, but the Pauli principle is accounted for. One might therefore infer that there should also be a semiclassical explanation for the bimodal distribution of transmission eigenvalues, which is the key ingredient of the quantum mechanical derivation. Such a derivation is given below [41].

Let us first introduce the transfer matrix M [42]. Whereas the scattering matrix S connects the incoming states with the outgoing states, see Eq. (1.15), the $2N \times 2N$ transfer matrix gives the relation between the states on the left side and the right side of the conductor (see Fig. 1.3)

$$M \begin{pmatrix} I_1 \\ O_1 \end{pmatrix} = \begin{pmatrix} O_2 \\ I_2 \end{pmatrix}. \quad (1.41)$$

The eigenvalues T_n of tt^\dagger are related to the eigenvalues $\exp(\pm 2\alpha_n L)$ of MM^\dagger by

$$T_n = \frac{1}{\cosh^2(\alpha_n L)}, \quad n = 1, 2, \dots, N. \quad (1.42)$$

which relates the eigenvalues T_n of tt^\dagger to the eigenvalues $\exp(\pm 2\alpha_n L)$ of MM^\dagger . The eigenvalues of MM^\dagger come in inverse pairs as a result of current conservation. The length $1/\alpha_n$ is the channel-dependent localization length [31]. Scattering channels are open or closed depending on whether $1/\alpha_n$ is larger or smaller than L . The bimodal distribution (1.39) of the transmission eigenvalues is equivalent to a *uniform* and *L-independent* distribution of the inverse localization lengths,

$$\rho(\alpha) = \begin{cases} N\bar{\ell}, & \text{if } 0 < \alpha\bar{\ell} < 1, \\ 0, & \text{otherwise,} \end{cases} \quad (1.43)$$

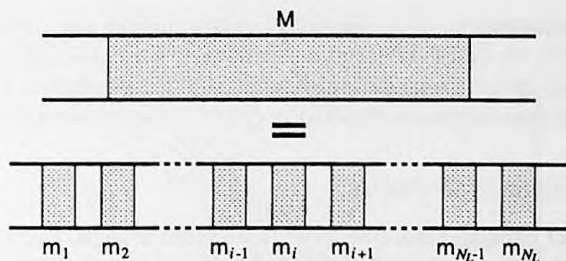


Figure 1.6: A diffusive wire can be constructed from a large number (N_L) of individual slices in series. The transfer matrix M of the wire is the product of the transfer matrices m_i of the individual slices.

where $\rho(\alpha) \equiv \langle \sum_n \delta(\alpha - \alpha_n) \rangle$. We will argue that these two properties, L -independence and uniformity, of $\rho(\alpha)$ follow from a law of classical physics, Ohm's law, and a mathematical theorem on eigenvalues, Oseledec's theorem [43].

We recall [42] that the transfer matrix has the multiplicative property that if two pieces of wire with transfer matrices M_1 and M_2 are connected in series, the transfer matrix of the combined system is the product $M_1 M_2$. In this way the transfer matrix of a disordered wire can be constructed from the product of N_L individual transfer matrices m_i (see Fig. 1.6),

$$M = \prod_{i=1}^{N_L} m_i, \quad (1.44)$$

where $N_L \simeq L/\lambda$ is a large number proportional to L . The m_i 's are assumed to be independently and identically distributed random matrices, each representing transport through a slice of conductor of length λ . In the theory of random matrix products [44], the limit $\lim_{L \rightarrow \infty} \alpha_n$ is known as a Lyapunov exponent. Oseledec's theorem [43] is the statement that this limit exists. Numerical simulations [42] indicate that the large- L limit is essentially reached for $L \gg \ell$, and does not require $L \gg N\ell$. This explains the L -independence of the distribution of the inverse localization lengths in the metallic, diffusive regime ($\ell \ll L \ll N\ell$).

Oseledec's theorem tells us that $\rho(\alpha)$ is independent of L , but it does not tell us how it depends on α . To deduce the uniformity of $\rho(\alpha)$ we invoke Ohm's law, $\langle G \rangle \propto 1/L$. This requires

$$L \int_0^\infty d\alpha \rho(\alpha) \frac{1}{\cosh^2(\alpha L)} = C, \quad (1.45)$$

where C is independent of L . Equation (1.45) implies the uniform distribution $\rho(\alpha) = C$. A cutoff at large α is allowed, since $1/\cosh^2(\alpha L)$ vanishes anyway for $\alpha L \gg 1$. From Drude's formula (1.36) we deduce $C = N\ell$, and normalization then implies a cutoff at $\alpha \gtrsim 1/\ell$, in accordance with Eq. (1.43).

1.1.6 Experimental results

The number of experimental papers on shot noise is remarkably smaller than the number of theoretical papers. Noise experiments are notoriously difficult. In particular, the combination of high frequencies (high enough to eliminate the $1/f$ -noise) and cryogenic temperatures is problematic, since the radiation of the measuring leads tends to heat up the device.

Li *et al.* have reported on low-frequency noise experiments in quantum point-contacts [45]. They observe an increase in the noise power at the conductance steps. However, an interpretation in terms of suppressed shot noise is still under debate, because it is known [46] that resistance fluctuations can also be quite sensitive to changes in the number of quantized modes in the point contact. Recently, the shot-noise suppression at the conductance plateaus has been measured at much higher frequencies by Reznikov *et al.* [47].

Shot noise in double-barrier resonant tunneling devices has been measured by Li *et al.* [48] and by Liu *et al.* [49]. The applied voltages are much larger than the width of the resonance. The observed noise depends on the symmetry of the device. Full shot noise is observed for asymmetric structures, where one tunnel barrier is much more opaque than the other. For symmetric structures, a suppression by one half is observed. This effect has been explained both from a quantum mechanical [50] as well as from a semiclassical [51] treatment. For the asymmetric structure, tunneling through the highest barrier dominates the current fluctuations, so that the noise is Poissonian. In less asymmetric devices, the tunneling through both barriers becomes correlated, so that the shot noise gets suppressed. The Coulomb interaction may have a strong effect on the noise in conductors with a small capacitance, such as single-electron-tunneling devices [52]. Theories which take the Coulomb blockade into account [53] predict a shot-noise suppression which is periodic in the applied voltage. This effect has recently been observed for a nanoparticle between a surface and the tip of a scanning tunneling microscope [54].

An experimental observation of suppressed shot noise in a diffusive wire has been presented by Liefrink *et al.* [55]. The system under investigation is a wire inside the two-dimensional electron gas of a (Al,Ga)As heterostructure defined by means of electrostatic gates on top of the structure. The wire has a lithographic length $L = 16.7 \mu\text{m}$ and width $W = 0.5 \mu\text{m}$. Upon application of a gate voltage the width becomes smaller than the lithographic width. Inside the wire the mean free path is estimated to be $\ell \simeq 1.4 \mu\text{m}$, so that the

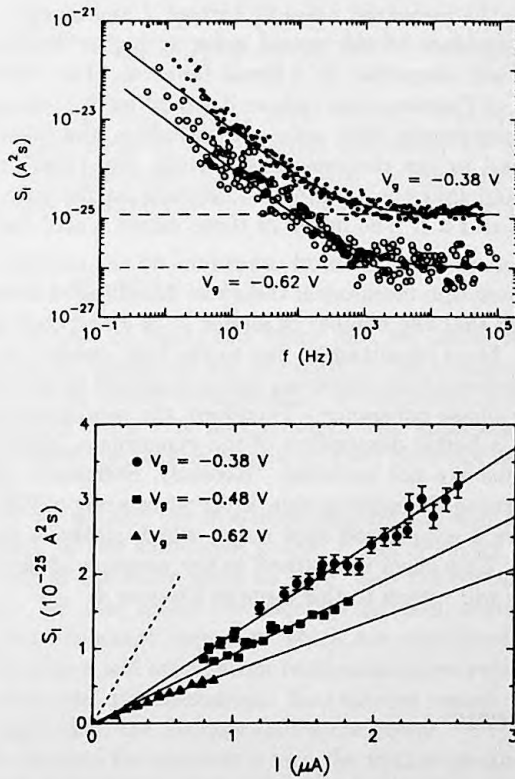


Figure 1.7: The noise in a (Al,Ga)As gate-defined wire of lithographic length $L = 16.7 \mu\text{m}$ and width $W = 0.5 \mu\text{m}$ at temperature $T = 4.2\text{K}$. Results are shown for gate voltages $V_g = -0.38\text{V}$, -0.48V , and -0.62V , where the resistance is $8.6\text{ k}\Omega$, $13\text{ k}\Omega$, and $26\text{ k}\Omega$, and where the number of transverse modes is $N \simeq 12$, 9 , and 5 , respectively. Top: Typical frequency spectrum of the excess noise S_I for gate voltage $V_g = -0.38\text{V}$ (closed circles) and $V_g = -0.62\text{V}$ (open circles). Solid curves represent fits to the data by the sum of a $1/f$ and a white-noise contribution. The latter is separately indicated by dashed lines. Bottom: Current dependence of the excess noise S_I (outside the $1/f$ range) for different gate voltages. Solid lines represent linear fits to the data. The dashed line shows the current dependence of S_I as expected for full shot noise. Taken from Liefrink *et al.* [55].

transport is in the diffusive regime. In Fig. 1.7 both the excess-noise spectrum and its dependence on the current are depicted. The excess noise S_I is the difference between the measured noise at current I and at zero current. We note that the dependence of the excess noise at higher frequencies on the current I is quite well described by a linear function. The slope of this line is well below that of Poisson noise (where it would be $2e$), clearly indicating the occurrence of suppressed shot noise. Nevertheless, the exact dependence does not correspond to the theoretical prediction, Eq. (1.40). Rather than one-third, it is found that the suppression depends on the gate voltage, and varies between 0.2 and 0.4. The origin of these values is still under debate.

We mention that the experimental conditions do not coincide with the assumptions of the quantum mechanical theory as described in Subsection 1.1.5. There it is assumed that the number of modes $N \gg 1$ and that the resistance $\ll h/2e^2 \simeq 13 \text{ k}\Omega$. More importantly, due to the high current densities inside the wire, the electron-electron scattering rate is expected to be high, thus completely destroying phase coherence. Therefore, the semiclassical theory [38] probably provides a better description of the experiment, although electron-electron interactions are not included. Recently, Steinbach, Martinis, and Devoret have measured the noise in thin silver wires using a SQUID amplifier [56]. They observe a suppressed shot noise, which is above the theoretical value of $\frac{1}{3}P_{\text{Poisson}}$. This effect is ascribed to the presence of electron-electron scattering, and we will return to this issue in Chapter 6.

1.2 This thesis

Chapter 2 Mesoscopic fluctuations in the shot-noise power of metals

As shown in Subsection 1.1.5 the shot-noise power of a metallic, diffusive conductor $\langle P \rangle = \frac{1}{3}P_{\text{Poisson}}$. This value is the average over an ensemble of macroscopically identical samples, with different impurity configurations. It is well known from experiments [57] and from theory [58, 59] that the sample-to-sample or mesoscopic fluctuations of the conductance of metallic, diffusive conductors have a universal magnitude of e^2/h . These "universal conductance fluctuations" (UCF) are independent of specific material and sample properties and are characteristic for phase-coherent transport in mesoscopic systems. The problem addressed in Chapter 2 concerns the sample-to-sample fluctuations in the shot-noise power. It will be shown that these fluctuations have the universal magnitude $e^3|V|/h$.

Our method is based on the scaling equation which describes the evolution

with increasing L of the distribution of transmission eigenvalues [34, 35],

$$\ell \frac{\partial w(\{\lambda_i\}, L)}{\partial L} = \frac{2}{\beta N + 2 - \beta} \sum_{n=1}^N \frac{\partial}{\partial \lambda_n} \lambda_n (1 + \lambda_n) J \frac{\partial}{\partial \lambda_n} J^{-1} w, \quad (1.46)$$

where $J \equiv \prod_{n < m} |\lambda_n - \lambda_m|^\beta$ and $\lambda_n \equiv (1 - T_n)/T_n$. The symmetry parameter β denotes whether there is time-reversal symmetry ($\beta = 1$) or not ($\beta = 2$). Time-reversal symmetry can be broken by applying a small magnetic field. The initial condition of the distribution function is that of ballistic transmission,

$$w(\{\lambda_i\}, 0) = \delta(\lambda_1) \delta(\lambda_2) \cdots \delta(\lambda_N). \quad (1.47)$$

Following the method of Mello and Stone [60], we derive from Eq. (1.46) an infinite hierarchy of equations for moments of the transmission eigenvalues. The hierarchy can be closed by expanding the moments in powers of $1/N$ and neglecting terms of order $1/N$ and smaller. The approach is restricted to a wire geometry, since the scaling equation (1.46) does not hold for a square or cube geometry.

As a result we recover the one-third suppression and find a weak-localization correction to the shot-noise power P . It is shown that the variance of P is universal in the same sense as UCF, and the precise numerical value is determined. We also study the effect of inelastic scattering by dividing the wire in phase-coherent segments which are connected through current-conserving, but phase and momentum randomizing reservoirs [37]. The weak-localization effect and the mesoscopic fluctuations vanish more rapidly as a function of length than the average shot-noise power.

Chapter 2 contains the research which the author performed as an undergraduate, and is included to make this thesis self-contained.

Chapter 3 Doubled shot noise in normal-metal–superconductor junctions

At low voltages electrical transport through a normal-metal–superconductor (NS) junction requires the conversion of the normal, dissipative current in the metal into the dissipationless supercurrent in the superconductor. The process by which this conversion occurs is known as Andreev reflection [61]: An electron excitation above the Fermi level in the normal metal is reflected at the NS interface into a hole excitation below the Fermi level, whereas the excess charge is carried away as a Cooper pair in the superconductor. We study the shot noise in an NS junction with an arbitrary scattering region in the normal metal.

The quasiparticle excitations in the NS system are eigenstates the Bogoliubov-de Gennes equation [62], which is a 2×2 matrix Schrödinger equation.

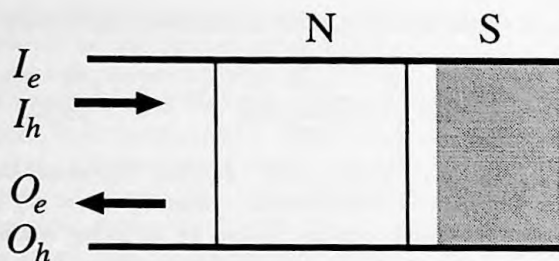


Figure 1.8: Schematic overview of the NS junction. Incoming electron and hole excitations in the normal metal are scattered by an arbitrary normal-metal scattering region in series with a superconductor. At excitation energies below the superconducting gap energy the electron and hole excitations are confined to the normal metal, so that all the incoming states (I) are reflected into outgoing states (O).

The calculation of the shot noise proceeds analogous to the normal-metal case described in Subsection 1.1.4. We assume low temperatures and an applied voltage $e|V|$ smaller than the excitation-gap energy Δ , so that the excitations are confined to the normal metal. The scattering of the incoming excitations into outgoing excitations is described by the $2N \times 2N$ reflection matrix R (see Fig. 1.8)

$$\begin{pmatrix} O_e \\ O_h \end{pmatrix} = R \begin{pmatrix} I_e \\ I_h \end{pmatrix}, \quad (1.48)$$

where I_e, I_h, O_e, O_h are the N -component vectors denoting the amplitudes of the incoming (I) and outgoing (O) electron (e) and hole (h) modes. The reflection matrix can be decomposed according to

$$R = \begin{pmatrix} r_{ee} & r_{eh} \\ r_{he} & r_{hh} \end{pmatrix}, \quad (1.49)$$

where e.g. the $N \times N$ submatrix r_{he} contains the reflection amplitudes from incoming electrons to reflected holes.

Within the scattering formalism we calculate the linear-response conductance of the NS junction [63, 64]

$$G_{NS} = 2G_0 \text{Tr} r_{he} r_{he}^\dagger. \quad (1.50)$$

The interpretation of Eq. (1.50) is that for each reflection of an electron into a hole there is a double contribution to the current, because the electrons and holes move in opposite direction with opposite charge. For the shot-noise power we obtain

$$P_{NS} = 4P_0 \text{Tr} r_{he} r_{he}^\dagger (1 - r_{he} r_{he}^\dagger). \quad (1.51)$$

On the basis of Eq. (1.51) we derive a formula which depends on the transmission eigenvalues of the normal region only. We then calculate the shot noise for an NS junction which contains a planar tunnel barrier, recovering previous results by Khlus [18]. For a high barrier $P = 2P_{\text{Poisson}}$, due to uncorrelated transport in units of $2e$. Subsequently, a disordered junction is considered, for which we find that $P = \frac{2}{3}P_{\text{Poisson}}$, as a consequence of noiseless open scattering channels. Finally, we treat a disordered region in series with a tunnel barrier.

Chapter 4 Andreev reflection in ferromagnet-superconductor junctions

In a conventional (spin-singlet) superconductor a Cooper pair consists of a spin-up and a spin-down electron. Therefore, in the Andreev-reflection process [61], the reflected quasiparticle must occupy the opposite spin band to that of the incoming quasiparticle. This change of spin band can be observed if the normal metal has a partial spin polarization as in a ferromagnet. The conductance and shot noise of ferromagnet-superconductor (FS) junctions are the subject of Chapter 4.

The first system that is considered is a ballistic FS point contact, where a ferromagnet is contacted through a small area with a superconductor. It is well known that in an ideal NS point contact, the conductance is twice the Sharvin conductance of the same point contact with the superconductor in the normal state. This is because all the scattering channels (transverse modes in the point contact at the Fermi level) which would be transmitted in the normal contact, are Andreev reflected in the NS contact, thereby giving a double contribution to the conductance. For the FS point contact the situation is different. Because of the exchange interaction the density of states at the Fermi level differs for both spins bands. Let $N_{\uparrow}(N_{\downarrow})$ be the number of up(down)-spin channels in the point contact, with $N_{\uparrow} \geq N_{\downarrow}$. At zero temperature, the spin channels do not mix and the conductance G_{FN} — where the superconductor is in the normal state — is given by

$$G_{\text{FN}} = \frac{e^2}{h} (N_{\downarrow} + N_{\uparrow}). \quad (1.52)$$

In the superconducting state, the spin-down electrons of all the N_{\downarrow} channels are Andreev reflected into spin-up holes. However, only a fraction $N_{\downarrow}/N_{\uparrow}$ of the N_{\uparrow} channels can be Andreev reflected, because the density of states in the spin-down band is smaller than in the spin-up band. Therefore, the resulting conductance is

$$G_{\text{FS}} = \frac{e^2}{h} (2N_{\downarrow} + 2\frac{N_{\downarrow}}{N_{\uparrow}}N_{\uparrow}) = 4\frac{e^2}{h} N_{\downarrow}. \quad (1.53)$$

Comparison of Eqs. (1.52) and (1.53) shows that G_{FS} may be either larger or smaller than G_{FN} depending on the ratio $N_{\uparrow}/N_{\downarrow}$, and hence on the magnitude of the exchange interaction.

The above argument is substantiated by applying the Stoner model [65] for the electrons inside the ferromagnet, which treats the exchange interaction on a mean field-level, and then determining the scattering states in this system by solving the Bogoliubov-de Gennes equation [62]. It is found that the Andreev reflection probability depends on the magnitude of the exchange interaction in the ferromagnet. The intuitive result Eq. (1.53), although not exact, is quite accurate. Subsequently, we consider the shot-noise power in the FS point contact, which is a sensitive probe for the Andreev-reflection probability at the FS interface.

In an NS junction the Andreev-reflected states close to the Fermi level are the phase-conjugates of the incoming states times a phase factor. One of the consequences is that the linear-response conductance G_{NINS} of an NINS junction with an insulating tunnel barrier (I) in the normal metal is independent of the length L between the barrier and the NS interface [63]. In the last part of Chapter 4 we study how this effect is modified in an FIFS junction. Due to the differences in wave vector between the spin-up (k_{\uparrow}) and spin-down (k_{\downarrow}) band, quasi-bound states are formed if the resonance condition

$$2L(k_{\uparrow} - k_{\downarrow}) = (2n + 1)\pi, \quad n = 0, 1, 2, \dots, \quad (1.54)$$

is fulfilled. As a consequence we find large resonances as a function of L in G_{FIFS} . These resonances are distinct from the Tomasch oscillations known to occur in the non-linear differential conductance of NINS junctions [66]. The Tomasch oscillations are due to the dispersion of electron and hole wave vectors at energies away from the Fermi level, and thus vanish in linear response. The oscillations in an FIFS junction are due to the change in spin band upon Andreev reflection. As a consequence, they do not vanish in linear response, but do disappear when the exchange interaction is zero, as in a normal metal.

Chapter 5 Transition from Sharvin to Drude resistance in high-mobility wires

The problems of Chapters 2–4 are solved in a fully quantum mechanical framework; the next three Chapters of this thesis contain semiclassical calculations. In Chapter 5 we study the resistance of a wire of length L for arbitrary ratio between L and the elastic mean free path ℓ . The two limiting cases are well known. In the ballistic regime $\ell \gg L$ the conductance is given by the Sharvin conductance [27]

$$G_S = G_0 N, \quad (1.55)$$

where N is the number of transverse modes in the wire. For a two-dimensional wire of width W we have $N = k_F W / \pi$ and for a three-dimensional wire, of cross-sectional area S , $N = k_F^2 S / 4\pi$, with k_F the Fermi wave number. In the diffusive regime $L \gg \ell$ the conductance is given by the Drude result

$$G_D = G_0 N \frac{\bar{\ell}}{L}, \quad (1.56)$$

with the normalized mean free path $\bar{\ell}$ proportional to ℓ [see Eq. (1.38)]. The aim of Chapter 5 is to derive a formula which describes the crossover from G_S to G_D when $\ell \simeq L$.

Our starting point is the semiclassical Landauer formula, which for two dimensions is given by

$$G = G_0 N \int_0^W \frac{dy}{W} \int_{-\pi/2}^{\pi/2} \frac{d\varphi}{2} \cos \varphi T(0, y, \varphi). \quad (1.57)$$

The transmission probability $T(0, y, \varphi)$ is the probability for transmission into lead 2 ($x = L$) of an electron which starts in lead 1 at $(x, y) = (0, y)$ with velocity $\mathbf{v} = v_F(\cos \varphi, \sin \varphi)$ (where v_F is the Fermi velocity). We assume specular boundary scattering, so that the transverse y -coordinate becomes irrelevant. For elastic and isotropic impurity scattering the transmission probabilities satisfy the integro-differential equation

$$\ell \cos \varphi \frac{\partial T(x, \varphi)}{\partial x} = T(x, \varphi) - \int_0^{2\pi} \frac{d\varphi'}{2\pi} T(x, \varphi'), \quad (1.58)$$

with the boundary conditions

$$T(0, \varphi) = 0, \quad \text{if } \varphi \in [\frac{1}{2}\pi, \frac{3}{2}\pi], \quad (1.59a)$$

$$T(L, \varphi) = 1, \quad \text{if } \varphi \in [0, \frac{1}{2}\pi] \cap [\frac{3}{2}\pi, 2\pi]. \quad (1.59b)$$

Equation (1.58) is valid both for two and three dimensions and can be obtained from the Boltzmann transport equation.

To determine the conductance for arbitrary ratio ℓ/L Eqs. (1.58) and (1.59) are transformed into an integral equation, which can be solved numerically. The result can be written as

$$G = G_0 N \left(1 + \gamma L / \bar{\ell}\right)^{-1}, \quad (1.60)$$

where γ is a number close to 1, which depends on the dimensionality and weakly on the ratio ℓ/L . Quite surprisingly, we find that the naive procedure

of simply adding the Sharvin and Drude resistances — according to $G^{-1} = G_S^{-1} + G_D^{-1}$, which is equivalent to setting $\gamma = 1$ in Eq. (1.60) — is just within a few percent from the exact solution.

Finally, we apply the result (1.60) to an experiment by Tarucha *et al.* [67], in which the resistances of wires, of different lengths, defined in a high-mobility two-dimensional electron gas are measured. Good agreement is obtained.

Chapter 6 Semiclassical theory of shot-noise suppression

The original derivation of the one-third suppression of the shot-noise power in a metallic, diffusive conductor [37] was quantum mechanical, based on the bimodal distribution of transmission eigenvalues. We have seen in Subsection 1.1.5 that the bimodal distribution can be obtained from a semiclassical argument. This suggests that it should be possible to derive the one-third suppression in the framework of a semiclassical transport theory. Nagaev [38] has presented such a derivation, in which the Pauli principle is taken into account, but the motion of the electrons is treated classically. Nagaev's approach does not yield a formula with the same generality as Büttiker's formula (1.30), but is only applicable for diffusive transport. In Chapter 6 we use the semiclassical approach to evaluate the shot noise in a wider class of mesoscopic conductors and we compare the outcomes of our theory with the quantum mechanical calculations.

Our starting point is the Boltzmann-Langevin equation [68, 69] for the fluctuating distribution function $f(\mathbf{r}, \mathbf{k}, t)$, which denotes the occupation number of electrons at position \mathbf{r} , with wave vector \mathbf{k} , at time t . The average over time-dependent fluctuations $\langle f \rangle \equiv \bar{f}$ satisfies the Boltzmann equation

$$\left(\frac{d}{dt} + \mathcal{S} \right) \bar{f}(\mathbf{r}, \mathbf{k}, t) = 0, \quad (1.61a)$$

$$\frac{d}{dt} \equiv \frac{\partial}{\partial t} + \mathbf{v} \cdot \frac{\partial}{\partial \mathbf{r}} + \mathcal{F} \cdot \frac{\partial}{\hbar \partial \mathbf{k}}. \quad (1.61b)$$

The derivative (1.61b) (with $\mathbf{v} = \hbar \mathbf{k} / m$) describes the classical, deterministic motion in the force field $\mathcal{F}(\mathbf{r})$ and the term $\mathcal{S} \bar{f}$ accounts for the stochastic effects of scattering. In the Boltzmann equation the scattering occurs into all wave vectors \mathbf{k} with some probability distribution. However, at a certain instant in time an electron is only scattered into one particular \mathbf{k} . Thus the stochastic nature of the scattering leads to time-dependent fluctuations $\delta f \equiv f - \bar{f}$ in the distribution function. The time-dependent fluctuations obey the Boltzmann-Langevin equation [68, 69]

$$\left(\frac{d}{dt} + \mathcal{S} \right) \delta f(\mathbf{r}, \mathbf{k}, t) = j(\mathbf{r}, \mathbf{k}, t). \quad (1.62)$$

The fluctuating source term j represents the stochastic fluctuations induced by each scattering event. The flux j has zero average, $\langle j \rangle = 0$, and covariance

$$\langle j(\mathbf{r}, \mathbf{k}, t) j(\mathbf{r}', \mathbf{k}', t') \rangle = (2\pi)^d \delta(\mathbf{r} - \mathbf{r}') \delta(t - t') J(\mathbf{r}, \mathbf{k}, \mathbf{k}'). \quad (1.63)$$

The delta functions ensure that fluxes are only correlated if they are induced by the same scattering process. The correlator J depends on the type of scattering and on \bar{f} , but not on δf .

On the basis of Eqs. (1.61)–(1.63) we can relate the shot-noise power P to classical transmission probabilities at the Fermi level. In the diffusive regime, we recover the one-third suppression of the shot-noise power [38]. It is shown, that this suppression does neither depend on the details of the scattering, nor on the dimensionality of the conductor. Furthermore, we calculate how the shot noise crosses over from complete suppression in the ballistic regime to one-third of the Poisson noise in the diffusive regime, complementing the study for the crossover of the conductance in Chapter 5. We also apply our theory to tunneling through n planar barriers in series (tunnel probability Γ). For $n = 2$ and $\Gamma \ll 1$ we recover the results for a double-barrier junction of Refs. [50, 51]. Our calculation shows how the shot-noise suppression by one half which occurs in a symmetric double-barrier junction [48, 50, 51] crosses over to the one-third suppression as $n \rightarrow \infty$. In addition, our method is applied to determine the shot noise in a conductor consisting of a disordered region in series with a tunnel barrier. Our results fully agree with quantum mechanical calculations in the literature, establishing that phase coherence is not required for the occurrence of suppressed shot noise in mesoscopic systems.

In the last part of Chapter 6, we calculate the effects of electron-electron and inelastic scattering on the shot noise. In an experiment, these types of scattering may be enhanced due to the high currents, which are often required for noise measurements. Analogous to the work of Beenakker and Büttiker [37], this scattering is modeled by putting charge-conserving electron reservoirs between phase-coherent segments of the conductor. This allows us to model the effects of quasi-elastic scattering, electron heating, and inelastic scattering within the same theoretical framework.

Chapter 7 Hydrodynamic electron flow in high-mobility wires

In classical diffusive transport, the effects of electron-electron scattering on the resistivity are difficult to observe. The reason is that normal electron-electron (e-e) scattering does not change the total momentum of the electron distribution, while resistive *umklapp* processes are rare in bulk simple metals [70]. However, it has been pointed out [71–73] that normal e-e scattering should influence the resistance of narrow wires with non-specular boundary scattering, provided that the bulk mean free path l_b exceeds the wire width W . At low

electron temperatures, normal e-e scattering causes electrons whose original trajectory is along the wire axis, to be deflected towards the boundaries, where their momentum can be dissipated. This process, the electronic analog of the Knudsen effect in gas-flow dynamics, increases the resistivity [72]. At higher electron temperatures, the electron collision-rate increases strongly, causing an increase in the time needed for the electrons to reach the boundary of the wire. In this regime, where the mean free path l_{ee} between normal e-e scattering events drops below W , the resistivity actually decreases with increasing electron temperature, a situation known as the Gurzhi effect [71]. This is the electronic analog of the Poiseuille gas-flow regime.

The last Chapter of this thesis contains a theoretical study of Knudsen and Gurzhi flow phenomena, based on a series of experiments carried out by L. W. Molenkamp at Philips Research Laboratories, Eindhoven. These flow phenomena occur in electrostatically defined two-dimensional wires, fabricated from high-mobility (Al,Ga)As heterostructures. Using these semiconductor devices to study hydrodynamic electron flow offers several advantages over metal wires: First, due to the high purity of the material and the resolution of electron-beam lithography one can easily reach the condition $l_b > W$. Second, *umklapp* electron-electron scattering is completely absent, because of the low electron density and the perfectly circular Fermi surface. Third, the electron-acoustic phonon coupling is weak. This makes it possible to investigate the influence of e-e scattering *not* by changing the temperature T of the full sample, but by selectively changing the temperature T_e of the electrons inside the wire by passing a dc current I through the device. The wires are equipped with opposing pairs of quantum point-contacts in their boundaries, so that one can determine T_e in the wire as a function of I from a thermovoltage measurement [74]. In the experiments, the non-linear differential resistance of the wires is observed to first increase and then decrease with increasing I . This is identified as the Knudsen and Gurzhi effect, respectively.

We model the experiments by a Boltzmann theory, taking into account impurity, e-e, and boundary scattering. We write the distribution function $f(\mathbf{r}, \mathbf{k})$ for electrons at position $\mathbf{r} = (x, y)$ (with x along and y perpendicular to the wire axis) and with wave vector $\mathbf{k} = k(\cos \varphi, \sin \varphi)$ in the form

$$f(\mathbf{r}, \mathbf{k}) = f_0(\varepsilon) + \left(-\frac{\partial f_0}{\partial \varepsilon} \right) \chi(y, \varphi), \quad (1.64)$$

where $f_0(\varepsilon)$ is the Fermi-Dirac distribution function at energy ε . We have dropped the x -coordinate since there is translational invariance along the x -axis. The stationary Boltzmann transport equation, linearized with respect

to the applied electric field $\mathbf{E} = (E, 0)$ reads

$$-eEv_F \cos \varphi + v_F \sin \varphi \frac{\partial \chi(y, \varphi)}{\partial y} = \left. \frac{\partial \chi(y, \varphi)}{\partial t} \right|_{\text{scatt}} \quad (1.65)$$

The r. h. s. of Eq. (1.65) takes into account both impurity and e-e scattering. The impurity scattering is assumed to be elastic and isotropic. For the e-e scattering we use a model due to Callaway [75], which is the simplest possible scattering term with the requirement of conservation of total momentum,

$$\left. \frac{\partial \chi(y, \varphi)}{\partial t} \right|_{ee} = -\frac{\chi(y, \varphi)}{\tau_{ee}} + \frac{1}{\tau_{ee}} \int_0^{2\pi} \frac{d\varphi'}{2\pi} \chi(y, \varphi') [1 + 2 \cos(\varphi - \varphi')], \quad (1.66)$$

with $\tau_{ee} (= l_{ee}/v_F)$ the e-e scattering time. The scattering with the wire boundaries is described by a specularity coefficient $p(\varphi)$, denoting the fraction of electrons which is scattered specularly, the remainder being scattered diffusely. The coefficient p is a function of the angle of incidence φ , such that $p \rightarrow 1$ for grazing incidence ($\varphi \rightarrow 0$ or $\varphi \rightarrow \pi$) [76].

We have developed a scheme to determine the solution of Eq. (1.65) for arbitrary l_b, l_{ee}, W , and $p(\varphi)$. By calculating the flow profiles inside the wire, we show how normal flow evolves into Poiseuille flow. Good agreement is obtained between experiment and theory.

References

- [1] Y. Imry, in *Directions in Condensed Matter Physics*, Vol. 1, edited by G. Grinstein and G. Mazenko (World Scientific, Singapore, 1986).
- [2] C. W. J. Beenakker and H. van Houten, *Solid State Phys.* **44**, 1 (1991).
- [3] *Mesoscopic Phenomena in Solids*, edited by B. L. Altshuler, P. A. Lee, and R. A. Webb (North-Holland, Amsterdam, 1991).
- [4] *Mesoscopic Quantum Physics*, edited by E. Akkermans, G. Montambaux, and J.-L. Pichard (North Holland, Amsterdam, 1995).
- [5] A. van der Ziel, *Noise in Solid State Devices and Circuits* (Wiley, New York, 1986).
- [6] W. B. Davenport and W. L. Root, *An Introduction to the Theory of Random Signals and Noise* (IEEE Press, New York, 1987).
- [7] M. B. Johnson, *Phys. Rev.* **29**, 367 (1927); H. Nyquist, *ibid.* **32**, 110 (1928).
- [8] H. B. Callen and T. W. Welton, *Phys. Rev.* **83**, 34 (1951).
- [9] F. N. Hooge, *IEEE Trans. Electron Devices* **41**, 1926 (1994).
- [10] W. Schottky, *Ann. Phys. (Leipzig)* **57**, 541 (1918).
- [11] H. Cramér, *Mathematical Methods of Statistics* (Princeton University Press, Princeton, 1946).
- [12] R. Landauer, *J. Res. Dev.* **1**, 233 (1957); **32**, 306 (1988).
- [13] D. S. Fisher and P. A. Lee, *Phys. Rev. B* **23**, 6851 (1981).
- [14] M. Büttiker, *Phys. Rev. Lett.* **57**, 1761 (1986); *IBM J. Res. Dev.* **32**, 317 (1988).
- [15] A. D. Stone and A. Szafer, *IBM J. Res. Dev.* **32**, 384 (1988).
- [16] H. U. Baranger and A. D. Stone, *Phys. Rev. B* **40**, 8169 (1989).
- [17] K. Shepard, *Phys. Rev. B* **43**, 11623 (1991).
- [18] V. A. Khlus, *Zh. Eksp. Teor. Fiz.* **93**, 2179 (1987) [*Sov. Phys. JETP* **66**, 1243 (1987)].
- [19] R. Landauer, *Physica D* **38**, 226 (1989).
- [20] G. B. Lesovik, *Pis'ma Zh. Eksp. Teor. Fiz.* **49**, 513 (1989) [*JETP Lett.* **49**, 592 (1989)].
- [21] B. Yurke and G.P. Kochanski, *Phys. Rev. B* **41**, 8184 (1990).
- [22] M. Büttiker, *Phys. Rev. Lett.* **65**, 2901 (1990); *Phys. Rev. B* **46**, 12485 (1992).
- [23] R. Landauer and Th. Martin, *Physica B* **175**, 167 (1991).
- [24] R. C. Liu and Y. Yamamoto, to appear in *Quantum dynamics of submicron structures*, edited by H. A. Cerdeira, B. Kramer, and G.

Schön.

- [25] L. S. Levitov and G. B. Lesovik, *Pis'ma Zh. Eksp. Teor. Fiz.* **58**, 225 (1993) [*JETP Lett.* **58**, 230 (1993)].
- [26] Th. Martin and R. Landauer, *Phys. Rev. B* **45**, 1742 (1992).
- [27] Yu. V. Sharvin, *Zh. Eksp. Teor. Fiz.* **48**, 984 (1965) [*Sov. Phys. JETP* **21**, 655 (1965)].
- [28] B. J. van Wees, H. van Houten, C. W. J. Beenakker, J. G. Williamson, L. P. Kouwenhoven, D. van der Marel, and C. T. Foxon, *Phys. Rev. Lett.* **60**, 848 (1988).
- [29] D. A. Wharam, T. J. Thornton, R. Newbury, M. Pepper, H. Ahmed, J. E. F. Frost, D. G. Hasko, D. C. Peacock, D. A. Ritchie, and G. A. C. Jones, *J. Phys. C* **21**, L209 (1988).
- [30] M. Büttiker, *Phys. Rev. B* **41**, 7906 (1990).
- [31] O. N. Dorokhov, *Solid State Commun.* **51**, 381 (1984).
- [32] Y. Imry, *Europhys. Lett.* **1**, 249 (1986).
- [33] J. B. Pendry, A. MacKinnon, and P. J. Roberts, *Proc. R. Soc. London Ser. A* **437**, 67 (1992).
- [34] O. N. Dorokhov, *Pis'ma Zh. Eksp. Teor. Fiz.* **36**, 259 (1982) [*JETP Lett.* **36**, 318 (1982)].
- [35] P. A. Mello, P. Pereyra, and N. Kumar, *Ann. Phys. (New York)* **181**, 290 (1988).
- [36] Yu. V. Nazarov, *Phys. Rev. Lett.* **73**, 134 (1994).
- [37] C. W. J. Beenakker and M. Büttiker, *Phys. Rev. B* **46**, 1889 (1992).
- [38] K. E. Nagaev, *Phys. Lett. A* **169**, 103 (1992).
- [39] M. J. M. de Jong and C. W. J. Beenakker, *Phys. Rev. B* **46**, 13400 (1992) [Chapter 2].
- [40] B. L. Altshuler, L. S. Levitov, and A. Yu. Yakovets, *Pis'ma Zh. Eksp. Teor. Fiz.* **59**, 821 (1994) [*JETP Lett.* **59**, 857 (1994)].
- [41] M. J. M. de Jong and C. W. J. Beenakker, in *Coulomb and Interference Effects in Small Electronic Structures*, edited by D. C. Glatli, M. Sanquer, and J. Trân Thanh Vân (Editions Frontières, France, 1994).
- [42] A. D. Stone, P. A. Mello, K. A. Muttalib, and J.-L. Pichard, in Ref. [3].
- [43] V. I. Oseledec, *Trans. Moscow Math. Soc.* **19**, 197 (1968).
- [44] A. Crisanti, G. Paladin, and A. Vulpiani, *Products of Random Matrices in Statistical Physics* (Springer, Berlin, 1993).
- [45] Y. P. Li, D. C. Tsui, J. J. Heremans, J. A. Simmons, and G. W. Weimann, *Appl. Phys. Lett.* **57**, 774 (1990).

- [46] G. Timp, R. E. Behringer, and J. E. Cunningham, *Phys. Rev. B* **42**, 9259 (1990); C. Dekker, A. J. Scholten, F. Liefrink, R. Eppenga, H. van Houten, and C. T. Foxon, *Phys. Rev. Lett.* **66**, 2148 (1991).
- [47] M. Reznikov, M. Heiblum, H. Shtrikman, and D. Mahalu (preprint).
- [48] Y. P. Li, A. Zaslavsky, D. C. Tsui, M. Santos, and M. Shayegan, *Phys. Rev. B* **41**, 8388 (1990).
- [49] H. C. Liu, J. Li, G. C. Aers, C. R. Leavens, M. Buchanan, and Z. R. Wasilewski, *Phys. Rev. B* **51**, 5116 (1995).
- [50] L. Y. Chen and C. S. Ting, *Phys. Rev. B* **43**, 4534 (1991); K.-M. Hung and G. Y. Wu, *ibid.* **48**, 14687 (1993).
- [51] J. H. Davies, P. Hyldgaard, S. Hershfield, and J. W. Wilkins, *Phys. Rev. B* **46**, 9620 (1992).
- [52] D. V. Averin and K. K. Likharev, in Ref. [3]; A. N. Korotkov, D. V. Averin, K. K. Likharev, and S. A. Vasenko, in *Single-Electron Tunneling and Mesoscopic Devices*, edited by H. Koch, H. Lübbig (Springer, Berlin, 1992); A. N. Korotkov, *Phys. Rev. B* **49**, 10381 (1994).
- [53] S. Hershfield, J. H. Davies, P. Hyldgaard, C. J. Stanton, and J. W. Wilkins, *Phys. Rev. B* **47**, 1967 (1992); U. Hanke, Yu. M. Galperin, K. A. Chao, and N. Zou, *ibid.* **48**, 17209 (1993).
- [54] H. Birk, M. J. M. de Jong, and C. Schönenberger (preprint).
- [55] F. Liefrink, J. I. Dijkhuis, M. J. M. de Jong, L. W. Molenkamp, and H. van Houten, *Phys. Rev. B* **49**, 14066 (1994).
- [56] A. Steinbach, J. Martinis, and M. Devoret, *Bull. Am. Phys. Soc.* **40**, 400 (1995).
- [57] S. Washburn and R. A. Webb, *Adv. Phys.* **35**, 375 (1986).
- [58] B. L. Altshuler, *Pis'ma Zh. Eksp. Teor. Fiz.* **41**, 530 (1985) [*JETP Lett.* **41**, 648 (1985)].
- [59] P. A. Lee and A. D. Stone, *Phys. Rev. Lett.* **55**, 1622 (1985).
- [60] P. A. Mello and A. D. Stone, *Phys. Rev. B* **44**, 3559 (1991).
- [61] A. F. Andreev, *Zh. Eksp. Teor. Fiz.* **46**, 1823 (1964) [*Sov. Phys. JETP* **19**, 1228 (1964)].
- [62] P. G. de Gennes, *Superconductivity of Metals and Alloys* (Benjamin, New York, 1966).
- [63] G. E. Blonder, M. Tinkham, and T. M. Klapwijk, *Phys. Rev. B* **25**, 4515 (1982).
- [64] Y. Takane and H. Ebisawa, *J. Phys. Soc. Jpn.* **61**, 2858 (1992).
- [65] E. C. Stoner, *Proc. R. Soc. London Ser. A* **165**, 372 (1938).
- [66] W. J. Tomasch, *Phys. Rev. Lett.* **15**, 672 (1965); **16**, 16 (1966); W.

- L. McMillan and P. W. Anderson, *Phys. Rev. Lett.* **16**, 85 (1966); A. Hahn, *Phys. Rev. B* **31**, 2816 (1985).
- [67] S. Tarucha, T. Saku, Y. Tokura, and Y. Hirayama, *Phys. Rev. B* **47**, 4064 (1993).
- [68] B. B. Kadomtsev, *Zh. Eksp. Teor. Fiz.* **32**, 943 (1957) [*Sov. Phys. JETP* **5**, 771 (1957)].
- [69] Sh. M. Kogan and A. Ya. Shul'man, *Zh. Eksp. Teor. Fiz.* **56**, 862 (1969) [*Sov. Phys. JETP* **29**, 467 (1969)].
- [70] J. M. Ziman, *Electrons and Phonons* (Oxford University Press, Oxford, 1960).
- [71] R. N. Gurzhi, *Zh. Eksp. Teor. Fiz.* **44**, 771 (1963) [*Sov. Phys. JETP* **17**, 521 (1963)].
- [72] J. E. Black, *Phys. Rev. B* **21**, 3279 (1980).
- [73] M. Kaveh and N. Wiser, *Adv. Phys.* **33**, 257 (1984).
- [74] L. W. Molenkamp, Th. Gravier, H. van Houten, O. J. A. Buyk, M. A. A. Mabesoone, and C. T. Foxon, *Phys. Rev. Lett.* **68**, 3765 (1992).
- [75] J. Callaway, *Phys. Rev.* **113**, 1046 (1959).
- [76] S. B. Soffer, *J. Appl. Phys.* **38**, 1710 (1967).

- 1. The first step in the scientific process is to identify a problem or question.
- 2. Next, you need to gather information about the problem.
- 3. Then, you should develop a hypothesis, which is a testable prediction.
- 4. After that, you design an experiment to test your hypothesis.
- 5. You then collect data from the experiment.
- 6. Finally, you analyze the data to see if it supports your hypothesis.
- 7. If the data does not support your hypothesis, you may need to revise it.
- 8. The scientific process is a cycle that repeats itself.
- 9. It is important to keep accurate records of your work.
- 10. Communication is a key part of the scientific process.
- 11. Scientists share their findings with others in the field.
- 12. This allows them to be tested and verified.
- 13. The scientific process is a way to gain knowledge about the world.
- 14. It is based on evidence and logic.
- 15. The scientific process is a way to solve problems.
- 16. It is a way to test ideas and theories.
- 17. The scientific process is a way to learn from mistakes.
- 18. It is a way to improve our understanding of the world.
- 19. The scientific process is a way to make progress.
- 20. It is a way to discover new things.

Chapter 2

Mesoscopic fluctuations in the shot-noise power of metals

2.1 Introduction

Recently, the classical problem of shot noise has been reinvestigated for quantum systems [1]. Shot noise is the time-dependent fluctuation in the electrical current due to the discreteness of the charge of the carriers. It has been found that the shot-noise power P is suppressed below the classical value of a Poisson process [2] ($P_{\text{Poisson}} = 2e|I|$, with I the time-averaged current) as a consequence of noiseless open quantum channels. In particular, it was shown by Beenakker and Büttiker [3] that the *average* noise power (P) in the diffusive transport regime is one third of the Poisson value. The “average” here refers to an average over an ensemble of impurity configurations. It is well known in mesoscopic physics that transport properties may have large fluctuations around the average from sample to sample [4]. Such “mesoscopic fluctuations” in the conductance were shown [5, 6] to have the root-mean-square value e^2/h times a coefficient of order unity, independent of the size of the sample and the degree of disorder. Hence the name “universal conductance fluctuations” (UCF). In Ref. [3] it was argued on general grounds that the shot-noise power has mesoscopic fluctuations of order $(e^2/h)e|V|$, with V the applied voltage. The purpose of this Chapter is to give an explicit calculation of the root-mean-square value of the shot-noise power, rms P , of disordered conductors, much longer than wide, but shorter than the localization length. It will be shown that, in the case of phase-coherent transport, these fluctuations are universal in the same sense as UCF and the precise numerical value will be calculated.

Starting point is the shot-noise formula derived by Büttiker [7]. It expresses the zero-temperature, zero-frequency shot-noise power P of a spin-

degenerate two-probe conductor over which a small voltage V is applied, entirely in terms of transmission matrices t at the Fermi energy:

$$P = P_0 \text{Tr} t t^\dagger (1 - t t^\dagger) = P_0 \sum_{n=1}^N T_n (1 - T_n), \quad (2.1)$$

where T_n denotes an eigenvalue of $t t^\dagger$, N is the number of channels, and $P_0 \equiv 2e|V|G_0$, with $G_0 \equiv 2e^2/h$ the unit of conductance. Equation (2.1) is the multi-channel generalization of the single-channel formulas found earlier [8–10]. Using the Landauer formula

$$G = G_0 \text{Tr} t t^\dagger = G_0 \sum_{n=1}^N T_n \quad (2.2)$$

for the conductance $G = I/V$, one finds from Eq. (2.1) that $P = P_{\text{Poisson}}$ if all transmission eigenvalues are small ($T_n \ll 1$, for all n). In a phase-coherent conductor, however, the T_n 's are either exponentially small (closed channels) or of order unity (open channels) [11]. This leads to sub-Poissonian shot noise when the ensemble average is taken [3].

To determine the fluctuations in P around $\langle P \rangle$ one can, in principle, use a diagrammatic Green's function method, as in the original theories of UCF [5, 6]. In this paper, however, the equivalent random-matrix method [11–17] will be used, as it makes contact naturally with Eq. (2.1), where the shot-noise power is expressed as a function of random transmission matrices. The central quantity in the random-matrix theory of quantum transport is the distribution $w(\{\lambda_1, \lambda_2, \dots, \lambda_N\})$ of eigenparameters $\lambda_n \in [0, \infty)$, related to the transmission eigenvalues by $T_n \equiv (1 + \lambda_n)^{-1}$. The so-called *local* approach, which is based on the properties of small segments of the conductor, leads to a diffusion equation for the evolution of this distribution with length L [13–16]. The diffusion equation depends on the symmetry properties of the random-matrix ensemble. It can be written in a unified way using the symmetry parameter β , where $\beta = 1$ in the presence and $\beta = 2$ in the absence of time-reversal symmetry. For a sample with N channels, a length L and an elastic mean free path $\tilde{\ell}$, with the definition $s \equiv L/\tilde{\ell}$, the diffusion equation is given by [13, 14, 16]

$$\begin{aligned} \frac{\partial}{\partial s} w_s^{(\beta)}(\{\lambda_i\}) &= \frac{2}{\beta N + 2 - \beta} \sum_{n=1}^N \frac{\partial}{\partial \lambda_n} \\ &\times \left[\lambda_n (1 + \lambda_n) J_\beta(\{\lambda_i\}) \frac{\partial}{\partial \lambda_n} \frac{w_s^{(\beta)}(\{\lambda_i\})}{J_\beta(\{\lambda_i\})} \right], \end{aligned} \quad (2.3)$$

where $J_\beta(\{\lambda_i\}) \equiv \prod_{n < m} |\lambda_n - \lambda_m|^\beta$. The initial condition is that of perfect transmission,

$$w_0^{(\beta)}(\{\lambda_i\}) = \delta(\lambda_1)\delta(\lambda_2)\cdots\delta(\lambda_N). \quad (2.4)$$

The diffusion equation (2.3) is based on (a) the difference in symmetry properties of the ensemble of scattering matrices in the presence or absence of time-reversal symmetry; (b) an isotropy assumption, which implies that flux incident in one channel is, on average, equally distributed among all outgoing channels; and (c) a maximum-entropy assumption for the distribution $w_{\delta_s}^{(\beta)}(\{\lambda_i\})$ for a small segment of the conductor. Assumption (b) requires a conductor much longer than wide, i.e. the *quasi-one-dimensional* limit. Assumption (c) has been justified by a "central-limit theorem" [17]. Calculations for the conductance starting from Eq. (2.3) [15, 16] have indeed produced the same ohmic conductance and quantum-interference effects (weak localization and UCF) as obtained earlier by Green's function techniques in the quasi-one-dimensional limit.

The outline of this Chapter is as follows. In Section 2.2 the diffusion equation (2.3) is used to determine the mesoscopic fluctuations in the shot-noise power. Furthermore, a weak-localization effect and the earlier found suppression by one third are obtained for the ensemble-averaged shot-noise power. The calculation is straightforward, but lengthy. The key intermediate steps are given in Appendix 2A. Finally, the effect of inelastic scattering on the shot-noise power of conductors longer than the phase-coherence length is discussed in Section 2.3.

2.2 Average and variance of the shot-noise power

The regime of interest is the metallic, diffusive regime: The sample must be much longer than the mean free path, but much shorter than the 1D localization length $\xi \sim N\bar{\ell}$, requiring

$$1 \ll s \ll N. \quad (2.5)$$

With the definition of the moment

$$\mathcal{T}_q^r \equiv \left(\sum_{n=1}^N \mathcal{T}_n^q \right)^r \equiv \left[\sum_{n=1}^N \frac{1}{(1 + \lambda_n)^q} \right]^r, \quad (2.6)$$

and the convention $\mathcal{T}^p \equiv \mathcal{T}_1^p$, $\mathcal{T}_q \equiv \mathcal{T}_q^1$, and $\mathcal{T} \equiv \mathcal{T}_1^1$, one finds from Eq. (2.1) for the average and the variance of the shot-noise power the expressions

$$\langle P \rangle = P_0 (\langle \mathcal{T} \rangle - \langle \mathcal{T}_2 \rangle), \quad (2.7)$$

$$\text{var } P = P_0^2 [\langle T^2 \rangle - \langle T \rangle^2 - 2(\langle T T_2 \rangle - \langle T \rangle \langle T_2 \rangle) + \langle T_2^2 \rangle - \langle T_2 \rangle^2] . \quad (2.8)$$

The brackets denote the ensemble average,

$$\langle F \rangle = \int_0^\infty d\lambda_1 \int_0^\infty d\lambda_2 \cdots \int_0^\infty d\lambda_N w_s^{(\beta)}(\{\lambda_i\}) F(\{\lambda_i\}) . \quad (2.9)$$

From the diffusion equation (2.3) one can derive the evolution of the different moments. For example, the evolution equation for $\langle T^p \rangle$ is given by [16]

$$(\beta N + 2 - \beta) \frac{\partial}{\partial s} \langle T^p \rangle = \langle -\beta p T^{p+1} - (2 - \beta) p T^{p-1} T_2 + 2p(p-1) T^{p-2} (T_2 - T_3) \rangle . \quad (2.10)$$

Obviously, this single evolution equation is not solvable because of the appearance of *new* moments. In Refs. [15,16] it is shown that the hierarchy of evolution equations can be closed by an expansion in powers of N^{-1} . The resulting set of coupled differential equations needed for the evaluation of Eqs. (2.7) and (2.8), and their solutions, are given in Appendix 2A. Here, only the results are presented.

For the average shot-noise power we find

$$\langle P \rangle = P_0 \left[\frac{N\bar{\ell}}{3L} - \frac{\delta\beta_1}{45} + \mathcal{O}\left(\frac{L}{N\bar{\ell}}\right) \right] . \quad (2.11)$$

Combining this with the result for the average conductance from Ref. [16],

$$\langle G \rangle = G_0 \left[\frac{N\bar{\ell}}{L} - \frac{\delta\beta_1}{3} + \mathcal{O}\left(\frac{L}{N\bar{\ell}}\right) \right] , \quad (2.12)$$

one can write

$$\langle P \rangle = \frac{1}{3} P_{\text{Poisson}} + \delta P_{\text{WL}} , \quad (2.13)$$

where $P_{\text{Poisson}} \equiv 2e|V|\langle G \rangle$ and $\delta P_{\text{WL}} \equiv P_0 4\delta\beta_1/45$. The suppression by a factor one third of the ensemble-averaged Poisson noise is in agreement with Ref. [3], where the alternative *global* approach to random-matrix theory was used. In the second term of Eq. (2.11) one recognizes a weak-localization correction for the shot noise, analogous to that in Eq. (2.12) for the conductance [16]. As it is caused by the interference between time-reversed pairs of trajectories, it disappears when time-reversal symmetry is broken ($\beta = 2$), i.e. in the presence of a magnetic field. The decrease in the conductance due to weak localization can be incorporated in the Poisson value. The remaining

correction δP_{WL} is positive, indicating that weak localization suppresses the conductance more than the shot noise.

Next the variance of the shot-noise power is determined. We find that the first two terms in the expansion of the right-hand-side of Eq. (2.8) — of order N^2 and N respectively — vanish *exactly*. The remaining term is

$$\text{var}(T - T_2) = \frac{1}{\beta} \frac{46}{2835} + \mathcal{O}\left(\frac{L}{N\bar{\ell}}\right). \quad (2.14)$$

Thus, the root-mean-square fluctuations in the shot-noise power are given by

$$\text{rms } P = P_0 C_\beta, \quad (2.15)$$

independent of the length L , the number of channels N , and the elastic mean free path $\bar{\ell}$. By analogy with the conductance, one could speak of “universal noise fluctuations.” The numerical coefficient is $C_1 = \sqrt{46/2835} \simeq 0.127$ in the presence of time-reversal symmetry and $C_2 = \sqrt{23/2835} \simeq 0.090$ in its absence.

2.3 Effect of inelastic scattering

The theory presented is valid at zero temperature, when shot noise is the only source of current fluctuations and when all scattering is elastic. At finite temperatures the theory should be modified to include thermal noise (important when $kT > eV$), the effects of thermal averaging (important when $L > l_T \equiv (\hbar D/kT)^{1/2}$, with D the diffusion constant), and inelastic scattering (important when L is greater than the inelastic-scattering length l_{in}). If $kT \ll eV$ and $l_{\text{in}} \ll l_T$ the effect of inelastic scattering dominates. Its effect on the shot noise can be estimated by considering a model in which the conductor is divided into $M_{\text{in}} \simeq L/l_{\text{in}}$ phase-coherent segments of length l_{in} , separated by phase and momentum randomizing reservoirs [3]. Quasi-one-dimensionality now requires that the width of the conductor is much smaller than l_{in} . Furthermore, phase-coherent diffusive transport requires $\bar{\ell} \ll l_{\text{in}}$. In Ref. [3] the following sum rule was derived

$$R^2 P = \sum_{i=1}^{M_{\text{in}}} R_i^2 P_i, \quad (2.16)$$

where R_i and P_i are the resistance and the shot-noise power of an individual segment, and $R \equiv \sum_{i=1}^{M_{\text{in}}} R_i$ and P are the resistance and the shot-noise power of the whole conductor. Using Eqs. (2.1) and (2.2), R_i and P_i can be expressed in terms of the moments $\mathcal{T}(i)$ and $\mathcal{T}_2(i)$ of the transmission eigenvalues of the

i -th segment. Since a fraction R_i/R of the total applied voltage V drops over the i -th segment, one has from Eq. (2.16)

$$P = P_0 \frac{\sum_{i=1}^{M_{\text{in}}} T(i)^{-3} [T(i) - T_2(i)]}{[\sum_{i=1}^{M_{\text{in}}} T(i)^{-1}]^3}. \quad (2.17)$$

Each moment in Eq. (2.17) can be written as the ensemble average plus a deviation, $T(i) \equiv \langle T \rangle_{\text{in}} + \delta T(i)$ and $T_2(i) \equiv \langle T_2 \rangle_{\text{in}} + \delta T_2(i)$. The brackets $\langle \dots \rangle_{\text{in}}$ denote the ensemble average for a phase-coherent conductor of length l_{in} . (All segments are assumed to have the same average properties.) Now, Eq. (2.17) is expanded in powers of $\delta T(i)$ and $\delta T_2(i)$, and the fact that moments of different segments are statistically independent (e.g. $\langle \delta T(i) \delta T(j) \rangle = \langle \delta T(i) \rangle \langle \delta T(j) \rangle$, if $i \neq j$) is used.

The ensemble-averaged shot-noise power becomes

$$\begin{aligned} \langle P \rangle = P_0 M_{\text{in}}^{-2} & \left[\langle T \rangle_{\text{in}} - \langle T_2 \rangle_{\text{in}} \right. \\ & \left. + 3 \frac{M_{\text{in}} - 1}{M_{\text{in}}} \left(\frac{\langle \delta T \delta T_2 \rangle_{\text{in}}}{\langle T \rangle_{\text{in}}} - \frac{\langle (\delta T)^2 \rangle_{\text{in}} \langle T_2 \rangle_{\text{in}}}{\langle T \rangle_{\text{in}}^2} \right) + \dots \right]. \end{aligned} \quad (2.18)$$

To determine the ensemble averages over a phase-coherent segment the results of Section 2.2 can be used (with L substituted by l_{in}). One has $\langle T \rangle_{\text{in}}, \langle T_2 \rangle_{\text{in}} = \mathcal{O}(N\bar{\ell}/l_{\text{in}})$, while $\langle (\delta T)^2 \rangle_{\text{in}}, \langle \delta T \delta T_2 \rangle_{\text{in}} = \mathcal{O}(1)$. It follows that the terms $\langle T \rangle_{\text{in}}$ and $\langle T_2 \rangle_{\text{in}}$ in Eq. (2.18) are two orders of magnitude in $(N\bar{\ell}/l_{\text{in}})$ higher than the terms containing the fluctuations δT and δT_2 , so that it is consistent to neglect these latter terms while retaining the weak-localization corrections to $\langle T \rangle_{\text{in}}$ and $\langle T_2 \rangle_{\text{in}}$. Equation (2.11) then implies

$$\langle P \rangle = P_0 \left[\frac{N\bar{\ell}}{3L} \left(\frac{l_{\text{in}}}{L} \right) - \frac{\delta\beta_1}{45} \left(\frac{l_{\text{in}}}{L} \right)^2 \right]. \quad (2.19)$$

Comparison with Eq. (2.11) shows that, while the leading term in the average shot-noise power is reduced by a factor (l_{in}/L) because of inelastic scattering [3], the weak-localization correction is suppressed more strongly, by a factor $(l_{\text{in}}/L)^2$.

Now, for the effect of inelastic scattering on the mesoscopic fluctuations of the shot-noise power. The variance $\langle P^2 \rangle - \langle P \rangle^2$ is determined by substitution of the expression for P given in Eq. (2.17), then an expansion in powers of δT and δT_2 , and finally taking the ensemble average. The result is

$$\text{var } P = P_0^2 M_{\text{in}}^{-5} [\langle (\delta T)^2 \rangle_{\text{in}} - 2\langle \delta T \delta T_2 \rangle_{\text{in}} + \langle (\delta T_2)^2 \rangle_{\text{in}} + \dots]. \quad (2.20)$$

The three terms between square brackets are, in fact, equal to the variance, $\text{var}(T - T_2)$, of a phase-coherent segment of length l_{in} . With Eqs. (2.14) and (2.15) one finds

$$\text{rms } P = P_0 C_\beta \left(\frac{l_{\text{in}}}{L} \right)^{5/2}. \quad (2.21)$$

The root-mean-square value of the mesoscopic fluctuations of the shot-noise power is suppressed by a factor $(l_{\text{in}}/L)^{5/2}$ due to inelastic scattering. Hence, at the breakdown of phase-coherent transport the mesoscopic fluctuations cease being universal and become dependent on the length of the conductor.

The division of the conductor in phase-coherent segments separated by phase and momentum randomizing reservoirs is a simplified model of inelastic scattering, which occurs throughout the conductor. A more realistic treatment is expected to leave the parametric dependence on the ratio (l_{in}/L) unaffected. It is interesting to compare the above results with the corresponding results for the conductance [18],

$$\delta G_{\text{WL}} = \text{constant} \times G_0 \left(\frac{l_{\text{in}}}{L} \right), \quad (2.22a)$$

$$\text{rms } G = \text{constant} \times G_0 \left(\frac{l_{\text{in}}}{L} \right)^{3/2}. \quad (2.22b)$$

One notes for the shot-noise power that the value of the exponent of (l_{in}/L) occurring in the expressions for the average, for the weak-localization effect, and for the root-mean-square value of the mesoscopic fluctuations, is equal to the exponent in the corresponding expressions for the conductance *plus one*.

Appendix 2A Moment expansion and solution

Consider a compound moment

$$\prod_{i=1}^m T_{q_i}^{r_i} \equiv \left[\sum_{n=1}^N \frac{1}{(1 + \lambda_n)^{q_1}} \right]^{r_1} \cdots \left[\sum_{n=1}^N \frac{1}{(1 + \lambda_n)^{q_m}} \right]^{r_m}, \quad (2.23)$$

where $q_i \neq q_j$ if $i \neq j$. From Eqs. (2.4) and (2.9) the initial condition of the ensemble average is

$$\lim_{s \rightarrow 0} \langle \prod_i T_{q_i}^{r_i} \rangle = N^\nu, \quad \nu \equiv \sum_{i=1}^m r_i. \quad (2.24)$$

The evolution of a compound moment can be derived from the diffusion equation (2.3). This leads to the general evolution equation

$$\begin{aligned}
 & (\beta N + 2 - \beta) \frac{\partial}{\partial s} \left\langle \prod_i \mathcal{T}_{q_i}^{r_i} \right\rangle = \\
 & \beta \sum_i \left\langle q_i r_i \mathcal{T}_{q_i}^{r_i-1} \left(\sum_{n=0}^{q_i-2} \mathcal{T}_{n+1} \mathcal{T}_{q_i-n-1} - \sum_{n=0}^{q_i-1} \mathcal{T}_{n+1} \mathcal{T}_{q_i-n} \right) \prod_{j \neq i} \mathcal{T}_{q_j}^{r_j} \right\rangle \\
 & + (2 - \beta) \sum_i \left\langle [q_i(q_i - 1) r_i \mathcal{T}_{q_i}^{r_i} - q_i^2 r_i \mathcal{T}_{q_i}^{r_i-1} \mathcal{T}_{q_i+1}] \prod_{j \neq i} \mathcal{T}_{q_j}^{r_j} \right\rangle \\
 & + \sum_i \left\langle 2q_i^2 r_i (r_i - 1) \mathcal{T}_{q_i}^{r_i-2} (\mathcal{T}_{2q_i} - \mathcal{T}_{2q_i+1}) \prod_{j \neq i} \mathcal{T}_{q_j}^{r_j} \right\rangle \\
 & + \sum_{i < j} \left\langle 4q_i q_j r_i r_j \mathcal{T}_{q_i}^{r_i-1} \mathcal{T}_{q_j}^{r_j-1} (\mathcal{T}_{q_i+q_j} - \mathcal{T}_{q_i+q_j+1}) \prod_{k \neq i, j} \mathcal{T}_{q_k}^{r_k} \right\rangle, \quad (2.25)
 \end{aligned}$$

where $\sum_{n=a}^b \equiv 0$ if $a > b$. Equation (2.10) is a special case of Eq. (2.25). The moments required for the average and the variance of the shot-noise power are $\langle \mathcal{T} \rangle$, $\langle \mathcal{T}_2 \rangle$, $\langle \mathcal{T}^2 \rangle$, $\langle \mathcal{T} \mathcal{T}_2 \rangle$, and $\langle \mathcal{T}_2^2 \rangle$, as can be seen from Eqs. (2.7) and (2.8). However, their evolution equations are not exactly solvable, because these cannot be written in a closed form. Mello and Stone [15, 16] have developed a method of solution by expanding the moments in descending powers of N . Here, their general method is applied to the moments listed above. For this purpose the following expansions are necessary:

$$\langle \mathcal{T}^p \rangle = N^p f_{p,0}(s) + N^{p-1} f_{p,1}(s) + N^{p-2} f_{p,2}(s) + \dots, \quad (2.26a)$$

$$\langle \mathcal{T}^p \mathcal{T}_2 \rangle = N^{p+1} g_{p+1,0}(s) + N^p g_{p+1,1}(s) + N^{p-1} g_{p+1,2}(s) + \dots, \quad (2.26b)$$

$$\langle \mathcal{T}^p \mathcal{T}_3 \rangle = N^{p+1} h_{p+1,0}(s) + N^p h_{p+1,1}(s) + \dots, \quad (2.26c)$$

$$\langle \mathcal{T}^p \mathcal{T}_4 \rangle = N^{p+1} i_{p+1,0}(s) + \dots, \quad (2.26d)$$

$$\langle \mathcal{T}^p \mathcal{T}_5 \rangle = N^{p+1} j_{p+1,0}(s) + \dots, \quad (2.26e)$$

$$\langle \mathcal{T}^p \mathcal{T}_2^2 \rangle = N^{p+2} l_{p+2,0}(s) + N^{p+1} l_{p+2,1}(s) + N^p l_{p+2,2}(s) + \dots, \quad (2.26f)$$

$$\langle \mathcal{T}^p \mathcal{T}_2 \mathcal{T}_3 \rangle = N^{p+2} m_{p+2,0}(s) + N^{p+1} m_{p+2,1}(s) + \dots, \quad (2.26g)$$

$$\langle \mathcal{T}^p \mathcal{T}_2^2 \mathcal{T}_4 \rangle = N^{p+2} n_{p+2,0}(s) + \dots, \quad (2.26h)$$

$$\langle \mathcal{T}^p \mathcal{T}_3^2 \rangle = N^{p+2} o_{p+2,0}(s) + \dots, \quad (2.26i)$$

$$\langle \mathcal{T}^p \mathcal{T}_2^3 \rangle = N^{p+3} t_{p+3,0}(s) + N^{p+2} t_{p+3,1}(s) + \dots, \quad (2.26j)$$

$$\langle \mathcal{T}^p \mathcal{T}_2^4 \rangle = N^{p+4} u_{p+4,0}(s) + \dots, \quad (2.26k)$$

$$\langle T^p T_2^2 T_3 \rangle = N^{p+3} v_{p+4,0}(s) + \dots \quad (2.26l)$$

The dependence of the coefficients of the powers of N on the symmetry parameter β is not explicitly mentioned. In this notation the expressions for the average (2.7) and the variance (2.8) of the shot noise can be obtained from

$$\begin{aligned} \langle T - T_2 \rangle &= [f_{1,0}(s) - g_{1,0}(s)]N + [f_{1,1}(s) - g_{1,1}(s)] \\ &\quad + [f_{1,2}(s) - g_{1,2}(s)]N^{-1} + \dots, \end{aligned} \quad (2.27a)$$

$$\begin{aligned} \langle T^2 \rangle - \langle T \rangle^2 &= [f_{2,0}(s) - f_{1,0}(s)^2]N^2 \\ &\quad + [f_{2,1}(s) - 2f_{1,0}(s)f_{1,1}(s)]N \\ &\quad + [f_{2,2}(s) - 2f_{1,0}(s)f_{1,2}(s) - f_{1,1}(s)^2] + \dots, \end{aligned} \quad (2.27b)$$

$$\begin{aligned} \langle T T_2 \rangle - \langle T \rangle \langle T_2 \rangle &= [g_{2,0}(s) - f_{1,0}(s)g_{1,0}(s)]N^2 \\ &\quad + [g_{2,1}(s) - f_{1,0}(s)g_{1,1}(s) - f_{1,1}(s)g_{1,0}(s)]N \\ &\quad + [g_{2,2}(s) - f_{1,0}(s)g_{1,2}(s) - f_{1,1}(s)g_{1,1}(s) \\ &\quad - f_{1,2}(s)g_{1,0}(s)] + \dots, \end{aligned} \quad (2.27c)$$

$$\begin{aligned} \langle T_2^2 \rangle - \langle T_2 \rangle^2 &= [l_{2,0}(s) - g_{1,0}(s)^2]N^2 \\ &\quad + [l_{2,1}(s) - 2g_{1,0}(s)g_{1,1}(s)]N \\ &\quad + [l_{2,2}(s) - 2g_{1,0}(s)g_{1,2}(s) - g_{1,1}(s)^2] + \dots \end{aligned} \quad (2.27d)$$

In order to determine the functions of s listed above, the evolution equations of the moments of interest are set up from the generalized evolution equation (2.25). One then finds that indeed all the moments of Eqs. (2.26a)–(2.26l) appear. Filling in the expansions and equating the coefficients of the same powers of N leads to a closed hierarchy of recurrent differential equations:

$$f'_{p,0}(s) + p f_{p+1,0}(s) = 0, \quad (2.28a)$$

$$g'_{p,0}(s) + (p+3)g_{p+1,0}(s) = 2f_{p+1,0}(s), \quad (2.28b)$$

$$f'_{p,1}(s) + p f_{p+1,1}(s) = -\delta_{\beta 1} [f'_{p,0}(s) + p g_{p,0}(s)], \quad (2.28c)$$

$$l'_{p,0}(s) + (p+6)l_{p+1,0}(s) = 4g_{p+1,0}(s), \quad (2.28d)$$

$$h'_{p,0}(s) + (p+5)h_{p+1,0}(s) = 6g_{p+1,0}(s) - 3l_{p+1,0}(s), \quad (2.28e)$$

$$\begin{aligned} g'_{p,1}(s) + (p+3)g_{p+1,1}(s) &= 2f_{p+1,1}(s) \\ &\quad + \delta_{\beta 1} [-g'_{p,0}(s) + 2g_{p,0}(s) - 4h_{p,0}(s) - (p-1)l_{p,0}(s)], \end{aligned} \quad (2.28f)$$

$$\begin{aligned} f'_{p,2}(s) + p f_{p+1,2}(s) &= -\delta_{\beta 1} [f'_{p,1}(s) + p g_{p,1}(s)] \\ &\quad + (\delta_{\beta 1} + 1)p(p-1)[g_{p-1,0}(s) - h_{p-1,0}(s)], \end{aligned} \quad (2.28g)$$

$$t'_{p,0}(s) + (p+9)t_{p+1,0}(s) = 6l_{p+1,0}(s), \quad (2.28h)$$

$$\begin{aligned} m'_{p,0}(s) + (p+8)m_{p+1,0}(s) &= \\ &= 2h_{p+1,0}(s) + 6l_{p+1,0}(s) - 3t_{p+1,0}(s), \end{aligned} \quad (2.28i)$$

$$l'_{p,1}(s) + (p+6)l_{p+1,1}(s) = 4g_{p+1,1}(s) + \delta_{\beta 1}[-l'_{p,0}(s) + 4l_{p,0}(s) - 8m_{p,0}(s) - (p-2)t_{p,0}(s)], \quad (2.28j)$$

$$u'_{p,0}(s) + (p+12)u_{p+1,0}(s) = 8t_{p+1,0}(s), \quad (2.28k)$$

$$i'_{p,0}(s) + (p+7)i_{p+1,0}(s) = 8h_{p+1,0}(s) + 4l_{p+1,0}(s) - 8m_{p+1,0}(s), \quad (2.28l)$$

$$v'_{p,0}(s) + (p+11)v_{p+1,0}(s) = 4m_{p+1,0}(s) + 6t_{p+1,0}(s) - 3u_{p+1,0}(s), \quad (2.28m)$$

$$n'_{p,0}(s) + (p+10)n_{p+1,0}(s) = 2i_{p+1,0}(s) + 8m_{p+1,0}(s) + 4t_{p+1,0}(s) - 8v_{p+1,0}(s), \quad (2.28n)$$

$$o'_{p,0}(s) + (p+10)o_{p+1,0}(s) = 12m_{p+1,0}(s) - 6v_{p+1,0}(s), \quad (2.28o)$$

$$j'_{p,0}(s) + (p+9)j_{p+1,0}(s) = 10i_{p+1,0}(s) + 10m_{p+1,0}(s) - 10n_{p+1,0}(s) - 5o_{p+1,0}(s), \quad (2.28p)$$

$$t'_{p,1}(s) + (p+9)t_{p+1,1}(s) = 6l_{p+1,1}(s) + \delta_{\beta 1}[-t'_{p,0}(s) + 6t_{p,0}(s) - 12v_{p,0}(s) - (p-3)u_{p,0}(s)], \quad (2.28q)$$

$$h'_{p,1}(s) + (p+5)h_{p+1,1}(s) = 6g_{p+1,1}(s) - 3l_{p+1,1}(s) + \delta_{\beta 1}[-h'_{p,0}(s) + 6h_{p,0}(s) - 9i_{p,0}(s) - (p-1)m_{p,0}(s)], \quad (2.28r)$$

$$m'_{p,1}(s) + (p+8)m_{p+1,1}(s) = 2h_{p+1,1}(s) + 6l_{p+1,1}(s) - 3t_{p+1,1}(s) + \delta_{\beta 1}[-m'_{p,0}(s) + 8m_{p,0}(s) - 4o_{p,0}(s) - 9n_{p,0}(s) - (p-2)v_{p,0}(s)], \quad (2.28s)$$

$$g'_{p,2}(s) + (p+3)g_{p+1,2}(s) = 2f_{p+1,2}(s) + \delta_{\beta 1}[-g'_{p,1}(s) + 2g_{p,1}(s) - 4h_{p,1}(s) - (p-1)l_{p,1}(s)] + (\delta_{\beta 1} + 1)\{4(p-1)[h_{p-1,0}(s) - i_{p-1,0}(s)] + (p-1)(p-2)[l_{p-1,0}(s) - m_{p-1,0}(s)]\}, \quad (2.28t)$$

$$l'_{p,2}(s) + (p+6)l_{p+1,2}(s) = 4g_{p+1,2}(s) + \delta_{\beta 1}[-l'_{p,1}(s) + 4l_{p,1}(s) - 8m_{p,1}(s) - (p-2)t_{p,1}(s)] + (\delta_{\beta 1} + 1)\{8[i_{p-1,0}(s) - j_{p-1,0}(s)] + 8(p-2)[m_{p-1,0}(s) - n_{p-1,0}(s)] + (p-2)(p-3)[t_{p-1,0}(s) - v_{p-1,0}(s)]\}. \quad (2.28u)$$

The equations are written in such order that each one can be solved with the solutions of the preceding ones. From Eq. (2.24) the initial conditions are

$$x_{p,0}(0) = 1, \quad x_{p,1}(0) = 0, \quad x_{p,2}(0) = 0, \quad (2.29)$$

where x stands for each of the functions $f, g, h \dots v$.

The first seven recurrent differential equations (2.28a)-(2.28g) were solved by Mello and Stone [16] to determine the variance of the conductance. Guided

by their results, the following ansatz for the solutions is made

$$x_{p,\dots}(s) = \frac{\pi(s) + p\sigma(s) + p^2\rho(s)}{(1+s)^q}, \quad (2.30)$$

where $\pi(s)$, $\sigma(s)$, and $\rho(s)$ are functions in s not dependent on p . The ansatz (2.30) is then verified by substitution. In this way the recurrent differential equations (2.28a)–(2.28u) reduce, after an appropriate value for q is chosen, to ordinary differential equations in s for the functions $\pi(s)$, $\sigma(s)$, and $\rho(s)$ which are easily solved. The functions are found to be polynomials in s . Here, only the solutions needed for substitution in Eqs. (2.27a)–(2.27d) are presented:

$$f_{p,0}(s) = \frac{1}{(1+s)^p}, \quad (2.31a)$$

$$f_{p,1}(s) = \frac{-\delta_{\beta 1} p s^3}{3(1+s)^{p+2}}, \quad (2.31b)$$

$$f_{p,2}(s) = \frac{s^2 p}{90(1+s)^{p+4}} \{ \delta_{\beta 1} [(8p-4)s^4 + (18p+6)s^3 + (45p+15)s^2 + (60p-60)s + 45p-45] + [(3p-5)s^4 + (18p-30)s^3 + (45p-75)s^2 + (60p-90)s + 45p-45] \}, \quad (2.31c)$$

$$g_{p,0}(s) = \frac{2s^3 + 6s^2 + 6s + 3}{3(1+s)^{p+3}}, \quad (2.31d)$$

$$g_{p,1}(s) = \frac{-\delta_{\beta 1} s^3}{45(1+s)^{p+5}} [(10p+4)s^3 + (30p+24)s^2 + (30p+60)s + 15p+75], \quad (2.31e)$$

$$g_{p,2}(s) = \frac{s^2}{1890(1+s)^{p+7}} \{ \delta_{\beta 1} [(112p^2 + 40p - 32)s^7 + (588p^2 + 612p - 120)s^6 + (1722p^2 + 2574p + 24)s^5 + (3654p^2 + 4326p + 924)s^4 + (5418p^2 + 2394p + 2772)s^3 + (5355p^2 + 315p + 5670)s^2 + (3150p^2 - 630p - 2520)s + 945p^2 + 945p - 1890] + [(42p^2 - 30p - 72)s^7 + (378p^2 - 270p - 648)s^6 + (1512p^2 - 1080p - 2592)s^5 + (3549p^2 - 2457p - 5964)s^4 + (5418p^2 - 3402p - 8568)s^3 + (5355p^2 - 2835p - 8190)s^2 + (3150p^2 - 1260p - 5670)s + 945p^2 + 945p - 1890] \}, \quad (2.31f)$$

$$l_{p,0}(s) = \frac{1}{9(1+s)^{p+6}} (4s^6 + 24s^5 + 60s^4 + 84s^3 + 72s^2 + 36s + 9),$$

(2.31g)

$$l_{p,1}(s) = \frac{-\delta_{\beta_1} s^3}{135(1+s)^{p+8}} [(20p+16)s^6 + (120p+144)s^5 + (300p+576)s^4 + (420p+1332)s^3 + (360p+1764)s^2 + (180p+1260)s + 45p+450], \quad (2.31h)$$

$$l_{p,2}(s) = \frac{s^2}{28350(1+s)^{p+10}} \{ \delta_{\beta_1} [(1120p^2 + 1360p + 4)s^{10} + (9240p^2 + 17160p + 3408)s^9 + (38220p^2 + 91860p + 33864)s^8 + (107520p^2 + 273840p + 152480)s^7 + (224280p^2 + 497880p + 413820)s^6 + (351540p^2 + 596340p + 780120)s^5 + (409500p^2 + 506520p + 917280)s^4 + (345870p^2 + 334530p + 517860)s^3 + (203175p^2 + 212625p + 66150)s^2 + (75600p^2 + 113400p - 151200)s + 14175p^2 + 42525p - 28350] + [(420p^2 + 100p - 1020)s^{10} + (5040p^2 + 1200p - 12240)s^9 + (27720p^2 + 6600p - 67320)s^8 + (92820p^2 + 22260p - 223840)s^7 + (211680p^2 + 51840p - 499860)s^6 + (345240p^2 + 88560p - 795240)s^5 + (407925p^2 + 114345p - 943110)s^4 + (345870p^2 + 134190p - 842940)s^3 + (203175p^2 + 146475p - 538650)s^2 + (75600p^2 + 103950p - 245700)s + 14175p^2 + 42525p - 28350] \}. \quad (2.31i)$$

The solutions (2.31a)–(2.31e) and (2.31g) have already been found by Mello and Stone [16]. We have checked by computer algebra that the complete set of solutions indeed satisfies the set of recurrent differential equations (2.28a)–(2.28u) and the initial conditions (2.29).

Using the solutions (2.31a)–(2.31f) one then obtains for Eq. (2.27a)

$$\begin{aligned} \langle T - T_2 \rangle = & \frac{s(s^2 + 3s + 3)}{3(1+s)^4} N - \frac{\delta_{\beta 1} s^3 (s^3 - 9s^2 + \dots)}{45(1+s)^6} \\ & - \frac{(2\delta_{\beta 1} - 1)s^3 (3s^6 + 27s^5 + \dots)}{315(1+s)^8} N^{-1} + \dots \end{aligned} \quad (2.32)$$

Equation (2.11) follows from Eq. (2.32) by omitting terms of order Ns^{-2} , s^{-1} , and sN^{-1} , while retaining terms of order Ns^{-1} and 1. This is a consistent approximation if $N^{1/2} \ll s \ll N$, which is a stronger condition than Eq. (2.5). As discussed in Ref. [16] this condition implies the quasi-one-dimensionality (length \gg width) of the conductor. The variance can be calculated by filling in the solutions (2.31a)–(2.31i) in Eqs. (2.27b)–(2.27d). The terms of order N^2 and N vanish and the remaining term is

$$\text{var}(T - T_2) = \frac{(1 + \delta_{\beta 1})s^2(23s^{10} + 276s^9 + 1518s^8 + \dots)}{2835(1+s)^{12}} + \dots \quad (2.33)$$

Taking the limit of a long system ($s \gg 1$) results in Eq. (2.14).

References

- [1] See, for example: R. Landauer and Th. Martin, *Physica B* **175**, 167 (1991); M. Büttiker, *ibid.* **175**, 199 (1991); and references therein.
- [2] A. van der Ziel, *Noise: Sources, Characterization, Measurement* (Prentice Hall, New Jersey, 1970).
- [3] C. W. J. Beenakker and M. Büttiker, *Phys. Rev. B* **46**, 1889 (1992).
- [4] A review of mesoscopic fluctuation phenomena is: *Mesoscopic Phenomena in Solids*, edited by B. L. Altshuler, P. A. Lee, and R. A. Webb (North-Holland, Amsterdam, 1991).
- [5] B. L. Altshuler, *Pis'ma Zh. Eksp. Teor. Fiz.* **41**, 530 (1985) [*JETP Lett.* **41**, 648 (1985)].
- [6] P. A. Lee and A. D. Stone, *Phys. Rev. Lett.* **55**, 1622 (1985).
- [7] M. Büttiker, *Phys. Rev. Lett.* **65**, 2901 (1990).
- [8] V. A. Khlus, *Zh. Eksp. Teor. Fiz.* **93**, 2179 (1987) [*Sov. Phys. JETP* **66**, 1243 (1987)].
- [9] G. B. Lesovik, *Pis'ma Zh. Eksp. Teor. Fiz.* **49**, 513 (1989) [*JETP Lett.* **49**, 592 (1989)].
- [10] B. Yurke and G. P. Kochanski, *Phys. Rev. B* **41**, 8184 (1990).
- [11] Y. Imry, *Europhys. Lett.* **1**, 249 (1986).
- [12] K. A. Muttalib, J.-L. Pichard, and A. D. Stone, *Phys. Rev. Lett.* **59**, 2475 (1987).
- [13] O. N. Dorokhov, *Pis'ma Zh. Eksp. Teor. Fiz.* **36**, 259 (1982) [*JETP Lett.* **36**, 318 (1982)].
- [14] P. A. Mello, P. Pereyra, and N. Kumar, *Ann. Phys.* **181**, 290 (1988).
- [15] P. A. Mello, *Phys. Rev. Lett.* **60**, 1089 (1988).
- [16] P. A. Mello and A. D. Stone, *Phys. Rev. B* **44**, 3559 (1991).
- [17] A. D. Stone, P. A. Mello, K. A. Muttalib, and J.-L. Pichard, in Ref. [4].
- [18] P. A. Lee, A. D. Stone, and H. Fukuyama, *Phys. Rev. B* **35**, 1039 (1987); C. W. J. Beenakker and H. van Houten, *Solid State Phys.* **44**, 1 (1991).

Chapter 3

Doubled shot noise in disordered normal-metal–superconductor junctions

Electrical shot noise is the time-dependent fluctuation of the current around the average I , due to the discreteness of the charge carriers. The shot-noise power P gives information on the conduction process which is not contained in the resistance. A well-known example is a vacuum diode, where $P = 2e|I| \equiv P_{\text{Poisson}}$. This tells us that the electrons traverse the diode in completely uncorrelated fashion, as in a Poisson process. A noise power of P_{Poisson} is the maximum value in the normal state (N). In macroscopic samples shot noise is fully suppressed due to inelastic processes. For samples of dimensions smaller than the inelastic scattering length shot noise is observable, but may be suppressed below P_{Poisson} due to correlated electron transmission [1]. In this Chapter we investigate theoretically the enhancement of shot noise at zero temperature in disordered normal-metal–superconductor (NS) junctions. Naively, one would expect $P = 4e|I| = 2P_{\text{Poisson}}$, since the current in the superconductor is carried by Cooper pairs in units of $2e$. Instead, we find $P = \frac{2}{3}P_{\text{Poisson}}$, due to noiseless open scattering channels. We also consider the more general case of a disordered region in series with a tunnel barrier. In the absence of disorder we recover previous results by Khlus [2]. As far as we know, no measurements of shot noise in NS junctions have been reported, yet. Independent work on the problem has been carried out by Muzykantskii and Khmel'nitskii [3]. We furthermore would like to mention recent work on shot noise in a normal-metal–superconductor–normal-metal junction [4].

We first review the results for phase-coherent transport in the normal state. The conductance at zero temperature and small applied voltage V is given by

the Landauer formula

$$G_N = G_0 \text{Tr} \, t t^\dagger = G_0 \sum_{n=1}^N T_n, \quad (3.1)$$

where $G_0 \equiv 2e^2/h$. The matrix product $t t^\dagger$ has eigenvalues T_n , $n = 1, 2, \dots, N$, with N the number of scattering channels at the Fermi energy E_F and t the transmission matrix. From current conservation it follows that $T_n \in [0, 1]$. A formula for the zero-frequency shot-noise power has been derived by Büttiker [5],

$$P_N = P_0 \text{Tr} \, t t^\dagger (1 - t t^\dagger) = P_0 \sum_{n=1}^N T_n (1 - T_n), \quad (3.2)$$

with $P_0 \equiv 2e|V|G_0$. Equation (3.2) is the multi-channel generalization of earlier single-channel formulas [2, 6]. It is a consequence of the Pauli principle that closed ($T_n = 0$) as well as open ($T_n = 1$) scattering channels do not fluctuate and therefore give no contribution to the shot noise.

In the case of a tunnel barrier, all transmission eigenvalues are small ($T_n \ll 1$, for all n), so that the quadratic terms in Eq. (3.2) can be neglected. Then it follows from comparison with Eq. (3.1) that $P_N = 2e|V|G_N = 2e|I| = P_{\text{Poisson}}$. In contrast, for a quantum point-contact $P_N \ll P_{\text{Poisson}}$. Since on the plateaus of quantized conductance all the T_n 's are either 0 or 1, the shot noise is expected to be only observable at the steps between the plateaus [6]. This is indeed confirmed in an experiment by Li *et al.* [7]. For a diffusive conductor of length L much longer than the elastic mean free path $\bar{\ell}$ it has been predicted that $P_N = \frac{1}{3}P_{\text{Poisson}}$, as a consequence of noiseless open scattering channels [8–11]. Recently, an experimental observation of suppressed shot noise in a disordered wire has been reported [12].

Now, let us turn to transport through an NS junction. The conducting properties have originally been described by Blonder, Tinkham, and Klapwijk [13], and more recently in Refs. [14–16]. If the applied voltage is smaller than the superconducting gap ($e|V| < \Delta$), the dissipative normal current is converted at the NS interface into dissipationless supercurrent, by means of Andreev reflection: Electrons in the normal metal are retro-reflected at the NS interface into holes, with the transfer of a Cooper pair to the superconducting condensate. The scattering geometry is illustrated in the inset to Fig. 3.1. Electrons and holes, incident from a reservoir via an ideal (impurity-free) lead, are scattered by an arbitrarily disordered, normal region in series with a superconductor. The applied voltage is taken to be small, and the temperature low, so that transmission of excitations into the superconductor is prohibited. All incident quasiparticles are therefore reflected back into the reservoir.

The calculation of the shot-noise power of the NS junction proceeds along the lines of Büttiker's method for normal-metal conductors [5]. In the present case the scattering states are solutions of the Bogoliubov-de Gennes equation [13–16], rather than of a single-particle Schrödinger equation. The current operator in the lead towards the NS junction is given by

$$\hat{I}(t) = \frac{e}{h} \sum_{\alpha, \beta} \int_0^{\infty} d\epsilon \int_0^{\infty} d\epsilon' I_{\alpha\beta}(\epsilon, \epsilon') \hat{a}_{\alpha}^{\dagger}(\epsilon) \hat{a}_{\beta}(\epsilon') e^{it(\epsilon - \epsilon')/\hbar}, \quad (3.3)$$

where $\hat{a}_{\alpha}^{\dagger}(\epsilon)$ [$\hat{a}_{\alpha}(\epsilon)$] is the creation (annihilation) operator of scattering state $\psi_{\alpha}(\epsilon)$, and $I_{\alpha\beta}(\epsilon, \epsilon')$ is the matrix element of the current operator between states $\psi_{\alpha}(\epsilon)$ and $\psi_{\beta}(\epsilon')$. The quasiparticle energy ϵ is measured with respect to E_F . In the lead, the state ψ_{α} consists of one incoming mode φ_{α}^{+} and several, reflected, outgoing modes φ_{β}^{-} ,

$$\psi_{\alpha}(\epsilon) = \varphi_{\alpha}^{+}(\epsilon) + \sum_{\beta} r_{\beta\alpha}(\epsilon) \varphi_{\beta}^{-}(\epsilon). \quad (3.4)$$

The indices α, β denote mode number (m) as well as whether it concerns electron [$\alpha = (m, e)$] or hole [$\alpha = (m, h)$] propagation. The modes $\varphi_{\alpha}^{+}, \varphi_{\alpha}^{-}$ are normalized to carry unit quasiparticle flux. The reflection amplitudes $r_{\beta\alpha}$ are contained in the unitary $2N \times 2N$ matrix R , which has the block form

$$R = \begin{pmatrix} r_{ee} & r_{eh} \\ r_{he} & r_{hh} \end{pmatrix}, \quad (3.5)$$

where e.g. the $N \times N$ submatrix r_{he} contains the reflection amplitudes from incoming electrons to reflected holes. The unitarity of the reflection matrix corresponds to conservation of the number of quasiparticles. The conductance of the NS junction is given by [15]

$$G_{\text{NS}} = 2G_0 \text{Tr} r_{he}^{\dagger} r_{he}. \quad (3.6)$$

In the zero-frequency limit we need the current-matrix elements $I_{\alpha\beta}(\epsilon, \epsilon)$ at equal energies. Following Ref. [5], we find

$$I_{\alpha\beta}(\epsilon, \epsilon) = [\Lambda - R^{\dagger}(\epsilon)\Lambda R(\epsilon)]_{\alpha\beta}. \quad (3.7)$$

The difference with Ref. [5] is the inclusion of the $2N \times 2N$ matrix Λ , defined by

$$\Lambda \equiv \begin{pmatrix} -1 & 0 \\ 0 & 1 \end{pmatrix}, \quad (3.8)$$

which accounts for the opposite charges of electrons and holes. The average current I can be determined from the expectation value of Eq. (3.3), using

$$\langle \hat{a}_\alpha^\dagger(\epsilon) \hat{a}_\beta(\epsilon') \rangle = \delta_{\alpha\beta} \delta(\epsilon - \epsilon') f_\alpha(\epsilon), \quad (3.9)$$

with $f_\alpha(\epsilon)$ the distribution function in the reservoir. At zero temperature and for $V < 0$ one has for the electron (f_e) and hole (f_h) distribution functions

$$f_e(\epsilon) = \Theta(e|V| - \epsilon), \quad f_h(\epsilon) = 0, \quad (3.10)$$

with $\Theta(x)$ the unit-step function. The conductance $G_{NS} \equiv \lim_{V \rightarrow 0} I/V$ can now easily be determined from Eqs. (3.3), (3.7), (3.9), and (3.10). This indeed provides the result Eq. (3.6) of Ref. [15], which serves as a check on the formalism.

We are now ready to compute the zero-frequency shot-noise power, defined by

$$P_{NS} \equiv 2 \int_{-\infty}^{\infty} dt \langle \Delta \hat{I}(t) \Delta \hat{I}(0) \rangle, \quad (3.11)$$

with $\Delta \hat{I}(t) \equiv \hat{I}(t) - I$. Substituting Eq. (3.3) and using Eq. (3.9) we find

$$P_{NS} = 2 \frac{e^2}{h} \int_0^\infty d\epsilon \sum_{\alpha, \beta} I_{\alpha\beta}(\epsilon, \epsilon) I_{\beta\alpha}(\epsilon, \epsilon) f_\alpha(\epsilon) [1 - f_\beta(\epsilon)]. \quad (3.12)$$

Equation (3.12) can be evaluated through Eqs. (3.7) and (3.10). In the zero-temperature, zero-voltage limit we find, making use of the unitarity of R ,

$$P_{NS} = 4P_0 \text{Tr} r_{he} r_{he}^\dagger (1 - r_{he} r_{he}^\dagger) = 4P_0 \sum_{n=1}^N \mathcal{R}_n (1 - \mathcal{R}_n), \quad (3.13)$$

where \mathcal{R}_n is an eigenvalue of $r_{he} r_{he}^\dagger$, evaluated at $\epsilon = 0$.

It remains to relate the Andreev-reflection eigenvalues \mathcal{R}_n to the scattering properties of the normal region. In the presence of time-reversal symmetry, i.e. in zero magnetic field, the eigenvalues \mathcal{R}_n can be expressed entirely in terms of the transmission eigenvalues T_n of the *normal* region [16] :

$$\mathcal{R}_n = T_n^2 (2 - T_n)^{-2}. \quad (3.14)$$

Equation (3.14) assumes a step function (at the NS interface) for the pair potential and neglects terms of order $(\Delta/E_F)^2$. Substitution into Eq. (3.6) yields the result of Ref. [16] for the conductance of the NS junction,

$$G_{NS} = G_0 \sum_{n=1}^N \frac{2T_n^2}{(2 - T_n)^2}. \quad (3.15)$$

We now apply the same method to our result (3.13) for the shot-noise power, and find

$$P_{\text{NS}} = P_0 \sum_{n=1}^N \frac{16T_n^2(1-T_n)}{(2-T_n)^4}. \quad (3.16)$$

This is our main result. It is a general formula for arbitrary disorder potential in the normal region. As in the normal state, scattering channels which have $T_n = 0$ or $T_n = 1$ do not contribute to the shot noise. However, the way in which partially transmitting channels contribute is entirely different from the normal state result (3.2). Before considering the case of a disordered conductor, we first briefly discuss the case of a planar tunneling barrier, which was previously studied by Khlus [2].

A planar tunnel barrier is modeled by a channel-independent barrier transparency: $T_n = \Gamma$, for all n . It follows from Eq. (3.2), that for a normal conductor this would yield $P_{\text{N}} = (1-\Gamma)P_{\text{Poisson}}$, implying full Poisson noise for a high barrier ($\Gamma \ll 1$). For the NS junction we find from Eqs. (3.15) and (3.16)

$$P_{\text{NS}} = P_0 N \frac{16\Gamma^2(1-\Gamma)}{(2-\Gamma)^4} = \frac{8(1-\Gamma)}{(2-\Gamma)^2} P_{\text{Poisson}}. \quad (3.17)$$

This agrees with the result of Khlus [2]*. If $\Gamma < 2(\sqrt{2}-1) \approx 0.83$, one observes a shot noise *above* the Poisson noise. For $\Gamma \ll 1$ one has

$$P_{\text{NS}} = 4e|I| = 2P_{\text{Poisson}}, \quad (3.18)$$

which is a *doubling* of the shot-noise power divided by the current with respect to the normal-state result. This can be interpreted as an uncorrelated current of $2e$ -charged particles.

We now turn to an NS junction with a disordered normal region, of length L much greater than the mean free path $\bar{\ell}$, but much smaller than the localization length, so that transport is in the metallic, diffusive regime. In Ref. [8] the average of the normal-state shot-noise power is computed. The method is applicable to any physical quantity of the form $\sum_n f(T_n)$ with $\lim_{T \rightarrow 0} f(T) = 0$. (Such a quantity is called a linear statistic on the transmission eigenvalues.) Our formula (3.16) for the shot noise in the NS junction is of this form. According to Ref. [8] one has the general formula

$$\left\langle \sum_{n=1}^N f(T_n) \right\rangle = \left\langle \sum_{n=1}^N T_n \right\rangle \int_0^{\infty} dx f(\cosh^{-2} x). \quad (3.19)$$

*To see this, one must evaluate Eq. (25a) of Ref. [2] for $eV \ll \Delta$. Note, that the first exponent 2 should be -2 .

Equation (3.19) is obtained from the relationship $T_n = \cosh^{-2}(L/\zeta_n)$ between the transmission eigenvalues and the channel-dependent localization lengths ζ_n , and from the fact that L/ζ is uniformly distributed between 0 and $L/\bar{\ell} \gg 1$. This uniform distribution is a general result of random-matrix theory [17], but has also been derived from a microscopic Green's function theory [11]. The ensemble-averaged shot-noise power is now easily calculated by application of Eq. (3.19) to Eqs. (3.15) and (3.16), with the result

$$\frac{\langle P_{\text{NS}} \rangle}{\langle G_{\text{NS}} \rangle} = \frac{2}{3} \frac{P_0}{G_0}, \quad (3.20)$$

hence

$$\langle P_{\text{NS}} \rangle = \frac{4}{3} e|I| = \frac{2}{3} P_{\text{Poisson}}. \quad (3.21)$$

Equation (3.21) is twice the result in the normal state, but still smaller than the Poisson noise. Corrections to (3.21) are of lower order in N and due to quantum-interference effects [10].

Finally, we discuss a normal region which contains a disordered part as well as a tunnel barrier. This is most relevant to experiments, because in practice the NS interface is almost never ideal, but has a transparency $\Gamma < 1$. However, the uniform distribution of L/ζ does not apply to such a system. In Refs. [11] and [18] the distribution of transmission eigenvalues of such a system is studied and an expression for $\langle G_{\text{NS}} \rangle$ as a function of $s \equiv L/\bar{\ell}$ and Γ is obtained. The shot-noise power can be derived in a similar fashion. Here we merely present the final expressions,

$$\langle G_{\text{NS}} \rangle = G_0 N \frac{2v'(\phi)}{2sv'(\phi) - 1}, \quad (3.22a)$$

$$\langle P_{\text{NS}} \rangle = P_0 N \left(\frac{4v'(\phi)}{3(2sv'(\phi) - 1)} - \frac{4sv''(\phi)^2}{(2sv'(\phi) - 1)^5} + \frac{2v'''(\phi)}{3(2sv'(\phi) - 1)^4} \right), \quad (3.22b)$$

with $v'(\phi)$, $v''(\phi)$, $v'''(\phi)$ the first, second, and third derivative of

$$v(\phi) \equiv \frac{\cos \phi}{2/\Gamma + \sin \phi - 1}. \quad (3.23)$$

The auxiliary variable $\phi \in (0, \pi/2)$ is the solution of

$$\phi = 2sv(\phi). \quad (3.24)$$

The result is given in Fig. 3.1, where $\langle P_{\text{NS}} \rangle / P_{\text{Poisson}}$ is plotted against $\Gamma L/\bar{\ell}$ for various Γ . Note, the crossover from the ballistic (3.17) to the diffusive

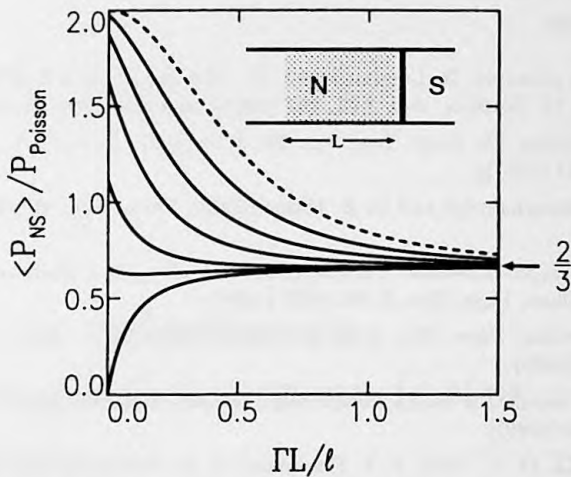


Figure 3.1: The shot-noise power of an NS junction (in units of $P_{\text{Poisson}} \equiv 2e|I|$) as a function of the length L (in units of ℓ/Γ), for barrier transparencies $\Gamma = 1, 0.9, 0.8, 0.6, 0.4, 0.2$ from bottom to top. The dashed curve gives the limiting result for $\Gamma \ll 1$. For $L = 0$ the noise power varies as a function of Γ according to Eq. (3.17), between doubled shot noise ($\langle P_{NS} \rangle = 4e|I|$) for high barriers ($\Gamma \ll 1$) and zero in the absence of a barrier ($\Gamma = 1$). If L increases the noise power approaches the limiting value $\langle P_{NS} \rangle = \frac{4}{3}e|I|$ for each Γ . The inset shows schematically the NS junction.

result (3.21). For a high barrier ($\Gamma \ll 1$), the shot noise decreases from twice the Poisson noise to two-thirds the Poisson noise as the amount of disorder increases.

In summary, we have presented a theory for the shot noise in normal-superconductor junctions for arbitrary normal region. The general result (3.16) can be applied to many mesoscopic systems. We predict that for a disordered normal region the shot noise is suppressed below the Poisson noise by a factor $\frac{2}{3}$, due to the presence of noiseless open scattering channels. This result is double the normal-state result, a consequence of the Cooper-pair transport in the superconductor. For a normal region consisting of a disordered part and a barrier (at the NS interface), the shot-noise power may vary between zero and a doubled Poisson noise, depending on the junction parameters. We feel that observation of our predictions is within reach of present technology and presents a challenge for experimentalists.

References

- [1] See, for example: R. Landauer and Th. Martin, *Physica B* **175**, 167 (1991); M. Büttiker, *ibid.* **175**, 199 (1991); and references therein.
- [2] V. A. Khlus, *Zh. Eksp. Teor. Fiz.* **93**, 2179 (1987) [*Sov. Phys. JETP* **66**, 1243 (1987)].
- [3] B. A. Muzykantskii and D. E. Khmel'nitskii, *Phys. Rev. B* **50**, 3982 (1994).
- [4] U. Hanke, M. Gissel'fält, Yu. Galperin, M. Jonson, R. I. Shekhter, and K. A. Chao, *Phys. Rev. B* **50**, 1953 (1994).
- [5] M. Büttiker, *Phys. Rev. Lett.* **65**, 2901 (1990); *Phys. Rev. B* **46**, 12485 (1992).
- [6] G. B. Lesovik, *Pis'ma Zh. Eksp. Teor. Fiz.* **49**, 513 (1989) [*JETP Lett.* **49**, 592 (1989)].
- [7] Y. P. Li, D. C. Tsui, J. J. Heremans, J. A. Simmons, and G. W. Weimann, *Appl. Phys. Lett.* **57**, 774 (1990).
- [8] C. W. J. Beenakker and M. Büttiker, *Phys. Rev. B* **46**, 1889 (1992).
- [9] K. E. Nagaev, *Phys. Lett. A* **169**, 103 (1992).
- [10] M. J. M. de Jong and C. W. J. Beenakker, *Phys. Rev. B* **46**, 13400 (1992) [Chapter 2].
- [11] Yu. V. Nazarov, *Phys. Rev. Lett.* **73**, 134 (1994).
- [12] F. Liefink, J. I. Dijkhuis, M. J. M. de Jong, L. W. Molenkamp, and H. van Houten, *Phys. Rev. B* **49**, 14066 (1994).
- [13] G. E. Blonder, M. Tinkham, and T. M. Klapwijk, *Phys. Rev. B* **25**, 4515 (1982).
- [14] C. J. Lambert, *J. Phys. Condens. Matter* **3**, 6579 (1991).
- [15] Y. Takane and H. Ebisawa, *J. Phys. Soc. Jpn.* **61**, 2858 (1992).
- [16] C. W. J. Beenakker, *Phys. Rev. B* **46**, 12841 (1992).
- [17] For a review, see: A. D. Stone, P. A. Mello, K. A. Muttalib, and J.-L. Pichard, in *Mesoscopic Phenomena in Solids*, edited by B. L. Altshuler, P. A. Lee, and R. A. Webb (North-Holland, Amsterdam, 1991).
- [18] C. W. J. Beenakker, B. Rejaei, and J. A. Melsen, *Phys. Rev. Lett.* **72**, 2470 (1994).

Chapter 4

Andreev reflection in ferromagnet–superconductor junctions

Electrons in a metal can not penetrate into a superconductor if their excitation energy with respect to the Fermi level is below the superconducting gap Δ . Still, a current may flow through a normal-metal–superconductor (NS) junction in response to a small applied voltage $V < \Delta/e$, by means of a scattering process known as Andreev reflection [1]: An electron in the normal metal is retro-reflected at the NS interface as a hole and a Cooper pair is carried away in the superconductor. Andreev reflection near the Fermi level conserves energy and momentum but does not conserve spin — in the sense that the incoming electron and the Andreev reflected hole occupy opposite spin bands. This is irrelevant for materials with spin-rotation symmetry, as is the case for normal metals. However, the change in spin band associated with Andreev reflection may cause an anomaly in the conductance of (metallic) ferromagnet–superconductor (FS) junctions, because the spin-up and the spin-down band in the ferromagnet are different. This Chapter contains a theoretical study of Andreev reflection in FS junctions. We use a scattering approach based on the Bogoliubov-de Gennes equation to study the transport properties for zero temperature and small V ($eV \ll \Delta$). We will concentrate on two distinct effects, which we think are experimentally observable. First, due to the change in spin band there is no complete Andreev reflection at the FS interface. This has a clear influence on the conductance and the shot-noise power of clean FS point contacts. Second, the different spin-up and spin-down wave vector at the Fermi level may lead to quantum-interference effects. This shows up in the linear-response conductance of FIFS junctions, where the

ferromagnet contains an insulating tunnel barrier (I).

In the past, FS junctions with an insulating layer between the ferromagnet and the superconductor have been used in spin-dependent tunneling experiments [2]. There the emphasis was on the voltage scale $eV \gtrsim \Delta$ and Andreev reflection did not play a role. Tunneling through S-Fi-S junctions, where Fi is a magnetic insulator, has been studied both experimentally [3] and theoretically [4, 5]. In addition, there has been theoretical work on the Josephson effect in SFS junctions [6, 7]. An experimental investigation of the boundary resistance of sputtered SFS sandwiches has also been reported [8]. The importance of phase coherence was demonstrated in a recent experiment [9], in which the effect of a remote superconducting island on the conductance of a ferromagnet was observed. We do not know of any previous theoretical work on the influence of Andreev reflection on the sub-gap conductance of an FS junction.

In order to clarify the effects we are aiming at, let us first give an intuitive and simple description of the conductance through a ballistic FS point contact. A ferromagnet is contacted through a small area with a superconductor. The transverse dimensions of the contact area are much smaller than the mean free path and the interface is clean, so that the conductance is completely determined by the scattering processes that are intrinsic to the FS interface. In a semiclassical approximation all scattering channels (transverse modes in the point contact at the Fermi level) are fully transmitted, when the superconductor is in the normal state. Let $N_{\uparrow}(N_{\downarrow})$ be the number of up(down)-spin channels, so that $N_{\uparrow} \geq N_{\downarrow}$. At zero temperature, the spin channels do not mix and the conductance is given by the Landauer formula

$$G_{FN} = \frac{e^2}{h} (N_{\downarrow} + N_{\uparrow}). \quad (4.1)$$

In the superconducting state, the spin-down electrons of all the N_{\downarrow} channels are Andreev reflected into spin-up holes. They give a double contribution to the conductance since $2e$ is transferred at each Andreev reflection. However, only a fraction $N_{\downarrow}/N_{\uparrow}$ of the N_{\uparrow} channels can be Andreev reflected, because the density of states in the spin-down band is smaller than in the spin-up band. Therefore, the resulting conductance is

$$G_{FS} = \frac{e^2}{h} (2N_{\downarrow} + 2\frac{N_{\downarrow}}{N_{\uparrow}}N_{\uparrow}) = 4\frac{e^2}{h} N_{\downarrow}. \quad (4.2)$$

Comparison of Eqs. (4.1) and (4.2) shows that G_{FS} may be either larger or smaller than G_{FN} depending on the ratio $N_{\downarrow}/N_{\uparrow}$. If $N_{\downarrow}/N_{\uparrow} < 1/3$ then $G_{FS} < G_{FN}$, and vice versa. This qualitative argument can be substantiated by an explicit calculation, as we now show.

For the conduction electrons inside the ferromagnet we apply the Stoner model, using an effective one-electron Hamiltonian with an exchange interaction. The effect of the ferromagnet on the superconductor is twofold. First, there is the influence of the exchange interaction on states near the interface. This will be fully taken into account. Second, there is the effect of the magnetic field due to the magnetization of the ferromagnet. Since this field — which is typically a factor thousand smaller than the exchange field — does not break spin-rotation symmetry it will be neglected for simplicity. Note that in typical layered structures the magnetization is parallel to the FS interface, so that it has no influence on the superconductor at all.

Transport through NS junctions has successfully been investigated through the Bogoliubov-de Gennes equation [10–13]. Here, we adopt this approach for an FS junction. In the absence of spin-flip scattering in the ferromagnet, the Bogoliubov-de Gennes equation breaks up into two independent matrix equations, one for the up-electron, down-hole quasiparticle wave function $(u_\uparrow, v_\downarrow)$ and another one for $(u_\downarrow, v_\uparrow)$. Each matrix equation has the form [14]

$$\begin{pmatrix} \mathcal{H}_0 - h & \Delta \\ \Delta^* & -(\mathcal{H}_0 + h) \end{pmatrix} \begin{pmatrix} u_\uparrow \\ v_\downarrow \end{pmatrix} = \epsilon \begin{pmatrix} u_\uparrow \\ v_\downarrow \end{pmatrix}. \quad (4.3)$$

Here, ϵ is the quasiparticle energy measured from the Fermi energy $E_F \equiv \hbar^2 k_F^2/2m$, $\mathcal{H}_0 \equiv \mathbf{p}^2/2m + V - E_F$ is the single-particle Hamiltonian, with $V(\mathbf{r})$ the potential energy, $h(\mathbf{r})$ is the exchange energy, and $\Delta(\mathbf{r})$ is the pair potential. For simplicity, it is assumed that the ferromagnet and the superconductor have identical \mathcal{H}_0 . For comparison with experiment, our model can easily be extended to include differences in effective mass and band bottom. We adopt the usual step-function model for the pair potential [10–13] and do the same for the exchange energy [6, 7]. Defining the FS interface at $x = 0$ with S at $x > 0$, we have $\Delta(\mathbf{r}) = \Delta\Theta(x)$ and $h(\mathbf{r}) = h_0\Theta(-x)$, with $\Theta(x)$ the unit step-function.

A scattering formula for the linear-response conductance of an NS junction is given by Takane and Ebisawa [12]. Application to the FS case is straightforward,

$$G_{\text{FS}} = 2 \frac{e^2}{h} \sum_{\sigma=\uparrow,\downarrow} \text{Tr} r_{h\bar{\sigma},e\sigma}^\dagger r_{h\bar{\sigma},e\sigma}, \quad (4.4)$$

where the matrix $r_{h\bar{\sigma},e\sigma}$ contains the reflection amplitudes from incoming electron modes with spin σ to outgoing hole modes with spin $\bar{\sigma}$ (opposite to σ) evaluated at the Fermi level ($\epsilon = 0$). We first consider a ballistic point contact. We assume that the dimensions of the contact are much greater than the Fermi wave length, as is appropriate for a metal, so that quantization effects can be neglected. The number N_\downarrow of minority spin modes in the point

contact (with area Ω) is $N_{\downarrow} = N_0(1 - h_0/E_F)$, with $N_0 \equiv k_F^2\Omega/4\pi$ the number of modes per spin for a non-ferromagnetic ($h_0 = 0$) contact of equal area. The reflection matrices for this case can be evaluated by matching the bulk solutions for the ferromagnet and for the superconductor at the interface. An incoming electron from the ferromagnet is either normally reflected as an electron of the same spin or Andreev reflected as a hole with the opposite spin. (Transmission into the superconductor is not possible at $\epsilon = 0$.) The reflection matrices are diagonal, with elements

$$r_{ee} \equiv r_{e\sigma, e\sigma} = r_{h\sigma, h\sigma} = \frac{k_{\uparrow}k_{\downarrow} - q^2}{k_{\uparrow}k_{\downarrow} + q^2}, \quad (4.5a)$$

$$r_{he} \equiv r_{h\bar{\sigma}, e\sigma} = r_{e\bar{\sigma}, h\sigma} = \frac{-2iq\sqrt{k_{\uparrow}k_{\downarrow}}}{k_{\uparrow}k_{\downarrow} + q^2}, \quad (4.5b)$$

where the longitudinal wave vectors $k_{\uparrow(\downarrow)}$ in the ferromagnet and q in the superconductor are defined in terms of the energy E_n of the n -th transverse mode by

$$q = \sqrt{(2m/\hbar^2)(E_F - E_n)}, \quad (4.6a)$$

$$k_{\uparrow} = \sqrt{(2m/\hbar^2)(E_F - E_n + h_0)}, \quad (4.6b)$$

$$k_{\downarrow} = \sqrt{(2m/\hbar^2)(E_F - E_n - h_0)}. \quad (4.6c)$$

In the above expressions terms of order Δ/E_F are neglected*. Note that $|r_{ee}|^2 + |r_{he}|^2 = 1$, as required from quasiparticle conservation. It follows from Eq. (4.5) that a clean FS junction does not exhibit complete Andreev reflection, in contrast to the NS case. This is due to the potential step the particle passes when being Andreev reflected to the opposite spin band.

Because of the large number of modes the trace in Eq. (4.4) can be replaced by an integration, which can be evaluated analytically. The result is

$$G_{FS} = 4 \frac{e^2}{h} N_0 \frac{4}{15\eta^4} [\sqrt{1 - \eta^2}(6 - 7\eta^2 + \eta^4) - 6 + 10\eta^2 - 4\eta^5], \quad (4.7)$$

where $\eta \equiv h_0/E_F$. The conductance is plotted in Fig. 4.1, and compared with the semiclassical estimate from Eq. (4.2), which turns out to be quite accurate. Since $N_{\uparrow} + N_{\downarrow} = 2N_0$ one has from Eq. (4.1) $G_{FN} > G_{FS}$ if $h_0 > 0.47E_F$, or equivalently $N_{\downarrow}/N_{\uparrow} < 0.36$.

*This is the Andreev approximation [1]. One can easily go beyond it by including terms of order Δ/E_F in Eqs. (4.5) and (4.6). We have checked that this has only a small influence on our final results. In fact, the larger h_0 , the more accurate is the Andreev approximation.

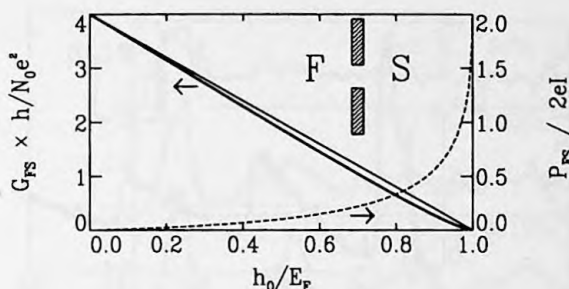


Figure 4.1: The conductance G_{FS} (full curves) and the shot-noise power P_{FS} (dashed) of a ballistic point contact in a ferromagnet–superconductor junction (see inset), as a function of the exchange energy h_0 . The thick line represents the exact result (4.7) for G_{FS} , the thin line the estimation (4.2).

Further information on the Andreev reflection at the FS interface can be obtained from the shot-noise power P of the junction. Shot noise is the time-dependent fluctuation in the current due to the discreteness of the charges. For uncorrelated electron transmission, one has the maximal noise power of a Poisson process $P_{\text{Poisson}} \equiv 2e|I|$, with I the mean current. On the one hand, correlations due to the Pauli principle reduce P below P_{Poisson} [15, 16]. On the other hand, Cooper-pair transport across an NS junction has been shown to manifest itself as a doubling of the maximal noise power [15, 17]. We apply the general result of Chapter 3 to the FS junction

$$P_{\text{FS}} = 8e|V| \frac{e^2}{h} \sum_{\sigma=\uparrow, \downarrow} \text{Tr} r_{h\bar{\sigma}, e\sigma}^\dagger r_{h\bar{\sigma}, e\sigma} (1 - r_{h\bar{\sigma}, e\sigma}^\dagger r_{h\bar{\sigma}, e\sigma}). \quad (4.8)$$

Substitution of Eq. (4.5b) into Eq. (4.8) yields the shot-noise power of a ballistic point contact, plotted in Fig. 4.1. The shot noise increases from complete suppression for a non-ferromagnetic ($h_0 = 0$) junction to twice the Poisson noise for a half-metallic ferromagnet ($h_0 = E_F$). The initial increase is slow, indicating that the N_1 modes undergo nearly complete Andreev reflection. However, for higher exchange energies the Andreev reflection probability decreases in favor of the normal reflection probability. This is manifested by the increase in the shot-noise power.

The second system we consider is an FIFS junction which contains a planar tunnel barrier (I) at $x = -L$. The barrier is modeled by a channel- and spin-independent transmission probability $\Gamma \in [0, 1]$. The matrix $r_{h\bar{\sigma}, e\sigma}^\dagger r_{h\bar{\sigma}, e\sigma}$ in Eq. (4.4) is diagonal, with elements

$$|r_{h\bar{\sigma}, e\sigma}|^2 = \Gamma^2 |r_{he}|^2 \left\{ 1 + 2\rho^2 \cos(\chi_\uparrow - \chi_\downarrow) + \rho^4 \right.$$

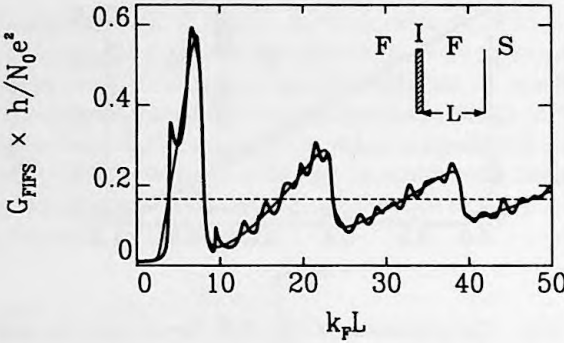


Figure 4.2: The conductance G_{FIFS} of a clean FIFS junction containing a planar tunnel barrier (transparency Γ) on the ferromagnetic side, as a function of the separation L from the interface (see inset). The thick solid line is computed from Eq. (4.9) for $\Gamma = 0.1$, $h_0 = 0.2E_F$. For the thin line normal reflection at the FS interface is neglected ($r_{ee} = 0$). The dashed line is the classical large- L limit.

$$\begin{aligned}
 &+ 2r_{ee}\rho(1 + \rho^2)(\cos \chi_{\uparrow} + \cos \chi_{\downarrow}) \\
 &+ 2r_{ee}^2\rho^2[1 + \cos(\chi_{\uparrow} + \chi_{\downarrow})] \}^{-1}, \quad (4.9)
 \end{aligned}$$

where $\rho \equiv \sqrt{1 - \Gamma}$ and $\chi_{\sigma} \equiv 2k_{\sigma}L$. Equation (4.9) describes resonant Andreev reflection: Due to the different wave vector of up electrons and down holes, $|r_{h\bar{\sigma},e\sigma}|^2$ varies as a function of χ_{\uparrow} and χ_{\downarrow} between Γ^2 , the value for a two-particle tunneling process, and 1 for full resonance. The conductance G_{FIFS} is evaluated by substitution of Eq. (4.9) into Eq. (4.4). It is depicted in Fig. 4.2 as a function of L for $h_0 = 0.2E_F$ and $\Gamma = 0.1$. The resonances have a dominant period $\delta L = \pi\hbar v_F/2h_0 (= 5\pi k_F^{-1}$ in Fig. 4.2), which is caused by the simplest round-trip containing two Andreev reflections and two barrier reflections. Superimposed one sees oscillations with smaller period, caused by longer trajectories in which also normal reflections at the FS interface occur. This becomes clear when we calculate G_{FS} with r_{ee} set to zero, which is also shown in Fig. 4.2. For large L , G_{FIFS} approaches the classical (i.e. all interferences are neglected) value $4(e^2/h)N_1\Gamma/(2 - \Gamma)$. The oscillations in Fig. 4.2 are distinct from the Tomasch oscillations known to occur in the *non-linear* differential conductance of NINS junctions [18]. There, quasi-bound states arise because electron and hole wave vectors disperse if $\epsilon > 0$. However, in linear response $G_{\text{NINS}} = 4(e^2/h)N_0\Gamma^2/(2 - \Gamma)^2$, independent of L [10]. In the ferromagnetic junction the resonances do not vanish in linear response, in contrast to the Tomasch oscillations. The quasi-bound states at the Fermi level are a direct consequence of the change in spin band upon Andreev reflection.

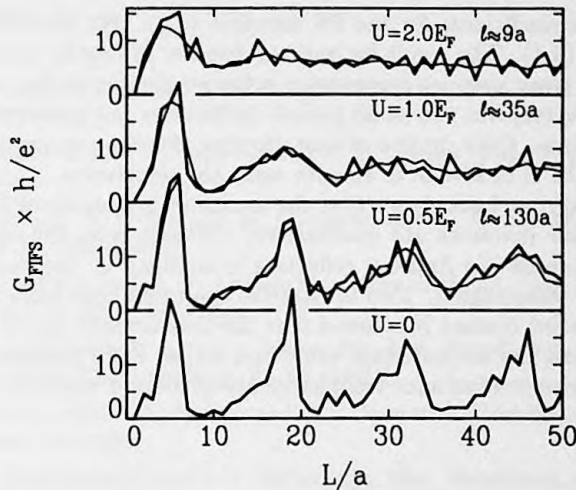


Figure 4.3: Numerical calculation of the effect of disorder in the ferromagnet on the oscillations shown in Fig. 4.2 for a clean junction. The disordered region is modeled by a $L \times W$ square lattice (lattice constant a) with random on-site disorder (uniformly distributed between $\pm U/2$). The width $W = 101a$ is fixed and the length L is varied on the horizontal axis. The results shown are for $E_F = \hbar^2/2ma^2$, $h_0 = 0.2E_F$, $\Gamma = 0.1$, and for various U . For each disorder strength U the bulk mean free path ℓ is given. Thick lines belong to one realization of disorder, thin to an average over 20 realizations.

We believe that both phenomena are experimentally accessible. The FS point contact can be constructed according to the nanofabrication technique of Ref. [19]. The FIFS junction can be made by growing a wedge-shaped layer of ferromagnet on a superconducting substrate and then depositing a thin oxide layer. This allows a measurement of G_{FIFS} for different values of L . It is not necessary for the contact area to be small, so that no nanofabrication techniques are needed. (Note, that in order to observe the resonances due to the quasi-bound states it is not essential that the contact on top of the barrier is a ferromagnet.) To estimate the effect of disorder (growth imperfections and impurities) on the resonances, we have numerically calculated G_{FIFS} for a disordered ferromagnet between the barrier and the FS interface. The computations are similar to the NS case treated in Ref. [20]. The disordered region is modeled by a tight-binding Hamiltonian on a square lattice with a random impurity potential at each site. (For computational efficiency the geometry is two-dimensional, but this makes no qualitative difference.) The matrix $r_{h\bar{\sigma},e\sigma}$ is obtained by combining the scattering matrix of the disordered region with

the reflection coefficients for the FS interface (4.5). We then calculate G_{FS} through Eq. (4.4). The result for various disorder strengths is shown in Fig. 4.3. For the clean case we recognize a behavior similar to Fig. 4.2. Adding some disorder removes the small-period oscillations but preserves the dominant oscillations. Only quite a strong disorder (for the top curve $k_F \times$ bulk mean free path $\simeq 9$) is able to smooth away the resonances.

In summary, we have shown that the transport properties of ferromagnet-superconductor junctions are qualitatively different from the non-ferromagnetic case, because the Andreev reflection is modified by the exchange interaction in the ferromagnet. Two illustrative examples have been given: For a ballistic FS point contact it is found that the conductance can be both larger or smaller than the normal-state value and for an FIFS junction containing a tunnel barrier conductance resonances are predicted to occur in linear response.

References

- [1] A. F. Andreev, Zh. Eksp. Teor. Fiz. **46**, 1823 (1964) [Sov. Phys. JETP **19**, 1228 (1964)].
- [2] A recent review is: R. Meservey and P. M. Tedrow, Phys. Rep. **238**, 173 (1994).
- [3] F. Stageberg, R. Cantor, A. M. Goldman, and G. B. Arnold, Phys. Rev. B **32**, 3292 (1985).
- [4] M. J. DeWeert and G. B. Arnold, Phys. Rev. Lett. **55**, 1522 (1985); Phys. Rev. B **39**, 11307 (1989).
- [5] S. V. Kuplevakhskii and I. I. Fal'ko, Fiz. Met. Metalloved. **71**, 68 (1991) [Phys. Met. Metallogr. **71**, 65 (1991)].
- [6] L. N. Bulaevskii, A. I. Buzdin, and S. V. Panjukov, Solid State Commun. **44**, 539 (1982).
- [7] S. V. Kuplevakhskii and I. I. Fal'ko, Fiz. Met. Metalloved. **62**, 13 (1986) [Phys. Met. Metallogr. **62**, 8 (1986)]; Pis'ma Zh. Eksp. Teor. Fiz. **52**, 957 (1990) [JETP Lett. **52**, 340 (1990)].
- [8] C. Fierz, S.-F. Lee, J. Bass, W. P. Pratt, Jr., and P. A. Schroeder, J. Phys. Condens. Matter **2**, 9701 (1990).
- [9] V. T. Petrashov, V. N. Antonov, S. V. Maksimov, and R. Sh. Shaikhaidarov, Pis'ma Zh. Eksp. Teor. Fiz. **59**, 523 (1994) [JETP Lett. **59**, 551 (1994)].
- [10] G. E. Blonder, M. Tinkham, and T. M. Klapwijk, Phys. Rev. B **25**, 4515 (1982).
- [11] C. J. Lambert, J. Phys. Condens. Matter **3**, 6579 (1991).
- [12] Y. Takane and H. Ebisawa, J. Phys. Soc. Jpn. **61**, 1685 (1992).
- [13] C. W. J. Beenakker, Phys. Rev. B **46**, 12841 (1992).
- [14] P. G. de Gennes, *Superconductivity of Metals and Alloys* (Benjamin, New York, 1966).
- [15] V. A. Khlus, Zh. Eksp. Teor. Fiz. **93**, 2179 (1987) [Sov. Phys. JETP **66**, 1243 (1987)].
- [16] G. B. Lesovik, Pis'ma Zh. Eksp. Teor. Fiz. **49**, 513 (1989) [JETP Lett. **49**, 592 (1989)]; M. Büttiker, Phys. Rev. Lett. **65**, 2901 (1990).
- [17] M. J. M. de Jong and C. W. J. Beenakker, Phys. Rev. B **49**, 16070 (1994) [Chapter 3].
- [18] W. J. Tomasch, Phys. Rev. Lett. **15**, 672 (1965); **16**, 16 (1966); W. L. McMillan and P. W. Anderson, Phys. Rev. Lett. **16**, 85 (1966); A. Hahn, Phys. Rev. B **31**, 2816 (1985).
- [19] P. A. M. Holweg, J. A. Kokkedee, J. Caro, A. H. Verbruggen, S.

Radelaar, A. G. M. Jansen, and P. Wyder, *Phys. Rev. Lett.* **67**, 2549 (1991).

- [20] I. K. Marmorkos, C. W. J. Beenakker, and R. A. Jalabert, *Phys. Rev. B* **48**, 2811 (1993).

Chapter 5

Transition from Sharvin to Drude resistance in high-mobility wires

5.1 Introduction

In 1891 Maxwell [1] computed the electrical resistance of a narrow and short constriction (or point contact) in a metal, in the *diffusive* transport regime in which the width W of the constriction is large compared to the mean free path ℓ . In 1965 Sharvin [2] calculated the resistance in the opposite regime $\ell \gg W$ of *ballistic* transport. Subsequently, Wexler [3] studied the intermediate regime $\ell \simeq W$, where the resistance crosses over from the Maxwell to the Sharvin result.

Interestingly, the transition between the ballistic and the diffusive transport regime still has been scarcely investigated for a wire, of length $L > W$. Only recently, Tarucha *et al.* [4] published measurements on the resistance of wires, of different lengths, defined in a high-mobility two-dimensional electron gas. Motivated by their paper, we present a theoretical study on the resistance of wires from the ballistic to the diffusive regime. The two-dimensional case, which applies to high-mobility wires, is considered extensively, whereafter the three-dimensional case is briefly dealt with. We assume elastic impurity scattering and specular boundary scattering, which is the relevant condition for the experiment. We restrict our investigation to semi-classical transport, and use a novel technique to evaluate the Landauer formula exactly in this limit. The main outcome is that the resistance of a wire is the sum of the Sharvin resistance and the diffusive Drude resistance multiplied by a factor which we compute numerically, and find to be of order unity. Our exact calculation shows that — somewhat unexpectedly — the naive procedure of summing the Sharvin and Drude resistances is correct within 2.5% (3.5% for the three-

dimensional case) over the range from $L \ll \ell$ to $L \gg \ell$. To illustrate the usefulness of our theory, we apply it to the experiment of Tarucha *et al.* [4] and find good agreement with no adjustable parameters. In addition, in Appendix 5A it is shown that our approach based on the Landauer formula is equivalent with the more conventional approach based on the Boltzmann equation. Finally, we like to mention two recent, related papers. Nieuwenhuizen and Luck [5] calculate the conductance of a diffusive slab from Milne's equation, and Bauer *et al.* [6] obtain results similar to ours by concatenation of scattering matrices.

5.2 Integro-differential equation for the transmission probability

We study transport of non-interacting electrons through a two-dimensional wire, of width W and length L (see inset of Fig. 5.1). The electrons are scattered specularly at the wire boundaries. The wire is made of material with an ideal circular Fermi surface and a mean free path ℓ for elastic and isotropic impurity scattering. The modeling of impurity scattering by one single parameter implies that our results will be averages over the ensemble of all possible impurity configurations. We assume low temperatures, and thus neglect inelastic electron-phonon and electron-electron scattering. A voltage V is applied over the wire, inducing a current I . In linear response, the zero-temperature conductance $G = I/V$ of the wire is given by the Landauer formula

$$G = G_0 \text{Tr} \, t t^\dagger, \quad (5.1)$$

with t the transmission matrix at the Fermi energy $E_F = \frac{1}{2} m v_F^2$ and $G_0 \equiv 2e^2/h$, the quantum unit of conductance in the case of spin degeneracy.

As mentioned in the Introduction, our interest is in the semi-classical regime, where quantum-interference effects may be neglected, but Fermi-Dirac statistics must be retained. Beenakker and Van Houten have shown [7] that the semi-classical approximation of the Landauer formula is able to give a good description of many transport phenomena observed experimentally at temperatures on the order of 1 K. For a hard-wall wire of width W the semi-classical limit of Eq. (5.1) is [7]

$$G = G_0 \frac{k_F W}{\pi} \int_0^W \frac{dy}{W} \int_{-\pi/2}^{\pi/2} \frac{d\varphi}{2} \cos \varphi T(0, y, \varphi) \quad (5.2a)$$

$$= G_0 \frac{k_F W}{\pi} \langle T \rangle. \quad (5.2b)$$

The transmission probability $T(0, y, \varphi)$ is the probability that an electron which is positioned in lead 1 at $(x, y) = (0, y)$ with velocity $\mathbf{v} = v_F(\cos \varphi, \sin \varphi)$ is transmitted into lead 2 (see inset of Fig. 5.1). Baranger *et al.* [8] have confirmed that Eq. (5.2) follows directly from Eq. (5.1) by using a Green function expression for the transmission amplitudes and then taking the semi-classical limit via a stationary-phase approximation.

Equation (5.2) is easily evaluated in two opposite regimes. Firstly, the ballistic regime $\ell \gg L$. Then $T(0, y, \varphi) = \langle T \rangle = 1$ and hence Eq. (5.2) reduces to the familiar two-dimensional Sharvin conductance

$$G_S = G_0 \frac{k_F W}{\pi}. \quad (5.3)$$

Secondly, the diffusive regime $\ell \ll L$. Then $\langle T \rangle = \pi \ell / 2L$ [9], so that Eq. (5.2b) becomes the Drude conductance

$$G_D = G_0 \frac{k_F \ell W}{2L}. \quad (5.4)$$

The purpose of this Chapter is to derive a formula which describes the transition from G_S to G_D when $\ell \simeq L$.

We first note that, because boundary scattering is specular, electrons starting with equal angle of incidence, but different transverse coordinates have the same transmission probability: $T(0, y, \varphi) = T(0, y', \varphi)$ for all y, y', φ . Furthermore, symmetry requires that $T(0, y, \varphi) = T(0, y, -\varphi)$. The average transmission probability $\langle T \rangle$ thus simplifies into

$$\langle T \rangle = \int_0^{\pi/2} d\varphi \cos \varphi T(0, \varphi), \quad (5.5)$$

where the irrelevant y -coordinate has been dropped. By integrating over all possible electron trajectories starting with incoming angle φ , $T(0, \varphi)$ can be determined. We now introduce $T(x, \varphi)$ with $x \in [0, L]$ and $\varphi \in [0, \pi]$ as the probability that an electron at position x in the wire with direction φ reaches lead 2. By definition, a mean free path ℓ implies that an electron traversing an infinitesimal distance $\Delta s = \Delta x / \cos \varphi$ has a scattering probability of $\Delta s / \ell$. If an electron is scattered at position x , it has a probability $\bar{T}(x)$ to reach lead 2. Since the scattering is isotropic, this conditional transmission probability is given by

$$\bar{T}(x) = \frac{1}{\pi} \int_0^{\pi} d\varphi T(x, \varphi). \quad (5.6)$$

An electron at position x with direction φ can be transmitted into lead 2 either after being scattered at x or by continuing in the direction φ . We thus find that for infinitesimal $\Delta x \geq 0$ the x -dependent transmission probability $T(x, \varphi)$ satisfies

$$T(x, \varphi) = \left(1 - \frac{\Delta x}{\ell \cos \varphi}\right) T(x + \Delta x, \varphi) + \frac{\Delta x}{\ell \cos \varphi} \bar{T}(x),$$

if $\varphi \in [0, \pi/2]$,

(5.7a)

$$T(x, \varphi) = \left(1 - \frac{\Delta x}{\ell |\cos \varphi|}\right) T(x - \Delta x, \varphi) + \frac{\Delta x}{\ell |\cos \varphi|} \bar{T}(x),$$

if $\varphi \in [\pi/2, \pi]$.

(5.7b)

Taken together, these two equations imply for all $\varphi \in [0, \pi]$ the integro-differential equation

$$\ell \cos \varphi \frac{\partial T(x, \varphi)}{\partial x} = T(x, \varphi) - \bar{T}(x). \quad (5.8)$$

At $x = 0$ and $x = L$ we have the boundary conditions

$$T(0, \varphi) = 0, \quad \text{if } \varphi \in [\pi/2, \pi], \quad (5.9a)$$

$$T(L, \varphi) = 1, \quad \text{if } \varphi \in [0, \pi/2]. \quad (5.9b)$$

Equations (5.8) and (5.9) are equivalent to the integral equation

$$T(x, \varphi) = \int_x^L \frac{dx'}{\ell \cos \varphi} e^{-(x'-x)/\ell \cos \varphi} \bar{T}(x') + e^{-(L-x)/\ell \cos \varphi},$$

if $\varphi \in [0, \pi/2]$,

(5.10a)

$$T(x, \varphi) = \int_0^x \frac{dx'}{\ell |\cos \varphi|} e^{-(x-x')/\ell |\cos \varphi|} \bar{T}(x'),$$

if $\varphi \in [\pi/2, \pi]$.

(5.10b)

Furthermore, from symmetry and from the fact that an electron exits the wire either through lead 1 or through lead 2, we deduce the sum rules

$$T(x, \varphi) + T(L - x, \pi - \varphi) = 1, \quad (5.11a)$$

$$\bar{T}(x) + \bar{T}(L - x) = 1. \quad (5.11b)$$

The integro-differential equation (5.8) [or the equivalent Eq. (5.10)] forms the basis of our calculation of the crossover from the ballistic to the diffusive regime. It is exact for isotropic impurity scattering and specular boundary scattering and can easily be solved numerically (as shown in the following Section). In Appendix 5A the exact relation between the transmission probability and the solution of the Boltzmann transport equation is derived.

5.3 Numerical solution

A closed expression for $\bar{T}(x)$ can be found by integrating Eq. (5.10) over ϕ . This leads to

$$\bar{T}(x) = \int_0^L dx' G(x, x') \bar{T}(x') + T_0(x), \quad (5.12)$$

with the definitions

$$G(x, x') = \frac{1}{\pi} \int_0^{\pi/2} \frac{d\varphi}{\ell \cos \varphi} e^{-|x-x'|/\ell \cos \varphi}, \quad (5.13)$$

$$T_0(x) = \frac{1}{\pi} \int_0^{\pi/2} d\varphi e^{-(L-x)/\ell \cos \varphi}. \quad (5.14)$$

Equation (5.12) is known as Milne's equation* [10], describing scattering of light through a diffusive medium. It is interesting to note that this similarity between electron and photon transport is due to the fact that in linear response the conductance is independent of the screening properties of the electron gas, as can be found in Appendix 5A. This justifies the use of the single-particle transmission approach.

An exact analytical solution of Eq. (5.13) is known for the case of an infinite system ($L = \infty$) [11]. Since our interest is in solutions for all possible ratios of ℓ/L we cannot make use of this method. Therefore we have computed $\bar{T}(x)$ by discretizing the x -values and numerically integrating Eqs. (5.13) and (5.14). Equation (5.12) then becomes a matrix equation which is easily solved. For good convergence, the size of the matrix is taken so large that the length of each discrete x -interval is at least an order of magnitude smaller than ℓ . Once $\bar{T}(x)$ is known, the transmission probability $T(x, \varphi)$ follows directly from Eq. (5.10). One further integration in Eq. (5.5) yields the average $\langle T \rangle$ and hence the conductance from Eq. (5.2b). Results for $\bar{T}(x)$ and G are plotted in Figs. 5.1 and 5.2a. Note that $\bar{T}(x)$ satisfies the sum rule (5.11b). Although it is difficult to see from Fig. 5.1, $\bar{T}(x)$ does not become linear in x for the diffusive regime. Deviations from linearity occur near the interfaces between the wire and the leads. Figure 5.2a also shows the interpolation formula

$$G_{\text{IP}}^{-1} = G_{\text{D}}^{-1} + G_{\text{S}}^{-1}, \quad (5.15)$$

*Actually, Milne's equation addresses the three-dimensional case.

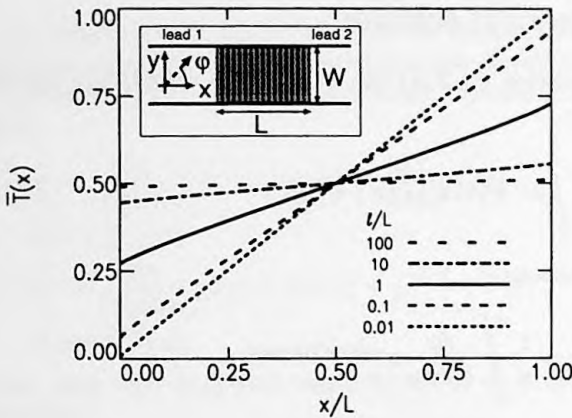


Figure 5.1: The conditional transmission probability $\bar{T}(x)$ as a function of the position along the wire, for various ℓ/L . The inset shows schematically the wire and its coordinates.

which approximates the resistance of the wire by the sum of the Sharvin and Drude resistances. It is remarkable how well the interpolation formula G_{IP} compares with the exact result G . In Fig. 5.2a the relative error $(G_{IP} - G)/G$ is also given. It is at most 2.5% when $\ell \simeq L$ and goes to zero for the ballistic as well as the diffusive limit.

By analogy with Wexler's result for a point contact [3], we write the exact solution in the form

$$G = G_0 \frac{k_F W}{\pi} \left[1 + \gamma_{2D} \frac{2L}{\pi \ell} \right]^{-1}, \quad (5.16)$$

where the dimensionless parameter γ_{2D} depends on the ratio ℓ/L as plotted in Fig. 5.2b. Its limiting values are in the ballistic limit

$$\lim_{\ell/L \rightarrow \infty} \gamma_{2D} = \frac{\pi^2}{8}, \quad (5.17)$$

and in the diffusive limit

$$\lim_{\ell/L \rightarrow 0} \gamma_{2D} = 1. \quad (5.18)$$

The diffusive limit follows from the condition $G \rightarrow G_D$ if $\ell/L \rightarrow 0$, with G_D given by Eq. (5.4). The ballistic limit is obtained by solving the integral equation (5.10) to first order in L/ℓ , which can be done analytically.

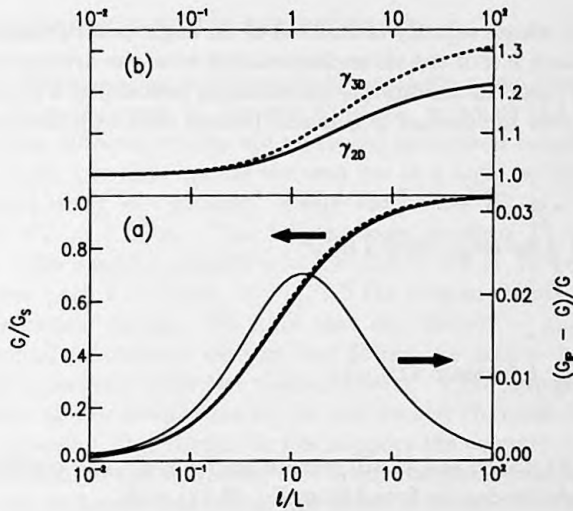


Figure 5.2: (a) The conductance [normalized by the Sharvin conductance (5.3)] plotted against the ratio l/L . The solid line is from the numerical solution of Eq. (5.12), the dotted line is G_{IP} according to the interpolation formula (5.15). The thin solid line shows the relative error of the interpolation formula. It remains below 2.5%. (b) The dependence on l/L of the factor γ_{2D} in Eq. (5.16) (solid line) and γ_{3D} in Eq. (5.24) (dotted line).

5.4 Three-dimensional wire

The previous Sections dealt with the two-dimensional case, which is relevant for the experiment [4]. The calculation for a three-dimensional wire is not very different and is briefly presented in this Section. In the semi-classical regime, the Landauer formula reads

$$G = G_0 \frac{k_F^2 S}{4\pi} \langle T \rangle, \quad (5.19)$$

where S is the cross-sectional area of the wire. (We assume that the wire has a constant cross section along the x -axis.) The Sharvin conductance G_S is given by Eq. (5.19) with $\langle T \rangle = 1$. From comparison with the Drude conductance it follows that in the diffusive regime $\langle T \rangle = 4\ell/3L$.

As in the two-dimensional case, we assume specular boundary scattering. Therefore, transverse coordinates are irrelevant. The transmission probability $T(x, \varphi)$ with $x \in [0, L]$ and $\varphi \in [0, \pi]$ gives the probability that an electron at

position x and whose velocity is directed at an angle φ with respect to the x -axis, reaches lead 2. For the three-dimensional wire, the average transmission probability $\langle T \rangle$ and the conditional transmission probability $\bar{T}(x)$ are obtained by averaging over the surface of a sphere (rather than over the circumference of a circle),

$$\langle T \rangle = 2 \int_0^{\pi/2} d\varphi \sin \varphi \cos \varphi T(0, \varphi), \quad (5.20)$$

$$\bar{T}(x) = \frac{1}{2} \int_0^{\pi} d\varphi \sin \varphi T(x, \varphi). \quad (5.21)$$

Equations (5.8), (5.9), and (5.10) remain unchanged. The conditional transmission probability can be found from Eq. (5.12) with

$$G(x, x') = \frac{1}{2} \int_0^{\pi/2} \frac{d\varphi}{\ell \cos \varphi} \sin \varphi e^{-|x-x'|/\ell \cos \varphi}, \quad (5.22)$$

$$T_0(x) = \frac{1}{2} \int_0^{\pi/2} d\varphi \sin \varphi e^{-(L-x)/\ell \cos \varphi}. \quad (5.23)$$

The results are similar to the two-dimensional case. A simple interpolation formula which adds the Sharvin and Drude resistances is within 3.5% different from the exact G . We write the exact solution as

$$G = G_0 \frac{k_F^2 S}{4\pi} \left[1 + \gamma_{3D} \frac{3L}{4\ell} \right]^{-1}. \quad (5.24)$$

The factor γ_{3D} is plotted against ℓ/L in Fig. 5.2b. Its limiting values are in the ballistic limit

$$\lim_{\ell/L \rightarrow \infty} \gamma_{3D} = \frac{4}{3}, \quad (5.25)$$

and in the diffusive limit

$$\lim_{\ell/L \rightarrow 0} \gamma_{3D} = 1. \quad (5.26)$$

5.5 Comparison with experiment

We conclude by comparing our theoretical result for a two-dimensional wire (5.16) with the experiment by Tarucha *et al.* [4], in which the resistances of wires with three different widths are measured for several lengths. The wires are defined in the two-dimensional electron gas in a high-mobility (Al,Ga)As heterostructure using wet etching. Their widths are $W_1 = 1.5 \mu\text{m}$, $W_2 = 3.5 \mu\text{m}$, and $W_3 = 7.5 \mu\text{m}$. The lengths vary between $L = 4.0 \mu\text{m}$ and $L = 60 \mu\text{m}$. The electron density $n = k_F^2/2\pi = 2.6 \times 10^{11} \text{cm}^{-2}$ and the bulk mean free path $\ell = 67 \mu\text{m}$. In Fig. 5.3 the measurements are compared with the theoretical curves. We note that our theory — in which simply the experimental parameters without any fitting are used — provides quite a reasonable agreement with the measurements. This agreement indicates that reflection at the boundaries of the wet-etched channels is indeed predominantly specular. Our results do not support the surmise of Ref. [4] that the mean free path in the narrowest wire is substantially enhanced above the bulk value due to lateral restriction (an effect attributed to the presence of one-dimensional subbands in the wire). It would be of interest to compare our theory with measurements further into the diffusive regime.

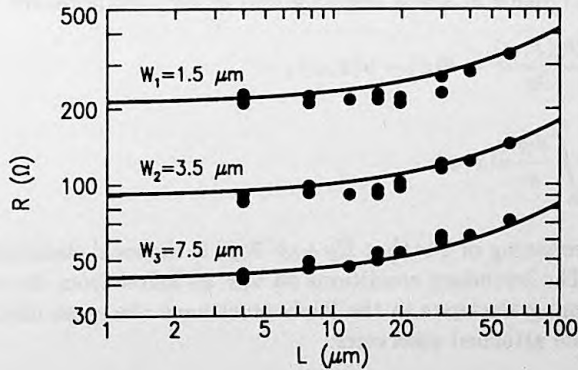


Figure 5.3: Comparison between the experimental resistance data of Tarucha *et al.* (Ref. [4]) (dots) and the results of our theory (curves). There are no adjustable parameters.

Appendix 5A Boltzmann approach

In this Appendix it is shown that the semi-classical transmission approach as described in the main text is equivalent with Boltzmann transport theory.

We investigate the wire of Section 5.2. The wire is connected via two perfect leads to two electron reservoirs, with electrochemical potentials $\mu_1 = E_F + eV$ and $\mu_2 = E_F$. The electrons inside the wire at the position $\mathbf{r} = (x, y)$ and with wave vector $\mathbf{k} = k(\cos \varphi, \sin \varphi)$ have the Boltzmann distribution function $f(\mathbf{r}, \mathbf{k})$. In the presence of an electric field $\mathbf{E}(\mathbf{r})$ the stationary Boltzmann equation reads

$$e\mathbf{E}(\mathbf{r}) \cdot \frac{\partial f(\mathbf{r}, \mathbf{k})}{\hbar \partial \mathbf{k}} + \mathbf{v} \cdot \frac{\partial f(\mathbf{r}, \mathbf{k})}{\partial \mathbf{r}} = -\frac{1}{\tau} f(\mathbf{r}, \mathbf{k}) + \int_0^{2\pi} \frac{d\varphi'}{2\pi\tau} f(\mathbf{r}, \mathbf{k}'), \quad (5.27)$$

where the r. h. s. is the impurity-scattering term (with scattering time τ). We assume translational invariance along the x -axis and retain only the relevant x, φ coordinates. Following Wexler [3], we introduce a new function u by

$$f(\mathbf{r}, \mathbf{k}) = f_0(\varepsilon) + e \left(\frac{\partial f_0}{\partial \varepsilon} \right) [\phi(x) - Vu(x, \varphi)], \quad (5.28)$$

where $f_0(\varepsilon) = \Theta(E_F - \varepsilon)$ is the Fermi-Dirac distribution function at energy $\varepsilon = \hbar^2 k^2 / 2m$ and $\phi(x)$ is the electrostatic potential. Substitution of Eq. (5.28) into Eq. (5.27) yields in linear response and at zero temperature

$$\ell \cos \varphi \frac{\partial u(x, \varphi)}{\partial x} = \bar{u}(x) - u(x, \varphi), \quad (5.29)$$

$$\bar{u}(x) = \int_0^\pi \frac{d\varphi}{\pi} u(x, \varphi). \quad (5.30)$$

The physical meaning of \bar{u} is that $E_F + eV \bar{u}(x)$ is the local electrochemical potential at x . The boundary conditions on $u(x, \varphi)$ follow from the requirement that the incoming electrons in the leads must have the same electrochemical potential as the attached reservoirs:

$$u(0, \varphi) = 1, \quad \text{if } \varphi \in [0, \pi/2], \quad (5.31a)$$

$$u(L, \varphi) = 0, \quad \text{if } \varphi \in [\pi/2, \pi]. \quad (5.31b)$$

The conductance is determined by calculating the current from Eq. (5.28) and dividing by the applied voltage. In terms of u one obtains

$$G = G_0 \frac{k_F W}{\pi} \int_0^\pi d\varphi \cos \varphi u(x, \varphi), \quad (5.32)$$

which is independent of x because of Eq. (5.29).

By comparing Eqs. (5.29), (5.31), and (5.32) with Eqs. (5.8), (5.9), and (5.5) of Section 5.2, we conclude that the semiclassical transmission approach is equivalent to the Boltzmann approach, upon the identification

$$u(x, \varphi) = 1 - T(x, \pi - \varphi). \quad (5.33)$$

This is a simple but instructive example of the equivalence between the Landauer formula and conventional transport theory: previously this equivalence has been derived for the full quantum mechanical case, starting from the Kubo formula [12]. (Of course, neither the derivation in Ref. [12] nor the present one do fully justice to the connection between the reservoirs and the leads [13].) Since the electrostatic potential $\phi(x)$ does not appear in Eq. (5.29), we conclude that the conductance is independent of the screening properties of the electron gas. This is a generic feature of linear response [9].

References

- [1] J. C. Maxwell, *A Treatise on Electricity and Magnetism* (Dover Press, New York, 1891).
- [2] Yu. V. Sharvin, Zh. Eksp. Teor. Fiz. **48**, 984 (1965) [Sov. Phys. JETP **21**, 655 (1965)].
- [3] G. Wexler, Proc. Phys. Soc. London **89**, 927 (1966).
- [4] S. Tarucha, T. Saku, Y. Tokura, and Y. Hirayama, Phys. Rev. B **47**, 4064 (1993).
- [5] Th. M. Nieuwenhuizen and J. M. Luck, Phys. Rev. E **48**, 569 (1993).
- [6] G. E. W. Bauer, A. Brataas, C. M. Schep, and P. J. Kelly, J. Appl. Phys. **75**, 6704 (1994); A. Brataas and G. E. W. Bauer, Phys. Rev. B **49**, 14684 (1994).
- [7] C. W. J. Beenakker and H. van Houten, Phys. Rev. Lett. **63**, 1857 (1989); in *Electronic Properties of Multilayers and Low-Dimensional Semiconductor Structures*, edited by J. M. Chamberlain, L. Eaves, and J. C. Portal (Plenum, New York, 1990).
- [8] H. U. Baranger, D. P. DiVincenzo, R. A. Jalabert, and A. D. Stone, Phys. Rev. B **44**, 10637 (1991).
- [9] C. W. J. Beenakker and H. van Houten, Solid State Phys. **44**, 1 (1991).
- [10] S. Chandrasekhar, *Radiative Transfer* (Oxford University Press, London, 1950).
- [11] See, for example, P. M. Morse and H. Feshbach, *Methods of Theoretical Physics I & II* (McGraw-Hill, New York, 1953).
- [12] D. S. Fisher and P. A. Lee, Phys. Rev. B **23**, 6851 (1981).
- [13] See, for example, R. Landauer, in *Analogies in Optics and Micro Electronics*, edited by W. van Haeringen and D. Lenstra (Kluwer, Dordrecht, 1990).

Chapter 6

Semiclassical theory of shot-noise suppression

6.1 Introduction

The discreteness of the electron charge causes time-dependent fluctuations in the electrical current, known as shot noise. These fluctuations are characterized by a white noise spectrum and persist down to zero temperature. The shot-noise power P contains information on the conduction process, which is not given by the resistance. A well-known example is a vacuum diode, where $P = 2e|\bar{I}| \equiv P_{\text{Poisson}}$, with \bar{I} the average current. This tells us that the electrons traverse the conductor in a completely uncorrelated fashion, as in a Poisson process. In macroscopic samples, the shot noise is averaged out to zero by inelastic scattering.

In the past few years, the shot noise has been investigated in mesoscopic conductors, smaller than the inelastic scattering length. Theoretical analysis shows that the shot noise can be suppressed below P_{Poisson} , due to correlations in the electron transmission imposed by the Pauli principle [1–5]. Most intriguingly, it has been found that $P = \frac{1}{3}P_{\text{Poisson}}$ in a metallic, diffusive conductor [6–10]. The factor one-third is universal in the sense that it is independent of the material, sample size, or degree of disorder, as long as the length L of the conductor is greater than the mean free path ℓ and shorter than the localization length. An observation of suppressed shot noise in a diffusive conductor has been reported [11]. In a quantum mechanical description [6], the suppression follows from the bimodal distribution of transmission eigenvalues [12]. Surprisingly, Nagaev [7] finds the same one-third suppression from a semiclassical approach, in which the Pauli principle is accounted for, but the motion of electrons is treated classically. This implies that phase co-

herence is not essential for the suppression. A similar conclusion is obtained in Ref. [13]. However, the relationship between the quantum mechanical and semiclassical theories remains unclear.

In this Chapter, we reinvestigate the semiclassical approach and present a detailed comparison with quantum mechanical calculations in the literature. In particular, we study how the shot noise crosses over from the ballistic to the diffusive regime. This complements the study of the crossover of the conductance in Chapter 5. We use the Boltzmann-Langevin equation [14, 15], which is a semiclassical kinetic equation for nonequilibrium fluctuations. This equation has previously been applied to shot noise by Kulik and Omel'yanchuk [16] for a ballistic point contact, and by Nagaev [7] for a diffusive conductor. Below we will demonstrate how the Boltzmann-Langevin equation can be applied to an arbitrary mesoscopic conductor. Our analysis corrects previous work by Beenakker and van Houten [17].

The outline of this Chapter is as follows: In Section 6.2 we discuss the Boltzmann-Langevin equation. It is demonstrated how the shot-noise power can be expressed in terms of semiclassical transmission probabilities. Impurity scattering is treated in Section 6.3. The shot-noise power increases from zero in the ballistic regime to $\frac{1}{3}P_{\text{Poisson}}$ in the diffusive regime. We consider both isotropic and nonisotropic impurity scattering, and both a two- and three-dimensional density of states. We also present a one-dimensional model, which can be solved analytically. Exact agreement is found with a previous quantum mechanical evaluation [8], in the limit of a conductance $\gg e^2/h$. Section 6.4 deals with barrier scattering. We consider tunneling through n planar barriers in series (tunnel probability Γ). For $n = 2$ and $\Gamma \ll 1$, we recover the results for a double-barrier junction of Refs. [18] and [19]. In the limit $n \rightarrow \infty$ the shot-noise power approaches $\frac{1}{3}P_{\text{Poisson}}$ independent of Γ . By taking the continuum limit, $n \rightarrow \infty$, $\Gamma \rightarrow 1$, at fixed $n(1 - \Gamma)$, we recover the one-dimensional model of Section 6.3. The case of a disordered region in series with a tunnel barrier concludes Section 6.4. In Section 6.5 we calculate the effects of inelastic scattering and of electron heating due to electron-electron scattering. Analogous to the work of Beenakker and Büttiker [6], this scattering is modeled by putting charge-conserving electron reservoirs between phase-coherent segments of the conductor. This allows us to model the effects of quasi-elastic scattering, electron heating, and inelastic scattering within a single theoretical framework. We conclude in Section 6.6.

Before proceeding with a description of the semiclassical approach, we briefly summarize the fully quantum mechanical theory. The zero-temperature, zero-frequency shot-noise power P of a phase-coherent conductor is related to

the transmission matrix t by the formula [2, 4]

$$P = P_0 \text{Tr} t t^\dagger (1 - t t^\dagger) = P_0 \sum_{n=1}^N T_n (1 - T_n), \quad (6.1)$$

where $P_0 \equiv 2e|V|G_0$, with V the applied voltage and $G_0 \equiv e^2/h$ the conductance quantum (we assume spinless electrons for simplicity of notation), $T_n \in [0, 1]$ an eigenvalue of $t t^\dagger$, and N the number of transverse modes at the Fermi energy E_F . The conductance is given by the Landauer formula

$$G = G_0 \text{Tr} t t^\dagger = G_0 \sum_{n=1}^N T_n. \quad (6.2)$$

One finds $P = 2e|V|G = P_{\text{Poisson}}$ if the conductor is such that all $T_n \ll 1$ (e.g., a high tunnel barrier). However, if some T_n are near 1 (open channels), then the shot noise is reduced below P_{Poisson} . In a metallic, diffusive conductor the T_n are either exponentially small or of order unity [12]. This bimodal distribution gives rise to the one-third suppression of the shot noise [6]. As we have demonstrated in Subsection 1.1.5, the universality of this bimodal distribution follows from very general requirements. It has been emphasized by Landauer [20], that Coulomb interactions may induce a further reduction of P . Here, we follow the quantum mechanical treatments in assuming noninteracting electrons, within the Boltzmann-Langevin approach. However, effects of electrostatic potential fluctuations are included in the theory of Section 6.5. We will briefly return to this issue in Section 6.6.

6.2 Boltzmann-Langevin equation

We now formulate the semiclassical kinetic theory [14, 15]. We consider a conductor with a d -dimensional density of states connected by ideal leads to two electron reservoirs (see Fig. 6.1). The reservoirs have a temperature T and a voltage difference V . The electrons in the left and the right reservoir are in equilibrium, with distribution function $f_L(\epsilon) = f_0(\epsilon - eV)$, $f_R(\epsilon) = f_0(\epsilon)$, respectively. Here f_0 is the Fermi-Dirac distribution

$$f_0(\epsilon) = \left[1 + \exp\left(\frac{\epsilon - E_F}{T}\right) \right]^{-1}. \quad (6.3)$$

The *fluctuating* distribution function $f(\mathbf{r}, \mathbf{k}, t)$ in the conductor equals $(2\pi)^d$ times the density of electrons with position \mathbf{r} , and wave vector \mathbf{k} , at time t . [The factor $(2\pi)^d$ is introduced so that f is the occupation number of a unit

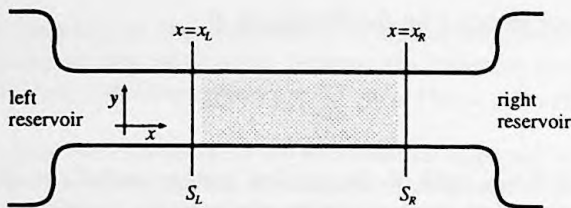


Figure 6.1: The conductor consists of a scattering region (shaded) connected by perfect leads to two electron reservoirs. Cross sections S_L and S_R in the left and right lead are indicated.

cell in phase space.] The average over time-dependent fluctuations $\langle f \rangle \equiv \bar{f}$ obeys the Boltzmann equation,

$$\left(\frac{d}{dt} + \mathcal{S} \right) \bar{f}(\mathbf{r}, \mathbf{k}, t) = 0, \quad (6.4a)$$

$$\frac{d}{dt} \equiv \frac{\partial}{\partial t} + \mathbf{v} \cdot \frac{\partial}{\partial \mathbf{r}} + \mathcal{F} \cdot \frac{\partial}{\hbar \partial \mathbf{k}}. \quad (6.4b)$$

The derivative (6.4b) (with $\mathbf{v} = \hbar \mathbf{k} / m$) describes the classical motion in the force field $\mathcal{F}(\mathbf{r}) = -e \partial \phi(\mathbf{r}) / \partial \mathbf{r} + e \mathbf{v} \times \mathbf{B}(\mathbf{r})$, with electrostatic potential $\phi(\mathbf{r})$ and magnetic field $\mathbf{B}(\mathbf{r})$. The term $\mathcal{S} \bar{f}$ accounts for the stochastic effects of scattering. Only elastic scattering is taken into account and electron-electron scattering is disregarded. In the case of impurity scattering, the scattering term in the Boltzmann equation (6.4) is given by

$$\begin{aligned} \mathcal{S} f(\mathbf{r}, \mathbf{k}, t) &= \int d\mathbf{k}' W_{\mathbf{k}\mathbf{k}'}(\mathbf{r}) \{ f(\mathbf{r}, \mathbf{k}, t) [1 - f(\mathbf{r}, \mathbf{k}', t)] \\ &\quad - f(\mathbf{r}, \mathbf{k}', t) [1 - f(\mathbf{r}, \mathbf{k}, t)] \} \\ &= \int d\mathbf{k}' W_{\mathbf{k}\mathbf{k}'}(\mathbf{r}) [f(\mathbf{r}, \mathbf{k}, t) - f(\mathbf{r}, \mathbf{k}', t)]. \end{aligned} \quad (6.5)$$

Here, $W_{\mathbf{k}\mathbf{k}'}(\mathbf{r})$ is the transition rate for scattering from \mathbf{k} to \mathbf{k}' , which may in principle also depend on \mathbf{r} . [We assume inversion symmetry, so that $W_{\mathbf{k}\mathbf{k}'}(\mathbf{r}) = W_{\mathbf{k}'\mathbf{k}}(\mathbf{r})$.]

We consider the stationary situation, where \bar{f} is independent of t . The time-dependent fluctuations $\delta f \equiv f - \bar{f}$ satisfy the Boltzmann-Langevin equation [14, 15],

$$\left(\frac{d}{dt} + \mathcal{S} \right) \delta f(\mathbf{r}, \mathbf{k}, t) = j(\mathbf{r}, \mathbf{k}, t), \quad (6.6)$$

where j is a fluctuating source term representing the fluctuations induced by the stochastic nature of the scattering. The flux j has zero average, $\langle j \rangle = 0$, and covariance

$$\langle j(\mathbf{r}, \mathbf{k}, t) j(\mathbf{r}', \mathbf{k}', t') \rangle = (2\pi)^d \delta(\mathbf{r} - \mathbf{r}') \delta(t - t') J(\mathbf{r}, \mathbf{k}, \mathbf{k}'). \quad (6.7)$$

The delta functions ensure that fluxes are only correlated if they are induced by the same scattering process. The flux correlator J depends on the type of scattering and on \bar{f} , but not on δf . The correlator J for the impurity-scattering term (6.5) has been derived by Kogan and Shul'man [15],

$$J(\mathbf{r}, \mathbf{k}, \mathbf{k}') = -W_{\mathbf{k}\mathbf{k}'}(\mathbf{r}) [\bar{f}(1 - \bar{f}') + \bar{f}'(1 - \bar{f})] \\ + \delta(\mathbf{k} - \mathbf{k}') \int d\mathbf{k}'' W_{\mathbf{k}\mathbf{k}''}(\mathbf{r}) [\bar{f}(1 - \bar{f}'') + \bar{f}''(1 - \bar{f})], \quad (6.8)$$

where $\bar{f} \equiv \bar{f}(\mathbf{r}, \mathbf{k})$, $\bar{f}' \equiv \bar{f}(\mathbf{r}, \mathbf{k}')$, and $\bar{f}'' \equiv \bar{f}(\mathbf{r}, \mathbf{k}'')$. One verifies that

$$\int d\mathbf{k} J(\mathbf{r}, \mathbf{k}, \mathbf{k}') = \int d\mathbf{k}' J(\mathbf{r}, \mathbf{k}, \mathbf{k}') = 0, \quad (6.9)$$

as it should, since the fluctuating source term conserves the number of particles [$\int d\mathbf{k} j(\mathbf{r}, \mathbf{k}, t) = 0$]. For the derivation of Eq. (6.8) we refer to Ref. [15]. In Section 6.4 we give a similar derivation for J in the case of barrier scattering.

Since j and j' are uncorrelated for $t > t'$, it follows from Eq. (6.6) that the correlation function $\langle \delta f \delta f' \rangle$ satisfies a Boltzmann equation in the variables $\mathbf{r}, \mathbf{k}, t$,

$$\left(\frac{d}{dt} + \mathcal{S} \right) \langle \delta f(\mathbf{r}, \mathbf{k}, t) \delta f(\mathbf{r}', \mathbf{k}', t') \rangle = 0. \quad (6.10)$$

Equation (6.10) forms the starting point of the method of moments of Gantsevich, Gurevich, and Katilius [21]. This method is very convenient to study equilibrium fluctuations, because the equal-time correlation is known,

$$\langle \delta f(\mathbf{r}, \mathbf{k}, t) \delta f(\mathbf{r}', \mathbf{k}', t) \rangle_{\text{equilibrium}} \\ = (2\pi)^d \bar{f}(\mathbf{r}, \mathbf{k}) [1 - \bar{f}(\mathbf{r}, \mathbf{k}')] \delta(\mathbf{k} - \mathbf{k}') \delta(\mathbf{r} - \mathbf{r}'), \quad (6.11)$$

and Eq. (6.10) can be used to compute the nonequal-time correlation. (For a recent study of thermal noise within this approach, see, for example, Ref. [22].) Out of equilibrium, Eq. (6.11) does not hold, except in the reservoirs, and one has to return to the full Boltzmann-Langevin equation (6.6) to determine the shot noise. In particular, it is only in equilibrium that the equal-time correlation $\langle \delta f \delta f' \rangle$ vanishes for $\mathbf{r} \neq \mathbf{r}'$, $\mathbf{k} \neq \mathbf{k}'$. Out of equilibrium, scattering correlates fluctuations δf at different momenta and different points in space.

To obtain the shot-noise power we compute the current $I(t) \equiv \bar{I} + \delta I(t)$ through a cross section S_R in the right lead. The average current \bar{I} and the fluctuations $\delta I(t)$ are given by

$$\bar{I} = \frac{e}{(2\pi)^d} \int_{S_R} dy \int dk v_x \bar{f}(\mathbf{r}, \mathbf{k}), \quad (6.12)$$

$$\delta I(t) = \frac{e}{(2\pi)^d} \int_{S_R} dy \int dk v_x \delta f(\mathbf{r}, \mathbf{k}, t). \quad (6.13)$$

We denote $\mathbf{r} = (x, y)$, with the x -coordinate along and y perpendicular to the wire (see Fig. 6.1). The zero-frequency noise power is defined as

$$P \equiv 2 \int_{-\infty}^{\infty} dt \langle \delta I(t) \delta I(0) \rangle. \quad (6.14)$$

The formal solution of Eq. (6.6) is

$$\delta f(\mathbf{r}, \mathbf{k}, t) = \int_{-\infty}^t dt' \int dr' \int dk' \mathcal{G}(\mathbf{r}, \mathbf{k}; \mathbf{r}', \mathbf{k}'; t - t') j(\mathbf{r}', \mathbf{k}', t'), \quad (6.15)$$

where the Green's function \mathcal{G} is a solution of

$$\left(\frac{d}{dt} + \mathcal{S} \right) \mathcal{G}(\mathbf{r}, \mathbf{k}; \mathbf{r}', \mathbf{k}'; t) = \delta(\mathbf{r} - \mathbf{r}') \delta(\mathbf{k} - \mathbf{k}') \delta(t), \quad (6.16)$$

such that $\mathcal{G} = 0$ if $t < 0$. The transmission probability $T(\mathbf{r}, \mathbf{k})$ is the probability that an electron at (\mathbf{r}, \mathbf{k}) leaves the wire through the right lead. It is related to \mathcal{G} by

$$T(\mathbf{r}, \mathbf{k}) = \int_0^{\infty} dt \int_{S_R} dy' \int dk' v'_x \mathcal{G}(\mathbf{r}', \mathbf{k}'; \mathbf{r}, \mathbf{k}; t). \quad (6.17)$$

Substitution of Eqs. (6.13) and (6.15) into Eq. (6.14) yield for the noise power the expression

$$P = \frac{2e^2}{(2\pi)^{2d}} \int_{S_R} dy \int dk v_x \int_{S_R} dy' \int dk' v'_x \\ \times \int_{-\infty}^t dt'' \int dr'' \int dk'' \mathcal{G}(\mathbf{r}, \mathbf{k}; \mathbf{r}'', \mathbf{k}''; t - t'')$$

$$\begin{aligned} & \times \int_{-\infty}^0 dt''' \int d\mathbf{r}''' \int d\mathbf{k}''' \mathcal{G}(\mathbf{r}', \mathbf{k}'; \mathbf{r}''', \mathbf{k}'''; -t''') \\ & \times \langle j(\mathbf{r}'', \mathbf{k}'', t'') j(\mathbf{r}''', \mathbf{k}''', t''') \rangle, \end{aligned} \quad (6.18)$$

which can be simplified using Eqs. (6.7) and (6.17)

$$P = \frac{2e^2}{(2\pi)^d} \int d\mathbf{r} \int d\mathbf{k} \int d\mathbf{k}' T(\mathbf{r}, \mathbf{k}) T(\mathbf{r}, \mathbf{k}') J(\mathbf{r}, \mathbf{k}, \mathbf{k}'). \quad (6.19)$$

Equation (6.19) applies generally to any conductor. It contains the noise due to the current fluctuations induced by the scattering processes inside the conductor. At non-zero temperatures, there is an additional source of noise from fluctuations which originate from the reservoirs. In Appendix 6A it is shown how this thermal noise can be incorporated. In what follows, we restrict to zero temperature.

A final remark concerns the x -coordinate of the cross section at which the current is evaluated [at $x = x_R$ in Eq. (6.13)]. From current conservation it follows that the zero-frequency noise power should not depend on the specific value of x . This is explicitly proven in Appendix 6B, as a check on the consistency of the formalism.

6.3 Impurity scattering

In this Section we specialize to elastic impurity scattering in a conductor made of a material with a spherical Fermi surface and in which the force field $\mathcal{F} = 0$ (so we do not consider the case that a magnetic field is present). The conductor has a length L and a constant width W ($d = 2$) or a constant cross-sectional area A ($d = 3$). (In general expressions, both W and A will be denoted by A .) We calculate the shot noise at zero temperature and small applied voltage, $eV \ll E_F$, so that we need to consider electrons at the Fermi energy only. The case of non-zero temperature is briefly discussed in Appendix 6A.

It is useful to change variables from wave vector \mathbf{k} to energy $\varepsilon = \hbar^2 k^2 / 2m$, and unit vector $\hat{\mathbf{n}} \equiv \mathbf{k}/k$. The integrations are modified accordingly,

$$\int \frac{d\mathbf{k}}{(2\pi)^d} \rightarrow \int d\varepsilon \mathcal{D}(\varepsilon) \int \frac{d\hat{\mathbf{n}}}{s_d}, \quad (6.20)$$

where $\mathcal{D}(\varepsilon) = s_d m (k/2\pi)^{d-2} \hbar^{-2}$ is the density of states, and s_d is the surface of a d -dimensional unit sphere ($s_1 = 2$, $s_2 = 2\pi$, $s_3 = 4\pi$). We consider the case of specular boundary scattering and assume that the elastic impurity-scattering rate $W_{\mathbf{k}\mathbf{k}'}(\mathbf{r}) \equiv W_{\hat{\mathbf{n}}\hat{\mathbf{n}}'} \delta(\varepsilon - \varepsilon') / \mathcal{D}(\varepsilon)$ is independent of \mathbf{r} . This allows us to drop the transverse coordinate \mathbf{y} and write $T(\mathbf{r}, \mathbf{k}) = T(x, \hat{\mathbf{n}})$ for

the transmission probability at the Fermi level. From Eqs. (6.16) and (6.17) we derive a Boltzmann equation for the transmission probability [23]

$$\begin{aligned} v_F n_x \frac{\partial T(x, \hat{n})}{\partial x} &= ST(x, \hat{n}), \\ &= \int \frac{d\hat{n}'}{s_d} W_{\hat{n}\hat{n}'} [T(x, \hat{n}) - T(x, \hat{n}')]. \end{aligned} \quad (6.21a)$$

The boundary conditions in the left and the right leads are

$$T(0, \hat{n}) = 0, \quad \text{if } n_x < 0, \quad (6.21b)$$

$$T(L, \hat{n}) = 1, \quad \text{if } n_x > 0, \quad (6.21c)$$

where $x_L = 0$ and $x_R = L$ are the x -coordinates of the left and right cross section S_L and S_R , respectively.

The average distribution function can be expressed as

$$\bar{f}(\mathbf{r}, \mathbf{k}) = [1 - T(\mathbf{r}, -\mathbf{k})]f_L(\varepsilon) + T(\mathbf{r}, -\mathbf{k})f_R(\varepsilon), \quad (6.22)$$

where (because of time-reversal symmetry in the absence of a magnetic field) $T(\mathbf{r}, -\mathbf{k})$ equals the probability that an electron at (\mathbf{r}, \mathbf{k}) has arrived there from the right reservoir. Combining Eqs. (6.12) and (6.22), we obtain the semiclassical Landauer formula for the linear-response conductance $G \equiv \lim_{V \rightarrow 0} \bar{I}/V$ [24]

$$\begin{aligned} G &= \frac{e^2}{(2\pi)^d} \int_{S_x} dy \int d\mathbf{k} \left(-\frac{\partial f_0(\varepsilon)}{\partial \varepsilon} \right) v_x T(\mathbf{r}, \mathbf{k}) \\ &= e^2 \int_{S_x} dy \int d\varepsilon \mathcal{D}(\varepsilon) \left(-\frac{\partial f_0(\varepsilon)}{\partial \varepsilon} \right) \int \frac{d\hat{n}}{s_d} v n_x T(x, \hat{n}) \\ &= G_0 N \int \frac{d\hat{n}}{v_{d-1}} n_x T(x, \hat{n}), \end{aligned} \quad (6.23)$$

with S_x the cross section at x . The number of transverse modes $N = v_{d-1}(k_F/2\pi)^{d-1}A$, where v_d is the volume of a d -dimensional unit sphere ($v_0 = 1$, $v_1 = 2$, $v_2 = \pi$). One has $N = k_F W/\pi$ for $d = 2$ and $N = k_F^2 A/4\pi$ for $d = 3$. One can verify that the conductance in Eq. (6.23) is independent of the value of x , as it should: By integrating Eq. (6.21a) over \hat{n} one finds that

$$\frac{\partial}{\partial x} \int d\hat{n} n_x T(x, \hat{n}) = 0. \quad (6.24)$$

We evaluate the noise power by substitution of Eqs. (6.8) and (6.22) into Eq. (6.19). Some intermediate steps are given in Appendix 6A. The resulting

zero-temperature shot-noise power is

$$P = \frac{P_0 N}{v_F s_d v_{d-1}} \int_0^L dx \int d\hat{n} \int d\hat{n}' W_{\hat{n}\hat{n}'} \times [T(x, \hat{n}) - T(x, \hat{n}')]^2 T(x, -\hat{n}) [1 - T(x, -\hat{n}')] . \quad (6.25)$$

This completes our general semiclassical theory. What remains is to compute the transmission probabilities from Eqs. (6.21) for a particular choice of the scattering rate W . Comparing Eqs. (6.2) and (6.23), we note that $\sum_n T_n$ corresponds semiclassically to $N \int d\hat{n} n_x T(x, \hat{n})$. Comparison of Eqs. (6.1) and (6.25) shows that the semiclassical correspondence to $\sum_n T_n (1 - T_n)$ is much more complicated, as it involves the transmission probabilities $T(x, \hat{n})$ at all scatterers inside the conductor [and not just the transmission probability $T(0, \hat{n})$ through the whole conductor].

In a ballistic conductor, where impurity scattering is absent, the transmission probabilities are given by $T(x, \hat{n}) = 1$, if $n_x > 0$, and $T(x, \hat{n}) = 0$, if $n_x < 0$. From Eq. (6.23), we then obtain the Sharvin conductance $G_S \equiv G_0 N$ [25]. Equation (6.25) implies that the shot-noise power is zero, in agreement with a previous semiclassical calculation by Kulik and Omel'yanchuk [16].

We now restrict ourselves to the case $W_{\hat{n}\hat{n}'} = v_F/\ell$ of isotropic impurity scattering. Let us first show that in the diffusive limit ($\ell \ll L$) the result of Nagaev [7] is recovered. For a diffusive wire the solution of Eq. (6.23) can be approximated by

$$T(x, \hat{n}) = \frac{x + \ell n_x}{L} . \quad (6.26)$$

Deviations from this approximation only occur within a thin layer, of order ℓ , at the ends $x = 0$ and $x = L$. Substitution of Eq. (6.26) into Eq. (6.23) yields the Drude conductance

$$G_D = G_0 N \frac{\bar{\ell}}{L} , \quad (6.27)$$

with the normalized mean free path $\bar{\ell} \equiv (v_d/v_{d-1})\ell$, i.e. for $d = 2$ we have $\bar{\ell} = \frac{1}{2}\pi\ell$ and for $d = 3$ we have $\bar{\ell} = \frac{4}{3}\ell$. For the shot-noise power we obtain from Eq. (6.25), neglecting terms of order $(\ell/L)^2$,

$$P = P_0 N \frac{2\bar{\ell}}{L} \int_0^L \frac{dx}{L} \frac{x}{L} \left(1 - \frac{x}{L}\right) = \frac{1}{3} P_{\text{Poisson}} , \quad (6.28)$$

in agreement with Nagaev [7]. This result is a direct consequence of the linear dependence of the transmission probability (6.26) on x , which is generic for

diffusive transport. In Appendix 6C it is demonstrated that for a diffusive conductor with arbitrary (nonisotropic) impurity scattering $W_{\hat{n}\hat{n}}$, $P = \frac{1}{3}P_{\text{Poisson}}$ remains valid.

We can go beyond Ref. [7] and apply our method to quasi-ballistic conductors, for which ℓ and L become comparable. In Chapter 5, we showed how in this case the probabilities $T(x, \hat{n})$ can be calculated numerically by solving Eqs. (6.21). With this numerical solution as input, we compute the conductance and the shot-noise power from Eqs. (6.23) and (6.25). The result is shown in Fig. 6.2. The conductance crosses over from the Sharvin conductance to the Drude conductance with increasing length [23]. This crossover is accompanied by a rise in the shot noise, from zero to $\frac{1}{3}P_{\text{Poisson}}$. We note small differences between the two and the three-dimensional case in the crossover regime. The crossover is only weakly dependent on the dimensionality of the Fermi surface.

The dimensions $d = 2$ and 3 require a numerical solution of Eqs. (6.21). For $d = 1$ an analytical solution is possible. We emphasize that this is not a model for true one-dimensional transport, where quantum interference leads to localization if $L > \ell$. The case $d = 1$ should rather be considered as a toy model, which displays similar behavior as the two and three-dimensional cases, but which allows us to evaluate both the conductance and the shot-noise power analytically for arbitrary ratio ℓ/L . In the one-dimensional conductor an electron can move either forward or backward, so $n_x \equiv n$ is either 1 or -1 . The solution of Eqs. (6.21) is

$$T(x, n) = \frac{x + \ell(n+1)}{L + 2\ell}. \quad (6.29)$$

Substitution into Eq. (6.23) yields

$$G = G_0 N \frac{1}{1 + L/\bar{\ell}}, \quad (6.30)$$

where $\bar{\ell} \equiv 2\ell$. Note that the resistance $1/G$ is precisely the sum of the Drude and the Sharvin resistance. The shot-noise power follows from Eq. (6.25)

$$\begin{aligned} P &= P_0 N \frac{\frac{2}{3}\ell L^3 + 4\ell^2 L^2 + 8\ell^3 L}{(L + 2\ell)^4}, \\ &= \frac{1}{3} \left(1 - \frac{1}{(1 + L/\bar{\ell})^3} \right) P_{\text{Poisson}}. \end{aligned} \quad (6.31)$$

In Fig. 6.2 we have plotted G and P according to Eqs. (6.30) and (6.31). The difference with $d = 2$ and $d = 3$ is very small.

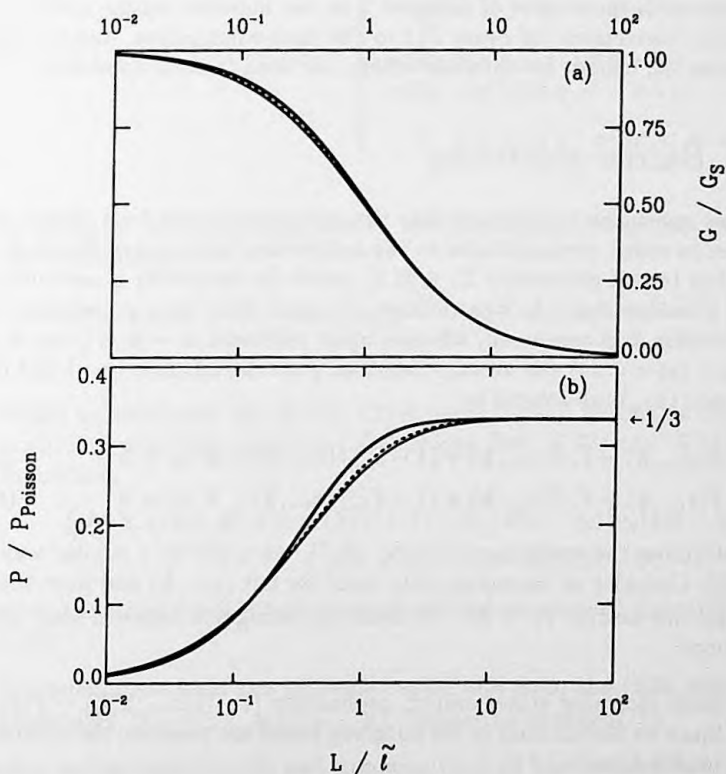


Figure 6.2: (a) The conductance (normalized by the Sharvin conductance G_S) and (b) the shot-noise power (in units of $P_{\text{Poisson}} \equiv 2e|I|$), as a function of the ratio L/\tilde{l} , computed from Eqs. (6.23) and (6.25) for isotropic impurity scattering. The curves correspond to a three-dimensional (thin solid), two-dimensional (dashed), and a one-dimensional wire (thick solid). The one-dimensional case is the analytical result Eqs. (6.30) and (6.31). The two- and three-dimensional cases are numerical results.

In Chapter 2, we have carried out a quantum mechanical study of the shot noise in a quasi-one-dimensional wire [8], on the basis of the Dorokhov-Mello-Pereyra-Kumar equation [26]. It is remarkable that the results from the one-dimensional model for both the conductance and the shot-noise power coincide precisely with the results of Chapter 2 in the metallic regime ($N\ell/L \gg 1$). Quantum corrections (of order P_0) to the shot-noise power, due to weak localization [8], cannot be obtained within our semiclassical approach.

6.4 Barrier scattering

We now specialize to the case that the scattering is due to n planar tunnel barriers in series, perpendicular to the x -direction (see inset of Fig. 6.3). Barrier i has tunnel probability $\Gamma_i \in [0, 1]$, which for simplicity is assumed to be \mathbf{k} and y -independent. In what follows, we again drop the y -coordinate. Upon transmission \mathbf{k} is conserved, whereas upon reflection $\mathbf{k} \rightarrow \tilde{\mathbf{k}} \equiv (-k_x, k_y)$. At barrier i (at $x = x_i$) the average densities \bar{f} on the left side (x_{i-}) and on the right side (x_{i+}) are related by

$$\bar{f}(x_{i+}, \mathbf{k}) = \Gamma_i \bar{f}(x_{i-}, \mathbf{k}) + (1 - \Gamma_i) \bar{f}(x_{i+}, \tilde{\mathbf{k}}), \quad \text{if } k_x > 0, \quad (6.32a)$$

$$\bar{f}(x_{i-}, \mathbf{k}) = \Gamma_i \bar{f}(x_{i+}, \mathbf{k}) + (1 - \Gamma_i) \bar{f}(x_{i-}, \tilde{\mathbf{k}}), \quad \text{if } k_x < 0. \quad (6.32b)$$

To determine the correlator J in Eq. (6.7), we argue in a similar way as in Ref. [5]. Consider an incoming state from the left (x_{i-}, \mathbf{k}) and from the right ($x_{i+}, \tilde{\mathbf{k}}$) (we assume $k_x > 0$). We need to distinguish between four different situations:

- (a) Both incoming states empty, probability $[1 - \bar{f}(x_{i-}, \mathbf{k})][1 - \bar{f}(x_{i+}, \tilde{\mathbf{k}})]$. Since no fluctuations in the outgoing states are possible, the contribution to J is zero.
- (b) Both incoming states occupied, probability $\bar{f}(x_{i-}, \mathbf{k}) \bar{f}(x_{i+}, \tilde{\mathbf{k}})$. Again, no contribution to J .
- (c) Incoming state from the left occupied and from the right empty, probability $\bar{f}(x_{i-}, \mathbf{k})[1 - \bar{f}(x_{i+}, \tilde{\mathbf{k}})]$. On the average, the outgoing states at the left and right have occupation $1 - \Gamma_i$ and Γ_i , respectively. However, since the incoming electron is either transmitted or reflected, the instantaneous occupation of the outgoing states differs from the average occupation. Upon transmission, the state at the right (left) has an excess (deficit) occupation of $1 - \Gamma_i$. Upon reflection, the state at the right (left) has a deficit (excess) occupation of Γ_i . Since transmission

occurs with probability Γ_i and reflection with probability $1 - \Gamma_i$, the equal-time correlation of the occupations is given by

$$\langle \delta f(\mathbf{r}, \mathbf{k}, t) \delta f(\mathbf{r}', \mathbf{k}', t) \rangle = \begin{cases} (2\pi)^d \Gamma_i (1 - \Gamma_i) \delta(\mathbf{k} - \mathbf{k}') \delta(\mathbf{r} - \mathbf{r}'), & \text{if } x, x' > x_i \text{ or } x, x' < x_i, \\ -(2\pi)^d \Gamma_i (1 - \Gamma_i) \delta(\mathbf{k} - \tilde{\mathbf{k}}') \\ \times \delta(\mathbf{y} - \mathbf{y}') \delta(x + x' - 2x_i), & \text{if } x < x_i < x' \text{ or } x' < x_i < x, \end{cases} \quad (6.33)$$

In terms of the fluctuating source, the fluctuating occupation number can be expressed as

$$\delta f(\mathbf{r}, \mathbf{k}, t) = \frac{1}{|v_x|} \int dx_0 j\left(x_0, \mathbf{y} - \frac{v_y}{v_x}(x - x_0), \mathbf{k}, t - \frac{x - x_0}{v_x}\right), \quad (6.34)$$

where we have used Eq. (6.15). (This result is valid as long as only one scattering event has occurred.) Combining Eqs. (6.33) and (6.34), it is found that

$$\langle j(\mathbf{r}, \mathbf{k}, t) j(\mathbf{r}', \mathbf{k}', t') \rangle = (2\pi)^d \Gamma_i (1 - \Gamma_i) \delta(x - x_i) |v_x| \delta(\mathbf{r} - \mathbf{r}') \\ \times [\delta(\mathbf{k} - \mathbf{k}') - \delta(\mathbf{k} - \tilde{\mathbf{k}}')] \delta(t - t'), \quad (6.35)$$

upon the initial condition of occupied left and unoccupied right incoming state.

- (d) Incoming state from the left unoccupied and from the right occupied, probability $[1 - \bar{f}(x_{i-}, \mathbf{k})] \bar{f}(x_{i+}, \tilde{\mathbf{k}})$. Similar to situation (c).

Collecting results from (a)–(d) and summing over all barriers, we find

$$J(x, \mathbf{k}, \mathbf{k}') = \sum_{i=1}^n \delta(x - x_i) \Gamma_i (1 - \Gamma_i) |v_x| [\delta(\mathbf{k} - \mathbf{k}') - \delta(\mathbf{k} - \tilde{\mathbf{k}}')] \\ \times \left\{ \bar{f}(x_{i-}, \mathbf{k}) [1 - \bar{f}(x_{i+}, \tilde{\mathbf{k}})] + \bar{f}(x_{i+}, \tilde{\mathbf{k}}) [1 - \bar{f}(x_{i-}, \mathbf{k})] \right\}, \\ \text{if } k_x > 0, \quad (6.36a)$$

$$J(x, \mathbf{k}, \mathbf{k}') = \sum_{i=1}^n \delta(x - x_i) \Gamma_i (1 - \Gamma_i) |v_x| [\delta(\mathbf{k} - \mathbf{k}') - \delta(\mathbf{k} - \tilde{\mathbf{k}}')] \\ \times \left\{ \bar{f}(x_{i+}, \mathbf{k}) [1 - \bar{f}(x_{i-}, \tilde{\mathbf{k}})] + \bar{f}(x_{i-}, \tilde{\mathbf{k}}) [1 - \bar{f}(x_{i+}, \mathbf{k})] \right\}, \\ \text{if } k_x < 0. \quad (6.36b)$$

Substitution of Eqs. (6.22) and (6.36) into Eq. (6.19) and linearization in V yields

$$P = P_0 N \sum_{i=1}^n \Gamma_i (1 - \Gamma_i) (T_i^- - T_i^{+-})^2 (T_i^- + T_i^{+-} - 2T_i^- T_i^{+-}), \quad (6.37)$$

where $T_i^- \equiv T(x_{i+}, k_x > 0)$ [$T_i^{+-} \equiv T(x_{i-}, k_x < 0)$] is the transmission probability into the right reservoir of an electron at the Fermi level moving away from the right [left] side of barrier i . The conductance is given simply by

$$G = G_0 N T_0, \quad (6.38)$$

where $T_0 \equiv T(x_{1-}, k_x > 0)$ is the transmission probability through the whole conductor.

As a first application of Eq. (6.37), we calculate the shot noise for a single tunnel barrier. Using $T_0 = \Gamma$, $T_1^{+-} = 0$, $T_1^- = 1$, we find the expected result [1-5] $P = P_0 N \Gamma (1 - \Gamma) = (1 - \Gamma) P_{\text{Poisson}}$. The double-barrier case ($n = 2$) is less trivial. Experiments by Li *et al.* [27] and by Liu *et al.* [28] showed full Poisson noise, for asymmetric structures ($\Gamma_1 \ll \Gamma_2$) and a suppression by one half, for the symmetric case ($\Gamma_1 \simeq \Gamma_2$). This effect has been explained by Chen and Ting [18], by Davies *et al.* [19], and by others [29]. These theories assume resonant tunneling in the regime that the applied voltage V is much greater than the width of the resonance. This requires $\Gamma_1, \Gamma_2 \ll 1$. The present semiclassical approach makes no reference to transmission resonances and is valid for all Γ_1, Γ_2 . For the double-barrier system one has $T_0 = \Gamma_1 \Gamma_2 / \Delta$, $T_1^{+-} = 0$, $T_1^- = \Gamma_2 / \Delta$, $T_2^{+-} = (1 - \Gamma_1) \Gamma_2 / \Delta$, and $T_2^- = 1$, with $\Delta = \Gamma_1 + \Gamma_2 - \Gamma_1 \Gamma_2$. From Eqs. (6.37) and (6.38), it follows that

$$P = \frac{\Gamma_1^2 (1 - \Gamma_2) + \Gamma_2^2 (1 - \Gamma_1)}{(\Gamma_1 + \Gamma_2 - \Gamma_1 \Gamma_2)^2} P_{\text{Poisson}}. \quad (6.39)$$

In the limit $\Gamma_1, \Gamma_2 \ll 1$, Eq. (6.39) coincides precisely with the results of Refs. [18] and [19].

The shot-noise suppression of one half for a symmetric double-barrier junction has the same origin as the one-third suppression for a diffusive conductor. In our semiclassical model, this is evident from the fact that a diffusive conductor is the continuum limit of a series of tunnel barriers. We demonstrate this below. Quantum mechanically, the common origin is the bimodal distribution $\rho(T) \equiv \langle \sum_n \delta(T - T_n) \rangle$ of transmission eigenvalues, which for a double-barrier junction is given by [30]

$$\rho(T) = \frac{N \Gamma_1 \Gamma_2}{\pi T \sqrt{4 \Gamma_1 \Gamma_2 T - (\Delta T + \Gamma_1 \Gamma_2)^2}}, \quad (6.40)$$

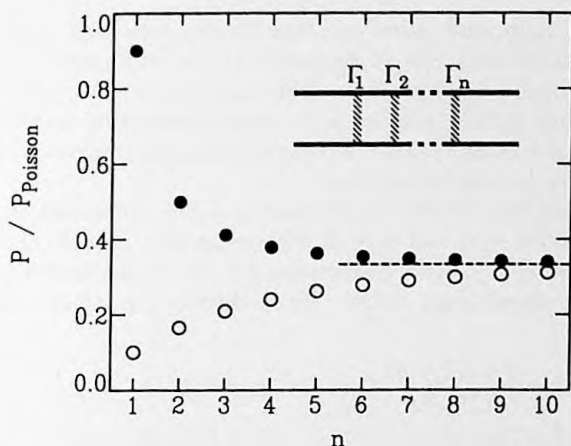


Figure 6.3: The shot-noise power P for n tunnel barriers in series with transmission probability $\Gamma = 0.1$ (dots) and $\Gamma = 0.9$ (circles), computed from Eq. (6.41). The dashed line is the large- n limit $P = \frac{1}{3}P_{\text{Poisson}}$. The inset shows schematically the geometry considered.

for $T \in [T_-, T_+]$, with $T_{\pm} = \Gamma_1\Gamma_2/(1 \mp \sqrt{1 - \Delta})^2$. For a symmetric junction ($\Gamma_1 = \Gamma_2 \ll 1$), the density (6.40) is strongly peaked near $T = 0$ and $T = 1$, leading to a suppression of shot noise, just as in the case of a diffusive conductor. In fact, one can verify that the average of Eqs. (6.1) and (6.2), with the bimodal distribution (6.40), gives precisely the result (6.39) from the Boltzmann-Langevin equation.

We now consider n barriers with equal Γ . We find $T_0 = \Gamma/\Delta$, $T_i^- = [\Gamma + i(1 - \Gamma)]/\Delta$, and $T_i^+ = (i - 1)(1 - \Gamma)/\Delta$, with $\Delta = \Gamma + n(1 - \Gamma)$. Substitution into Eqs. (6.37) and (6.38) yields

$$P = \frac{1}{3} \left(1 + \frac{n(1 - \Gamma)^2(2 + \Gamma) - \Gamma^3}{[\Gamma + n(1 - \Gamma)]^3} \right) P_{\text{Poisson}}. \quad (6.41)$$

The shot-noise suppression for a low barrier ($\Gamma = 0.9$) and for a high barrier ($\Gamma = 0.1$) is plotted against n in Fig. 6.3. For $\Gamma = 0.1$ we observe almost full shot noise if $n = 1$, one-half suppression if $n = 2$, and on increasing n the suppression rapidly reaches one-third. For $\Gamma = 0.9$, we observe that P/P_{Poisson} increases from almost zero to one-third. It is clear from Eq. (6.41) that $P \rightarrow \frac{1}{3}P_{\text{Poisson}}$ for $n \rightarrow \infty$ independent of Γ .

We can make the connection with elastic impurity scattering in a disordered wire as follows: The scattering occurs throughout the whole wire instead of at a discrete number of barriers. For the semiclassical evaluation we thus take the limit $n \rightarrow \infty$ and $\Gamma \rightarrow 1$, such that $n(1 - \Gamma) = L/\bar{\ell}$. For the conduc-

tance and the shot-noise power one then obtains from Eqs. (6.38) and (6.41) exactly the same results, Eqs. (6.30) and (6.31), as for impurity scattering with a one-dimensional density of states. This equivalence is expected, since in the one-dimensional model electrons move either forward or backward, whereas in the model of n planar tunnel barriers in series the transverse component of the wave vector becomes irrelevant.

We conclude this Section by considering a wire consisting of a disordered region, between $x = 0$ and $x = L$ with mean free path ℓ , in series with a barrier, at $x = x_b > L$ with transparency Γ . For analytical convenience, we study the one-dimensional model. By modifying Eqs. (6.21) and (6.32), we find

$$T(x, n) = \frac{x + \ell(1+n)}{L\Gamma + 2\ell} \Gamma, \quad \text{if } x \in [0, L], \quad (6.42a)$$

$$T(x, n) = T(x, L), \quad \text{if } x \in [L, x_b], \quad (6.42b)$$

$$T(x, -1) = 1 - \frac{2\ell\Gamma}{L\Gamma + 2\ell}, \quad \text{if } x > x_b, \quad (6.42c)$$

$$T(x, 1) = 1. \quad \text{if } x > x_b, \quad (6.42d)$$

The conductance is given by Eq. (6.23),

$$G = G_0 N \frac{\Gamma}{1 + \Gamma L/\ell}. \quad (6.43)$$

The total resistance is thus the sum of the Drude resistance $R_D = L/G_0 N \ell$ and the barrier resistance $R_\Gamma = 1/G_0 N \Gamma$. Combining Eqs. (6.25) and (6.37), we obtain for the shot-noise power

$$\begin{aligned} P &= \frac{P_0 N}{2\ell} \int_0^L dx [T(x, 1) - T(x, -1)]^2 \\ &\quad \times [T(x, 1) + T(x, -1) - 2T(x, 1)T(x, -1)] \\ &+ P_0 N \Gamma (1 - \Gamma) [T(x_{b+}, 1) - T(x_{b-}, -1)]^2 \\ &\quad \times [T(x_{b+}, 1) + T(x_{b-}, -1) - 2T(x_{b+}, 1)T(x_{b-}, -1)]. \end{aligned} \quad (6.44)$$

Substitution of Eqs. (6.42) yields

$$\begin{aligned} P &= P_0 N \left(\frac{2\Gamma^3 \ell L (12\ell^2 + 6\ell L + \Gamma L^2)}{3(2\ell + \Gamma L)^4} + \frac{8\Gamma(1 - \Gamma)\ell^3}{(2\ell + \Gamma L)^3} \right) \\ &= \left(\frac{1}{3} - \frac{1}{3(1 + \Gamma L/\ell)^3} + \frac{1 - \Gamma}{(1 + \Gamma L/\ell)^3} \right) P_{\text{Poisson}}, \end{aligned} \quad (6.45)$$

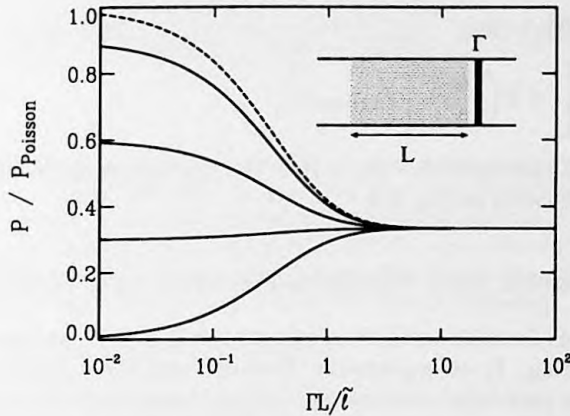


Figure 6.4: The shot-noise power P for a conductor consisting of a disordered region in series with a planar tunnel barrier (see inset) as a function of its length L (in units of $\bar{\ell}/\Gamma$), for barrier transparencies $\Gamma = 1, 0.7, 0.4$, and 0.1 (bottom to top). The dashed line is the limiting curve for $\Gamma \ll 1$. The curves are computed from Eq. (6.45) for a model with a one-dimensional density of states. The dimensionality dependence is expected to be small, compare Fig. 6.2.

where we have used Eq. (6.43). In Fig. 6.4 we have plotted the shot-noise power against the length of the disordered region for various values of the barrier transparency. In the absence of disorder, there is full shot noise for high barriers ($\Gamma \ll 1$) and complete suppression if the barrier is absent ($\Gamma = 1$). Upon increasing the disorder strength, we note that the shot-noise power approaches the limiting value $P = \frac{1}{3}P_{\text{Poisson}}$ independent of Γ : Once the disordered region dominates the resistance, the shot noise is suppressed by one-third. Note, that it follows from Eq. (6.45) that for $\Gamma = \frac{2}{3}$ the suppression is one-third for all ratios $\bar{\ell}/L$.

We have carried out a quantum mechanical calculation of the shot-noise power in this system in a wire geometry similar to the calculation in Chapter 2. The barrier can be incorporated in the Dorokhov-Mello-Pereyra-Kumar equation [26] by means of an initial condition (see Ref. [31]). In this way, we find exactly the same result as Eq. (6.45) in the metallic regime ($N\Gamma \gg 1$ and $N\bar{\ell}/L \gg 1$). For a high barrier ($\Gamma \ll 1$) in series with a diffusive wire ($L \gg \bar{\ell}$) our results for the shot noise coincide with previous work by Nazarov [9] using a different quantum mechanical theory. In this limit, the shot noise can be

expressed as [9]

$$P = \frac{1}{3} \left[1 + 2 \left(\frac{R_{\Gamma}}{R} \right)^3 \right] P_{\text{Poisson}}, \quad (6.46)$$

with the total resistance $R = R_D + R_{\Gamma}$. The limiting result (6.46) is depicted by the dashed curve in Fig. 6.4.

6.5 Inelastic and electron-electron scattering

In the previous Sections we have calculated the shot noise for several types of elastic scattering. In an experiment, however, additional types of scattering may occur. In particular, electron-electron and inelastic electron-phonon scattering will be enhanced due to the high currents which are often required for noise experiments. The purpose of this Section is to discuss the effects of these additional scattering processes. This can in principle be achieved by including additional scattering terms in the Boltzmann-Langevin equation. Below, we will adopt a different method, following Beenakker and Büttiker [6], in which inelastic scattering is modeled by dividing the conductor in separate, phase-coherent parts which are connected by charge-conserving reservoirs. We extend this model to include the following types of scattering:

- (a) *Quasi-elastic scattering.* Due to weak coupling with external degrees of freedom the electron wave function gets dephased, but its energy is conserved. In metals, this scattering is caused by fluctuations in the electromagnetic field [32].
- (b) *Electron heating.* Electron-electron scattering exchanges energy between the electrons, but the total energy of the electron system is conserved. The distribution function is therefore assumed to be a Fermi-Dirac distribution at a temperature above the lattice temperature.
- (c) *Inelastic scattering.* Due to electron-phonon interactions the electrons exchange energy with the lattice. The electrons emerging from the reservoir are distributed according to the Fermi-Dirac distribution (6.3), at the lattice temperature T . This is the model of Ref. [6].

First, we divide the conductor in two parts connected via one reservoir and determine the shot noise for case (a), (b), and (c). After that, we repeat the calculation for many intermediate reservoirs to take into account that the scattering occurs throughout the whole length of the conductor.

The model is depicted in Fig. 6.5. The conductors 1 and 2 are connected via a reservoir with distribution function $f_{12}(\epsilon)$. The time-averaged current

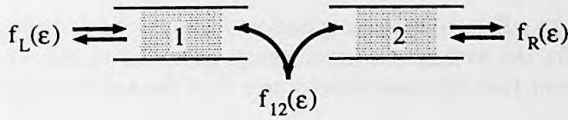


Figure 6.5: Both ends of the conductor are connected to an electron reservoir. Additional scattering inside the conductor is modeled by dividing it in two parts and connecting them through another reservoir. The electron distributions in the left and the right reservoir, $f_L(\epsilon)$ and $f_R(\epsilon)$, are Fermi-Dirac distributions. The distribution $f_{12}(\epsilon)$ in the intermediate reservoir depends on the type of scattering.

I_m through conductor $m = 1, 2$ is given by

$$I_1 = (G_1/e) \int d\epsilon [f_L(\epsilon) - f_{12}(\epsilon)], \quad (6.47a)$$

$$I_2 = (G_2/e) \int d\epsilon [f_{12}(\epsilon) - f_R(\epsilon)]. \quad (6.47b)$$

The conductance $G_m \equiv 1/R_m$ is expressed in terms of the transmission matrix t_m of conductor m at the Fermi energy,

$$G_m = G_0 \text{Tr} t_m t_m^\dagger = G_0 \sum_{n=1}^N T_n^{(m)}, \quad (6.48)$$

with $T_n^{(m)} \in [0, 1]$ an eigenvalue of $t_m t_m^\dagger$. We assume small eV and $k_B T$, so that we can neglect the energy dependence of the transmission eigenvalues.

Current conservation requires that

$$I_1 = I_2 \equiv I. \quad (6.49)$$

We define the total resistance of the conductor by

$$R = R_1 + R_2. \quad (6.50)$$

It will be shown that this incoherent addition of resistances is valid for all three types of scattering that we consider. Our model is not suitable for transport in the ballistic regime or in the quantum Hall regime, where a different type of “one-way” reservoirs are required [33]. Recently, Büttiker has calculated the effects of inelastic scattering along these lines [34].

The time-averaged current (6.47) depends on the average distribution $f_{12}(\epsilon)$ in the reservoir between conductors 1 and 2. In order to calculate the current fluctuations, we need to take into account that this distribution varies in time. We denote the time-dependent distribution by $\tilde{f}_{12}(\epsilon, t)$. The fluctuating current through conductor 1 or 2 causes electrostatic potential fluctuations $\delta\phi_{12}(t)$ in the reservoir, which enforce charge neutrality. In Ref. [6],

the reservoir has a Fermi-Dirac distribution $\tilde{f}_{12}(\varepsilon, t) = f_0[\varepsilon - eV_{12} - e\delta\phi_{12}(t)]$, with $E_F + eV_{12}$ the average electrochemical potential in the reservoir. As a result, it is found that the shot-noise power P of the entire conductor is given by [6]

$$R^2 P = R_1^2 P_1 + R_2^2 P_2. \quad (6.51)$$

In other words, the voltage fluctuations add. The noise powers P_1 and P_2 of the two segments depend solely on the time-averaged distribution [4],

$$P_1 = 2G_1 \int d\varepsilon [f_L(1 - f_L) + f_{12}(1 - f_{12})] + 2S_1 \int d\varepsilon (f_L - f_{12})^2, \quad (6.52a)$$

$$P_2 = 2G_2 \int d\varepsilon [f_{12}(1 - f_{12}) + f_R(1 - f_R)] + 2S_2 \int d\varepsilon (f_{12} - f_R)^2. \quad (6.52b)$$

Here, S_m is defined as

$$S_m = G_0 \text{Tr} \, t_m^\dagger t_m (1 - t_m^\dagger t_m) = G_0 \sum_{n=1}^N T_n^{(m)} (1 - T_n^{(m)}). \quad (6.53)$$

For example, for a single tunnel barrier we have $S_m = G_m$, whereas for a diffusive conductor $S_m = \frac{1}{3}G_m$. The analysis of Ref. [6] is easily generalized to arbitrary distribution f_{12} . Then, we have $\tilde{f}_{12}(\varepsilon, t) = f_{12}[\varepsilon - e\delta\phi_{12}(t)]$. It follows that Eqs. (6.51) and (6.52) remain valid, only the $f_{12}(\varepsilon)$ may be different. Let us determine the shot noise for the three types of scattering.

(a) *Quasi-elastic scattering.* Here, it is not just the total current which must be conserved, but the current in each energy range. This requires

$$f_{12}(\varepsilon) = \frac{G_1 f_L(\varepsilon) + G_2 f_R(\varepsilon)}{G_1 + G_2}. \quad (6.54)$$

We note that Eq. (6.54) implies the validity of Eq. (6.50). Substitution of Eq. (6.54) into Eqs. (6.51) and (6.52) yields at $T=0$

$$P = P_{\text{Poisson}} (R_1^4 S_1 + R_2^4 S_2 + R_1 R_2^2 + R_1^2 R_2) R^{-3}. \quad (6.55)$$

For the diffusive wire Eq. (6.55) implies $P = \frac{1}{3}P_{\text{Poisson}}$, independent of the ratio between R_1 and R_2 . Breaking phase coherence, but retaining the nonequilibrium electron distribution leaves the shot noise unaltered. The reservoir model for phase-breaking scattering is therefore consistent with the results of the Boltzmann-Langevin approach.

(b) *Electron heating.* We model electron-electron scattering, where energy can be exchanged between the electrons, at constant total energy. We assume that the exchange of energies establishes a Fermi-Dirac distribution $f_{12}(\varepsilon)$

at an electrochemical potential $E_F + eV_{12}$ and an elevated temperature T_{12} . From current conservation, Eq. (6.49), it follows that

$$V_{12} = \frac{R_2}{R} V. \quad (6.56)$$

Conservation of the energy of the electron system requires that T_{12} is such that no energy is absorbed or emitted by the reservoir. The energy current J_m through conductor m is given by

$$J_1 = (G_1/e^2) \int d\varepsilon \varepsilon [f_L(\varepsilon) - f_{12}(\varepsilon)], \quad (6.57a)$$

$$J_2 = (G_2/e^2) \int d\varepsilon \varepsilon [f_{12}(\varepsilon) - f_R(\varepsilon)]. \quad (6.57b)$$

Since f_{12} is a Fermi-Dirac distribution, Eqs. (6.57) equal

$$J_1 = Q_1 + \mu_1 I/e = K_1(T - T_{12}) + \mu_1 I/e, \quad (6.58a)$$

$$J_2 = Q_2 + \mu_2 I/e = K_2(T_{12} - T) + \mu_2 I/e, \quad (6.58b)$$

where $\mu_1 \equiv E_F + \frac{1}{2}e(V + V_{12})$ and $\mu_2 \equiv E_F + \frac{1}{2}eV_{12}$. The energy current J_m is thus the sum of the heat current Q_m and of the particle current I/e times the average energy μ_m of each electron. The heat current Q_m equals the difference in temperature times the thermal conductance $K_m = G_m \mathcal{L}_0 T_m$, with $T_m \equiv (T + T_{12})/2$ and the Lorentz number $\mathcal{L}_0 \equiv (k_B/e)^2 \pi^2/3$. There are no thermoelectric contributions in Eqs. (6.47) and (6.58), because of the assumption of energy independent transmission eigenvalues [35]. From the requirement of energy conservation, $J_1 = J_2$, we calculate the electron temperature in the intermediate reservoir:

$$T_{12}^2 = T^2 + \frac{V^2}{\mathcal{L}_0} \frac{R_1 R_2}{R^2}. \quad (6.59)$$

At zero temperature in the left and right reservoir and for $R_1 = R_2$ we have $k_B T_{12} = (\sqrt{3}/2\pi)e|V| \simeq 0.28e|V|$. For the shot noise at $T = 0$, we thus obtain using Eqs. (6.51) and (6.52),

$$\begin{aligned} P &= 2 \frac{k_B T_{12}}{R} \\ &+ 2 \frac{S_1 R_1^2}{R^2} \left\{ e(V - V_{12}) + k_B T_{12} [2 \ln(1 + e^{e(V_{12} - V)/k_B T_{12}}) - 1] \right\} \\ &+ 2 \frac{S_2 R_2^2}{R^2} \left\{ eV_{12} + k_B T_{12} [2 \ln(1 + e^{-eV_{12}/k_B T_{12}}) - 1] \right\}. \end{aligned} \quad (6.60)$$

The shot noise for two equal ($R_1 = R_2$) diffusive conductors,

$$P = P_{\text{Poisson}} \frac{1}{\pi\sqrt{3}} \left[1 + \ln 2 + \ln \cosh(\pi/2\sqrt{3}) \right] \simeq 0.38 P_{\text{Poisson}}, \quad (6.61)$$

is slightly above the one-third suppression. This shows that the current becomes less correlated due to the electron-electron scattering.

(c) *Inelastic scattering.* This is the model of Ref. [6]. The distribution function of the intermediate reservoir is the Fermi-Dirac distribution at the lattice temperature T , with an electrochemical potential $\mu_{12} \equiv E_F + eV_{12}$, where V_{12} is given by Eq. (6.56). This reservoir absorbs energy, in contrast to cases (a) and (b). The zero-temperature shot-noise power follows from Eqs. (6.51)–(6.52) [6]

$$P = P_{\text{Poisson}} \frac{R_1^3 S_1 + R_2^3 S_2}{R^2}. \quad (6.62)$$

For the diffusive case, with $R_1 = R_2$, one has $P = \frac{1}{6} P_{\text{Poisson}}$. The inelastic scattering gives an additional suppression [6].

For a double-barrier system it is plausible to model the additional scattering by a single reservoir between the barriers. In a diffusive conductor, however, these scattering processes occur throughout the system. It is therefore more realistic to divide the conductor into M segments, connected by reservoirs. Equation (6.51) becomes

$$R^2 P = \sum_{m=1}^M R_m^2 P_m, \quad (6.63)$$

where the noise power P_m of segment m is calculated analogous to Eq. (6.52). We take the continuum limit $M \rightarrow \infty$. The electron distribution at position x is denoted by $f(\varepsilon, x)$. At the ends of the conductor $f(\varepsilon, 0) = f_L(\varepsilon)$ and $f(\varepsilon, L) = f_R(\varepsilon)$, i.e. the electrons are Fermi-Dirac distributed at temperature T and with electrochemical potential $\mu(0) = E_F + eV$ and $\mu(L) = E_F$, respectively. The value of $f(\varepsilon, x)$ inside the conductor depends on the type of scattering, (a), (b), or (c), and is determined below.

In the expression for P_m only the first term of Eq. (6.52a) remains. It follows from Eq. (6.63) that the noise power is given by

$$P = \frac{4}{R^2} \int_0^L dx \frac{\rho(x)}{A} \int d\varepsilon f(\varepsilon, x) [1 - f(\varepsilon, x)], \quad (6.64)$$

where $\rho(x)$ is the resistivity at position x . The total resistance is given by

$$R = \frac{1}{A} \int_0^L dx \rho(x). \quad (6.65)$$

For a constant resistivity ρ we find from Eq. (6.64)

$$P = \frac{4}{RL} \int_0^L dx \int d\varepsilon f(\varepsilon, x) [1 - f(\varepsilon, x)]. \quad (6.66)$$

This formula has been derived by Nagaev from the Boltzmann-Langevin equation for isotropic impurity scattering in the diffusive limit [7]. Our semiclassical calculation in the previous Sections is worked out in terms of transmission probabilities rather than in terms of the electron distribution function. However, one can easily convince oneself that in the diffusive limit and at zero temperature, Eqs. (6.25) and (6.66) are equivalent. The present derivation shows that the quantum mechanical expression for the noise with phase-breaking reservoirs leads to the same result as the semiclassical approach. We evaluate Eq. (6.66) for the three types of scattering.

(a) *Quasi-elastic scattering.* This calculation has previously been performed by Nagaev [7] and is similar to the evaluation in Section 6.3. Current conservation and the absence of inelastic scattering requires

$$\frac{\partial^2}{\partial x^2} f(\varepsilon, x) = 0. \quad (6.67)$$

The solution is

$$f(\varepsilon, x) = \frac{L-x}{L} f(\varepsilon, 0) + \frac{x}{L} f(\varepsilon, L), \quad (6.68)$$

The electron distribution at $x = L/2$ is plotted in the left inset of Fig. 6.6. Substitution of Eq. (6.68) into Eq. (6.66) yields [7]

$$P = \frac{2}{3R} [4k_B T + eV \coth(eV/2k_B T)]. \quad (6.69)$$

At zero temperature the shot noise is one-third of the Poisson noise. The temperature dependence of P is given in Fig. 6.6.

(b) *Electron heating.* This calculation is due to Martinis and Devoret [36]. The electron distribution function is a Fermi-Dirac distribution at an elevated temperature $T_e(x)$,

$$f(\varepsilon, x) = \left\{ 1 + \exp \left[\frac{\varepsilon - \mu(x)}{k_B T_e(x)} \right] \right\}^{-1}. \quad (6.70)$$

The current density $j(x)$ at x is

$$j(x) = -eD\mathcal{D}(E_F) \frac{\partial}{\partial x} \int d\varepsilon f(\varepsilon, x), \quad (6.71)$$

where D is the diffusion constant and \mathcal{D} is the density of states. We neglect the energy dependence of D and \mathcal{D} . The resistivity ρ is given by the Einstein relation, $\rho^{-1} = e^2 D \mathcal{D}(E_F)$. Current conservation yields

$$\frac{\partial j(x)}{\partial x} = 0, \quad (6.72)$$

which implies for the electrochemical potential

$$\mu(x) = E_F + \frac{L-x}{L} eV. \quad (6.73)$$

The energy current $j_\epsilon(x)$ is determined according to

$$j_\epsilon(x) = -D \mathcal{D}(E_F) \frac{\partial}{\partial x} \int d\epsilon \epsilon f(\epsilon, x) = \mu(x) j(x)/e + j_Q(x), \quad (6.74a)$$

$$j_Q(x) \equiv -\kappa(x) \frac{\partial T_e(x)}{\partial x}. \quad (6.74b)$$

The heat current $j_Q(x)$ equals the temperature gradient times the heat conductivity $\kappa(x) = T_e(x) \mathcal{L}_0 / \rho$. Because of energy conservation the divergence of the energy current must be zero,

$$\frac{\partial j_\epsilon(x)}{\partial x} = 0. \quad (6.75)$$

Combining Eqs. (6.74) and (6.75), we obtain the following differential equation for the temperature

$$\frac{\partial^2}{\partial x^2} [T_e(x)^2] = -\frac{2}{\mathcal{L}_0} \left(\frac{V}{L} \right)^2. \quad (6.76)$$

Taking into account the boundary conditions the solution is

$$T_e(x) = \sqrt{T^2 + (x/L)[1 - (x/L)] V^2 / \mathcal{L}_0}. \quad (6.77)$$

In the middle of the wire the electron temperature takes its maximum value. For zero lattice temperature ($T = 0$) one has $k_B T_e(L/2) = (\sqrt{3}/2\pi)e|V| \simeq 0.28e|V|$. The electron distribution at $x = L/2$ is depicted in the left inset and the electron temperature profile (6.77) is plotted in the right inset of Fig. 6.6.

Equations (6.66), (6.70), and (6.77) yields for the noise power the result

$$\begin{aligned} P &= \frac{4}{RL} \int_0^L dx k_B T_e(x) \\ &= \frac{2k_B T}{R} + 2eI \left[\frac{2\pi}{\sqrt{3}} \left(\frac{k_B T}{eV} \right)^2 + \frac{\sqrt{3}}{2\pi} \right] \arctan \left(\frac{\sqrt{3}}{2\pi} \frac{eV}{k_B T} \right). \end{aligned} \quad (6.78)$$

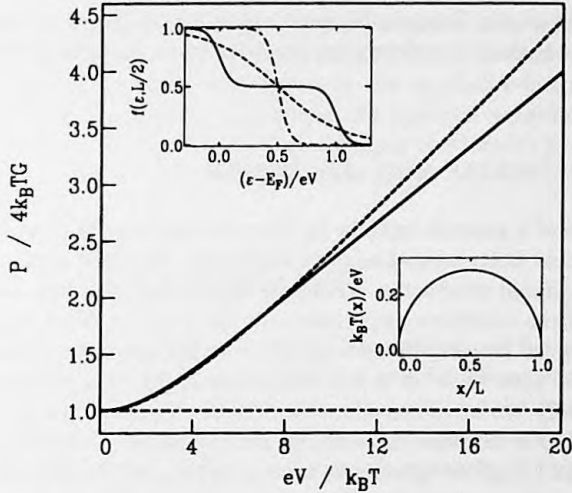


Figure 6.6: The noise power P (divided by the Johnson-Nyquist noise $4k_B T G$) versus applied voltage V for a disordered wire for model (a) (solid) quasi-elastic scattering, (b) (dashed) electron heating, (c) (dash-dotted) inelastic scattering, according to Eqs. (6.69), (6.78), and (6.81), respectively. The (upper) left inset gives the electron distribution in the middle of the wire $f(\epsilon, L/2)$ as a function of energy ϵ for model (a), (b), and (c). The (lower) right inset shows the temperature $T_e(x)$ as a function of the position x for model (b). For both insets, $k_B T = \frac{1}{20} e|V|$.

Equation (6.78) is plotted in Fig. 6.6. For the limit $eV \gg k_B T$ one finds [37]

$$P = \frac{1}{4} \sqrt{3} P_{\text{Poisson}} \simeq 0.43 P_{\text{Poisson}}. \quad (6.79)$$

Due to the electron-electron scattering the shot noise is increased. The exchange of energies among the electrons makes the current less correlated. The suppression factor of $\frac{1}{4} \sqrt{3}$ is close to the value observed in an experiment on silver wires by Steinbach, Martinis, and Devoret [37].

(c) *Inelastic scattering.* The electron distribution function is given by

$$f(\epsilon, x) = \left\{ 1 + \exp \left[\frac{\epsilon - \mu(x)}{k_B T} \right] \right\}^{-1}, \quad (6.80)$$

with $\mu(x)$ according to Eq. (6.73). For the noise power we obtain from Eqs. (6.66) and (6.80)

$$P = \frac{4k_B T}{R}, \quad (6.81)$$

which is equal to the Johnson-Nyquist noise for arbitrary V (see Fig. 6.6). The shot noise is thus completely suppressed by the inelastic scattering [6, 13, 38, 39].

6.6 Conclusions and discussion

We have derived a general formula for the shot noise within the framework of the semiclassical Boltzmann-Langevin equation. We have applied this to the case of a disordered conductor, where we have calculated how the shot noise crosses over from complete suppression in the ballistic limit to one-third of the Poisson noise for the diffusive limit. Furthermore, we have applied our formula to the shot noise in a conductor consisting of a sequence of tunnel barriers. Finally, we have considered a disordered conductor in series with a tunnel barrier. For all these systems, we have obtained a sub-Poissonian shot-noise power, in complete agreement with quantum mechanical calculations in the literature. This establishes that phase coherence is not required for the occurrence of suppressed shot noise in mesoscopic conductors. Moreover, it has been shown that for diffusive conductors the one-third suppression occurs quite generally. This phenomenon depends neither on the dimensionality of the conductor, nor on the microscopic details of the scattering potential.

We have modeled quasi-elastic scattering (which breaks phase coherence), electron heating (due to electron-electron scattering), and inelastic scattering (due to, e.g., electron-phonon scattering) by putting charge-conserving reservoirs between phase-coherent segments of the conductor. If the scattering occurs throughout the whole length of the conductor, we end up with the same formula for the noise as can be obtained directly from the Boltzmann-Langevin approach. In the case of electron heating, the shot noise is $\frac{1}{4}\sqrt{3}$ of the Poisson noise, which is slightly above the fully elastic case. This may be relevant for experiments [11, 37]. The inelastic scattering is shown to completely suppress the shot noise [6]. For future work, it might be worthwhile to investigate the influence of electron heating and inelastic scattering by taking them into account through the scattering terms in the Boltzmann-Langevin equation. This would allow the calculation of the crossover behavior between the different regimes.

In both the quantum mechanical theories and the semiclassical theories the electrons are treated as noninteracting particles. Some aspects of the electron-electron interaction are taken into account by the conditions for the reservoirs in our model of Section 6.5. Here, fluctuations in the electrostatic potential enforce charge-neutrality. We have shown that this only leads to a suppression of the noise in the presence of inelastic scattering. The Coulomb repulsion is known to have a strong effect on the noise in confined geometries with a small

capacitance [29]. This is relevant for the double-barrier case treated in Section 6.4. Theories which take the Coulomb blockade into account [29] predict a shot-noise suppression which is periodic in the applied voltage. This effect has recently been observed for a nanoparticle between a surface and the tip of a scanning tunneling microscope [40]. In open conductors we would expect these interaction effects to be less important [41].

Appendix 6A Thermal noise

In this Appendix it is shown how thermal fluctuation can be incorporated to the theory. These are ignored in Sections 6.3 and 6.4 where zero temperature is considered. At non-zero temperatures we need to take into account the time-dependent fluctuations in the occupation of the states in the reservoirs. The formal solution of the Boltzmann-Langevin equation (6.6) can be written as

$$\begin{aligned} \delta f(\mathbf{r}, \mathbf{k}, t) = & \int_{-\infty}^t dt' \int_{\mathcal{V}} d\mathbf{r}' \int d\mathbf{k}' \mathcal{G}(\mathbf{r}, \mathbf{k}; \mathbf{r}', \mathbf{k}'; t - t') j(\mathbf{r}', \mathbf{k}', t') \\ & + \int_{-\infty}^t dt' \int_{S_L} dy' \int_{k_x > 0} d\mathbf{k}' v_x \mathcal{G}(\mathbf{r}, \mathbf{k}; \mathbf{r}', \mathbf{k}'; t - t') \delta f(\mathbf{r}', \mathbf{k}', t') \\ & + \int_{-\infty}^t dt' \int_{S_R} dy' \int_{k_x < 0} d\mathbf{k}' |v_x| \mathcal{G}(\mathbf{r}, \mathbf{k}; \mathbf{r}', \mathbf{k}'; t - t') \delta f(\mathbf{r}', \mathbf{k}', t'), \end{aligned} \quad (6.82)$$

where \mathcal{V} denotes the scattering region of the conductor. The second and third term describe the time-dependent fluctuations of states originating from the reservoir which are ignored in Eq. (6.19). The correlation function of the incoming fluctuations which have not yet reached the scattering region [i.e. for the left lead $x, x' \leq x_L$, $k_x, k'_x > 0$ and for the right lead $x, x' \geq x_R$, $k_x, k'_x < 0$] follows from Eqs. (6.10) and (6.11):

$$\begin{aligned} \langle \delta f(\mathbf{r}, \mathbf{k}, t) \delta f(\mathbf{r}', \mathbf{k}', t') \rangle = & (2\pi)^d \delta[\mathbf{r} - \mathbf{r}' - \mathbf{v}(t - t')] \delta(\mathbf{k} - \mathbf{k}') \\ & \times f_{L,R}(\varepsilon) [1 - f_{L,R}(\varepsilon)]. \end{aligned} \quad (6.83)$$

The derivation of the noise power proceeds similar to the derivation of Eq. (6.19). Substitution of Eq. (6.82) into Eqs. (6.13) and (6.14) and using both

tions (6.7) and (6.83), yields

$$\begin{aligned} & \frac{1}{(2\pi)^d} \left(\int_V d\mathbf{r} \int d\mathbf{k} \int d\mathbf{k}' T(\mathbf{r}, \mathbf{k}) T(\mathbf{r}, \mathbf{k}') J(\mathbf{r}, \mathbf{k}, \mathbf{k}') \right. \\ & + \int_{S_L} d\mathbf{y} \int_{k_x > 0} d\mathbf{k} v_x T(\mathbf{r}, \mathbf{k})^2 f_L(\varepsilon) [1 - f_L(\varepsilon)] \\ & \left. + \int_{S_R} d\mathbf{y} \int_{k_x < 0} d\mathbf{k} |v_x| [1 - T(\mathbf{r}, \mathbf{k})]^2 f_R(\varepsilon) [1 - f_R(\varepsilon)] \right). \quad (6.84) \end{aligned}$$

Let us apply Eq. (6.84) to the case of impurity scattering, treated in Section 6.3 for zero temperature. By changing variables according to Eq. (6.20) and by substitution of Eqs. (6.8) and (6.22), we obtain

$$\begin{aligned} P &= 2e^2 A \int_0^L dx \int d\varepsilon \mathcal{D}(\varepsilon) \int \frac{d\hat{\mathbf{n}}}{s_d} \int \frac{d\hat{\mathbf{n}}'}{s_d} W_{\hat{\mathbf{n}}\hat{\mathbf{n}}'} [T(x, \hat{\mathbf{n}}) - T(x, \hat{\mathbf{n}}')]^2 \\ & \times \left\{ f_L(\varepsilon) [1 - f_L(\varepsilon)] [1 - T(x, -\hat{\mathbf{n}})] + f_R(\varepsilon) [1 - f_R(\varepsilon)] T(x, -\hat{\mathbf{n}}) \right. \\ & \quad \left. + [f_L(\varepsilon) - f_R(\varepsilon)]^2 T(x, -\hat{\mathbf{n}}) [1 - T(x, -\hat{\mathbf{n}}')] \right\} \\ & + 2e^2 A \int d\varepsilon \mathcal{D}(\varepsilon) f_L(\varepsilon) [1 - f_L(\varepsilon)] \int \frac{d\hat{\mathbf{n}}}{s_d} v n_x T^2(0, \hat{\mathbf{n}}) \\ & - 2e^2 A \int d\varepsilon \mathcal{D}(\varepsilon) f_R(\varepsilon) [1 - f_R(\varepsilon)] \int \frac{d\hat{\mathbf{n}}}{s_d} v n_x [1 - T(L, \hat{\mathbf{n}})]^2, \quad (6.85) \end{aligned}$$

where we have used Eq. (6.21) and $W_{\hat{\mathbf{n}}\hat{\mathbf{n}}'} = W_{\hat{\mathbf{n}}'\hat{\mathbf{n}}}$. Equation (6.85) can be simplified by means of the relations

$$\begin{aligned} & \int_0^L dx \int \frac{d\hat{\mathbf{n}}}{s_d} \int \frac{d\hat{\mathbf{n}}'}{s_d} W_{\hat{\mathbf{n}}\hat{\mathbf{n}}'} [T(x, \hat{\mathbf{n}}) - T(x, \hat{\mathbf{n}}')]^2 \\ & = v_F \int \frac{d\hat{\mathbf{n}}}{s_d} n_x [T^2(L, \hat{\mathbf{n}}) - T^2(0, \hat{\mathbf{n}})], \quad (6.86) \end{aligned}$$

$$\begin{aligned} & \int_0^L dx \int \frac{d\hat{\mathbf{n}}}{s_d} \int \frac{d\hat{\mathbf{n}}'}{s_d} W_{\hat{\mathbf{n}}\hat{\mathbf{n}}'} [T(x, \hat{\mathbf{n}}) - T(x, \hat{\mathbf{n}}')]^2 T(x, -\hat{\mathbf{n}}) \\ & = v_F \int \frac{d\hat{\mathbf{n}}}{s_d} n_x [T^2(L, \hat{\mathbf{n}}) T(L, -\hat{\mathbf{n}}) - T^2(0, \hat{\mathbf{n}}) T(0, -\hat{\mathbf{n}})], \quad (6.87) \end{aligned}$$

which can be derived from Eq. (6.21). For the distribution function we apply the identity $f_0(1 - f_0) = -k_B T \partial f_0 / \partial \epsilon$ and define

$$F(V, T) \equiv \int d\epsilon [f_L(\epsilon) - f_R(\epsilon)]^2 = e|V| \coth \left(\frac{e|V|}{2k_B T} \right) - 2k_B T. \quad (6.88)$$

Taken together, the noise is given by

$$P = \frac{2F(V, T)G_0 N}{v_F s_d v_{d-1}} \int_0^L dx \int d\hat{n} \int d\hat{n}' W_{\hat{n}\hat{n}'} \\ \times [T(x, \hat{n}) - T(x, \hat{n}')]^2 T(x, -\hat{n}) [1 - T(x, -\hat{n}')] \\ + 4k_B T G_0 N \int \frac{d\hat{n}}{v_{d-1}} n_x T(L, \hat{n}). \quad (6.89)$$

At zero voltage, we find from Eqs. (6.23) and (6.89) the Johnson-Nyquist noise $P = 4k_B T G$. At zero temperature, Eq. (6.89) reduces to Eq. (6.25). Applying Eq. (6.89) to impurity scattering (within the one-dimensional model) as treated in Section 6.3, we obtain

$$P = \frac{2G}{3} \left\{ eV \coth \left(\frac{eV}{2k_B T} \right) \left[1 - \frac{1}{(1 + L/\tilde{\ell})^3} \right] \right. \\ \left. + 2k_B T \left[2 + \frac{1}{(1 + L/\tilde{\ell})^3} \right] \right\}. \quad (6.90)$$

The voltage dependence of the noise is plotted in Fig. 6.7 for various values of $L/\tilde{\ell}$. The result for the diffusive limit is equal to Eq. (6.69). Also depicted is the classical result for a single high tunnel barrier ($\Gamma \ll 1$),

$$P = 2e|I| \coth \left(\frac{eV}{2k_B T} \right), \quad (6.91)$$

which can be derived within our theory by combining the results of Section 6.4 with the analysis of this Appendix.

Appendix 6B Noise at arbitrary cross section

Let us verify that the noise power does not depend on the location x of the cross section at which the current is evaluated. The fluctuating current through a cross section S_x at coordinate x is defined by

$$\delta I(t, x) \equiv \frac{e}{(2\pi)^d} \int_{S_x} dy \int d\mathbf{k} v_x \delta f(\mathbf{r}, \mathbf{k}, t), \quad (6.92)$$

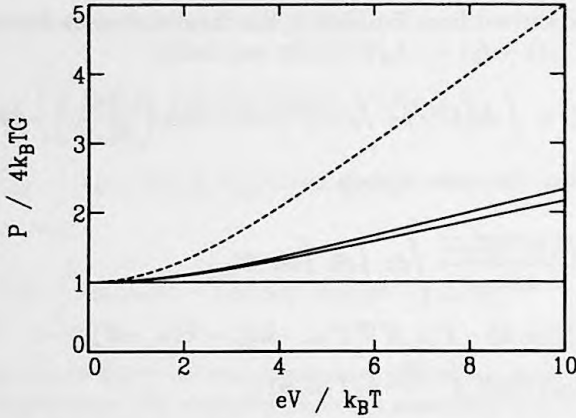


Figure 6.7: The noise power P (divided by the Johnson-Nyquist noise $4k_B T G$) versus applied voltage V for a disordered wire (bottom to top) in the ballistic limit $L/\bar{\ell} \rightarrow 0$, the intermediate regime $L/\bar{\ell} = 1$, and in the diffusive limit $L/\bar{\ell} \rightarrow \infty$, as given by Eq. (6.90). The dashed line is the noise in a tunnel barrier, according to Eq. (6.91).

and leads to

$$P(x, x') \equiv 2 \int_{-\infty}^{\infty} dt \langle \delta I(t, x) \delta I(0, x') \rangle. \quad (6.93)$$

We use the following relation

$$\int_0^{\infty} dt \int_{S_x} dy \int dk v_x \mathcal{G}(\mathbf{r}, \mathbf{k}; \mathbf{r}_0, \mathbf{k}_0; t) = T(\mathbf{r}_0, \mathbf{k}_0) - \Theta(x_0 - x), \quad (6.94)$$

which follows from Eqs. (6.16) and (6.17). Here, $\Theta(x)$ is the unit-step function. Evaluating Eq. (6.93) along the same lines as was done in Section 6.2, we find

$$P(x, x') = \frac{2e^2}{(2\pi)^d} \int d\mathbf{r}_0 \int d\mathbf{k}_0 \int d\mathbf{k}'_0 J(\mathbf{r}_0, \mathbf{k}_0, \mathbf{k}'_0) \times [T(\mathbf{r}_0, \mathbf{k}_0) - \Theta(x_0 - x)] [T(\mathbf{r}_0, \mathbf{k}'_0) - \Theta(x_0 - x')]. \quad (6.95)$$

We use that the integral over \mathbf{k} or over \mathbf{k}' of $J(\mathbf{r}, \mathbf{k}, \mathbf{k}')$ vanishes, Eq. (6.9), and find that $P(x, x')$ is independent of x, x' .

Appendix 6C Nonisotropic scattering

We wish to demonstrate that the occurrence of one-third suppressed shot noise in the diffusive regime is independent of the angle-dependence of the scattering rate. We write $W_{\hat{\mathbf{n}}\hat{\mathbf{n}}'} = w(\hat{\mathbf{n}} \cdot \hat{\mathbf{n}}')v_F$, with arbitrary w . In the diffusive limit, the transmission probability is given by

$$T(x, \hat{\mathbf{n}}) = T(x) + t(n_x), \quad (6.96)$$

where $T(x) = x/L$ and $t(n_x)$ of order $\bar{\ell}/L$, with $\int d\hat{\mathbf{n}} t(n_x) = 0$. The conductance is given by the Drude result, Eq. (6.27), where the normalized mean free path $\bar{\ell}$ can be derived as follows: By integration of Eq. (6.21a) over $d\hat{\mathbf{n}} n_x$ and substitution of Eq. (6.96), one obtains

$$\int \frac{d\hat{\mathbf{n}}}{s_d} n_x^2 \frac{dT(x)}{dx} = \int \frac{d\hat{\mathbf{n}}}{s_d} \int \frac{d\hat{\mathbf{n}}'}{s_d} n_x w(\hat{\mathbf{n}} \cdot \hat{\mathbf{n}}') [t(n_x) - t(n'_x)]. \quad (6.97)$$

Comparison with Eq. (6.23) yields

$$\bar{\ell} = \frac{v_d}{v_{d-1}} \left[\int \frac{d\hat{\mathbf{n}}}{s_d} w(n_x)(1 - n_x) \right]^{-1}. \quad (6.98)$$

From Eq. (6.21a) it also follows that

$$\begin{aligned} \int \frac{d\hat{\mathbf{n}}}{s_d} \int \frac{d\hat{\mathbf{n}}'}{s_d} W_{\hat{\mathbf{n}}\hat{\mathbf{n}}'} [T(x, \hat{\mathbf{n}}) - T(x, \hat{\mathbf{n}}')]^2 &= v_F \frac{\partial}{\partial x} \int \frac{d\hat{\mathbf{n}}}{s_d} n_x T^2(x, \hat{\mathbf{n}}) \\ &= \frac{2Gv_F v_{d-1}}{G_0 N s_d} \frac{dT(x)}{dx}, \end{aligned} \quad (6.99)$$

where we have used Eqs. (6.23) and (6.96). By substitution of Eq. (6.99) into Eq. (6.25) and neglecting terms of order $\bar{\ell}/L$, we find

$$P = 2P_{\text{Poisson}} \int_0^L dx T(x)[1 - T(x)] \frac{dT(x)}{dx} = \frac{1}{3} P_{\text{Poisson}}, \quad (6.100)$$

independent of w .

References

- [1] V. A. Khlus, Zh. Eksp. Teor. Fiz. **93**, 2179 (1987) [Sov. Phys. JETP **66**, 1243 (1987)].
- [2] G. B. Lesovik, Pis'ma Zh. Eksp. Teor. Fiz. **49**, 513 (1989) [JETP Lett. **49**, 592 (1989)].
- [3] B. Yurke and G. P. Kochanski, Phys. Rev. B **41**, 8184 (1990).
- [4] M. Büttiker, Phys. Rev. Lett. **65**, 2901 (1990); Phys. Rev. B **46**, 12485 (1992).
- [5] Th. Martin and R. Landauer, Phys. Rev. B **45**, 1742 (1992).
- [6] C. W. J. Beenakker and M. Büttiker, Phys. Rev. B **46**, 1889 (1992).
- [7] K. E. Nagaev, Phys. Lett. A **169**, 103 (1992).
- [8] M. J. M. de Jong and C. W. J. Beenakker, Phys. Rev. B **46**, 13400 (1992) [Chapter 2].
- [9] Yu. V. Nazarov, Phys. Rev. Lett. **73**, 134 (1994).
- [10] B. L. Altshuler, L. S. Levitov, and A. Yu. Yakovets, Pis'ma Zh. Eksp. Teor. Fiz. **59**, 821 (1994) [JETP Lett. **59**, 857 (1994)].
- [11] F. Liefrink, J. I. Dijkhuis, M. J. M. de Jong, L. W. Molenkamp, and H. van Houten, Phys. Rev. B **49**, 14066 (1994).
- [12] O. N. Dorokhov, Solid State Commun. **51**, 381 (1984); Y. Imry, Europhys. Lett. **1**, 249 (1986); J. B. Pendry, A. MacKinnon, and P. J. Roberts, Proc. R. Soc. London Ser. A **437**, 67 (1992).
- [13] A. Shimizu and M. Ueda, Phys. Rev. Lett. **69**, 1403 (1992).
- [14] B. B. Kadomtsev, Zh. Eksp. Teor. Fiz. **32**, 943 (1957) [Sov. Phys. JETP **5**, 771 (1957)].
- [15] Sh. M. Kogan and A. Ya. Shul'man, Zh. Eksp. Teor. Fiz. **56**, 862 (1969) [Sov. Phys. JETP **29**, 467 (1969)].
- [16] I. O. Kulik and A. N. Omel'yanchuk, Fiz. Nizk. Temp. **10**, 305 (1984) [Sov. J. Low Temp. Phys. **10**, 158 (1984)].
- [17] C. W. J. Beenakker and H. van Houten, Phys. Rev. B **43**, 12066 (1991).
- [18] L. Y. Chen and C. S. Ting, Phys. Rev. B **43**, 4534 (1991).
- [19] J. H. Davies, P. Hyldgaard, S. Hershfield, and J. W. Wilkins, Phys. Rev. B **46**, 9620 (1992).
- [20] R. Landauer, in *Fundamental Problems in Quantum Theory*, edited by D. Greenberger (New York, Acad. Sci., to be published).
- [21] S. V. Gantsevich, V. L. Gurevich, and R. Katilius, Rivista Nuovo Cimento **2** (5), 1 (1979).

- [22] O. M. Bulashenko and V. A. Kochelap, *J. Phys. Condens. Matter* **5**, L469 (1993).
- [23] M. J. M. de Jong, *Phys. Rev. B* **49**, 7778 (1994) [Chapter 5].
- [24] C. W. J. Beenakker and H. van Houten, *Phys. Rev. Lett.* **63**, 1857 (1989).
- [25] Yu. V. Sharvin, *Zh. Eksp. Teor. Fiz.* **48**, 984 (1965) [*Sov. Phys. JETP* **21**, 655 (1965)].
- [26] O. N. Dorokhov, *Pis'ma Zh. Eksp. Teor. Fiz.* **36**, 259 (1982) [*JETP Lett.* **36**, 318 (1982)]; P. A. Mello, P. Pereyra, and N. Kumar, *Ann. Phys.* **181**, 290 (1988).
- [27] Y. P. Li, A. Zaslavsky, D. C. Tsui, M. Santos, and M. Shayegan, *Phys. Rev. B* **41**, 8388 (1990).
- [28] H. C. Liu, J. Li, G. C. Aers, C. R. Leavens, M. Buchanan, and Z. R. Wasilewski, *Phys. Rev. B* **51**, 5116 (1995).
- [29] S. Hershfield, J. H. Davies, P. Hyldgaard, C. J. Stanton, and J. W. Wilkins, *Phys. Rev. B* **47**, 1967 (1992); K.-M. Hung and G. Y. Wu, *ibid.* **48**, 14687 (1993); U. Hanke, Yu. M. Galperin, K. A. Chao, and N. Zou, *ibid.* **48**, 17209 (1993); A. N. Korotkov, *ibid.* **49**, 10381 (1994).
- [30] J. A. Melsen and C. W. J. Beenakker, **203**, 219 (1994).
- [31] C. W. J. Beenakker, B. Rejaei, and J. A. Melsen, *Phys. Rev. Lett.* **72**, 2470 (1994).
- [32] B. L. Altshuler, A. G. Aronov, and D. E. Khmel'nitskii, *J. Phys. C* **15**, 7367 (1982); A. Stern, Y. Aharonov, and Y. Imry, *Phys. Rev. B* **41**, 3436 (1990).
- [33] M. Büttiker, *Phys. Rev. B* **38**, 9375 (1988).
- [34] M. Büttiker (preprint).
- [35] See, e.g., H. van Houten, L. W. Molenkamp, C. W. J. Beenakker, and C. T. Foxon, *Semicond. Sci. Technol.* **7**, B215 (1992).
- [36] M. Devoret (private communication).
- [37] A. Steinbach, J. Martinis, and M. Devoret, *Bull. Am. Phys. Soc.* **40**, 400 (1995).
- [38] R. Landauer, *Phys. Rev. B* **47**, 16427 (1993).
- [39] R. C. Liu and Y. Yamamoto, *Phys. Rev. B* **49**, 10520 (1994); **50**, 17411 (1994).
- [40] H. Birk, M. J. M. de Jong, and C. Schönenberger (preprint).
- [41] M. Büttiker, in *Noise in Physical Systems and 1/f Fluctuations*, edited by P. H. Handel and A. L. Chung (AIP, New York, 1993).

The following text is extremely faint and illegible. It appears to be a list of items or a series of paragraphs, but the content cannot be discerned. The text is organized into approximately 20 numbered lines, starting from the top of the page and continuing down to the bottom. Each line contains a small number followed by a block of text that is too light to read.

Chapter 7

Hydrodynamic electron flow in high-mobility wires

7.1 Introduction

In his 1909 paper on gas flow through a capillary, Knudsen demonstrated that the ratio between the pressure drop over the capillary and the gas-flow rate first increases and then decreases with increasing density [1]. The mechanism is that with increasing density of gas particles, the number of interparticle collisions increases. At low densities (what is now known as the Knudsen transport regime) the gas particles move almost independently, so that the flow is mainly carried by particles with a large velocity parallel to the wire axis. These particles travel long distances before colliding with the wall. An occasional interparticle collision, although not resistive by itself because of momentum conservation, drives the parallel-moving particles towards the wall and shortens their trajectories between subsequent collisions with the wall. Therefore, in this regime, an enhancement of the interparticle collision-rate leads to increasing dissipation of forward particle momentum at the capillary walls. At higher densities, however, many interparticle collisions between subsequent particle-wall collisions occur, resulting in a random-walk behavior. As a consequence a laminar (Poiseuille) flow evolves, in which the effective particle-wall interaction is decreased.

Because of the analogy between classical diffusive transport of electrons and gas particles, one anticipates that a similar transition between Knudsen and Poiseuille flow may occur in electron transport. In this case electron-electron (e-e) scattering events are the analogue of collisions between gas particles [2]. Electron-electron scattering * has no influence on the electri-

*In this Chapter electron-electron (e-e) scattering only refers to *momentum-conserving*

cal resistivity of bulk materials, because it conserves the total momentum of the electron distribution. Effects of e-e scattering in the classical transport regime can only be expected in the resistivity of films and wires of high purity and small dimensions [3], where conditions similar to those leading to hydrodynamic gas flow can be realized. Typically, the sample width W should be smaller than or comparable to the impurity mean free path l_b of the bulk material. These two lengths should be compared to l_{ee} , the average length an electron covers between two subsequent e-e scattering events. When $l_{ee} > W$ one expects an increase of the resistivity with increasing e-e scattering rate, which is the electronic Knudsen effect. In contrast, when $l_{ee} < W$ the resistivity should decrease with increasing e-e scattering rate, due to electronic Poiseuille flow. The latter effect has been predicted by Gurzhi in 1963 [4] and is now known as the Gurzhi effect. Experimentally, it proved difficult to obtain reliable data on these effects, because dissipation mechanisms not present in gas flow usually prevent the occurrence of electronic Knudsen and Gurzhi flow regimes: First of all, electrons in a metal are scattered by impurities. Moreover, since the e-e scattering rate is usually varied by changing the lattice temperature of the sample, the induced effects are overwhelmed by electron-phonon interactions. Furthermore, an increase in temperature also enhances the *umklapp* electron-electron scattering rate, which adds to the bulk resistivity. Finally, deviations from an ideal spherical Fermi surface may hinder interpretation of experimental data.

Due to these complications, only a few experimental indications of e-e scattering effects have been found [3]. Most experiments use potassium, as an exemplary simple metal, which to a good approximation has a spherical Fermi surface [5]. However, the observed changes in the resistivity as a function of lattice temperature are limited to about 0.01% of the total resistivity, because of the small l_b and the onset of electron-phonon scattering. Yu *et al.* [6] have reported a negative temperature derivative of the resistivity ($d\rho/dT$) of potassium wires at temperatures around and below 1 K. However, an interpretation in terms of the Gurzhi effect was disputed [3], since at these temperatures $l_{ee} > W$. In later publications of the same group, it was shown that the negative $d\rho/dT$ can be attributed to metallurgical imperfections [7], and also Kondo-like effects in the resistivity were reported [8]. Observations of a positive $d\rho/dT$ in wider wires [7] were interpreted by Movshovitz and Wiser [9] as a Knudsen-like behavior due to the combination of e-e and electron-phonon collisions. A similar mechanism was proposed to explain an anoma-

scattering. These processes are also known as *normal* electron-electron scattering. In contrast, *umklapp* electron-electron scattering does not conserve momentum, and is explicitly denoted each time it is mentioned in the text. As we argue in the main text *umklapp* electron-electron scattering is absent in the two-dimensional electron gas, which is studied in this Chapter.

lously strong, positive $d\rho/dT$ in very thin potassium films [10,11]. However, until now there has been no observation of electronic Poiseuille flow, nor has there been an observation of a 'Knudsen maximum' in the resistance at the crossover between Knudsen and Gurzhi flow regimes [2].

In this Chapter, we present a theoretical study of Knudsen and Gurzhi transport phenomena in two-dimensional wires, based on a series of experiments carried out by L. W. Molenkamp at Philips Research Laboratories, Eindhoven. The wires used for the experiments are defined electrostatically in the two-dimensional electron gas (2DEG) of (Al,Ga)As heterostructures [12]. Using these devices to study hydrodynamic electron-flow offers several advantages: First, due to the high purity of the material and the resolution of electron-beam lithography one can easily reach the condition $l_b > W$. Second, *umklapp* electron-electron scattering is absent, because of the low electron density and the perfectly circular Fermi surface. Third, the electron-acoustic phonon coupling is weak in the (Al,Ga)As-2DEG system. This makes it possible to investigate the influence of e-e scattering *not* by changing the temperature T of the full sample, but by selectively changing the temperature T_e of the electrons inside the wire by passing a dc current I through the device. Previously, this current-heating technique has proven very useful for the study of thermoelectric phenomena in nanostructures [13,14]. The wires studied here are equipped with opposing pairs of quantum point-contacts in their boundaries. Since the thermopower of the point contacts is quantized [14], one can determine the electron temperature T_e in the wire, as a function of I , from a thermovoltage measurement [15]. The ability to modify selectively the e-e scattering rate allows a clear and unambiguous demonstration of hydrodynamic effects on the resistance of the wire.

In the experiments the differential resistance dV/dI versus I is measured.[†] In the resistance curves we can distinguish three regimes: 1) Starting from $I = 0$ we observe an increase in dV/dI with increasing I . This is attributed to the Knudsen effect. Resistance changes as large as 10% of the total resistance have been found. 2) Then there is a range where dV/dI decreases with increasing I , which we identify as the Gurzhi effect. In this range, one sees relative resistance changes up to 20%. 3) Upon increasing I one comes into a regime where dV/dI increases again. Here, the heating due to the applied current also affects the lattice temperature, so that the resistance increase can be attributed to enhanced electron-phonon scattering. At the crossover between regime 1) and 2) the Knudsen maximum is reached. The minimum in the resistance between regime 2) and 3) was the actual subject of one of Gurzhi's first papers [4].

[†]The relation between the resistance and the differential resistance at a current I is: $dV/dI = R + IdR/dI$.

In order to understand the experimental results, we have developed a theory based on the Boltzmann transport equation, which yields quantitative agreement with the experiments. In the first half of this century the Boltzmann approach has been applied to study size effects on the resistance of small conductors. The thin film case has been addressed by Fuchs [16] and the case of a thin wire by Dingle [17]. A particularly insightful method to solve the Boltzmann equation is due to Chambers [18], who has expressed the solution in terms of the effective mean free path the electron covers between either bulk-impurity or boundary collisions. These treatments consider partially diffusive boundary scattering, in which part of the electrons colliding with the boundaries is specularly reflected and the remainder is diffusely scattered. The boundary scattering is modeled by a constant specular coefficient. In a more realistic treatment by Soffer [19] the wave nature of the electrons has been taken into account and results in a specular coefficient which depends on the angle of incidence. In Ref. [20] it is shown that inclusion of the angle-dependent specular coefficient in a calculation of the resistivity of thin wires gives a more satisfactory agreement with experiments than Dingle's original theory.

The inclusion of e-e scattering in the Boltzmann approach to the resistivity of wires is not trivial and has been limited to a certain parameter range in most treatments. In the pioneering work by Gurzhi [4], the situation $l_{ee} \ll l_b, W$ is considered. It is shown that under these conditions the Boltzmann equation can be mapped on a Navier-Stokes type of equation. The opposite Knudsen regime $l_{ee} \gg l_b, W$ has been treated by Movshovitz and Wiser [9,10], who use the Chambers method to calculate effective mean free paths with the approximation that at most one e-e scattering event in each electron trajectory is taken into account. In Ref. [21] Gurzhi and coworkers provide an alternative approach for this regime, by solving the Boltzmann equation perturbatively. This also allows including specific features of the e-e scattering, such as the distinction between isotropic and small-angle scattering. We know of only two approaches that describe the resistivity of wires from the Knudsen up to the Gurzhi regime. The first is due to Black [22], who employs a Monte Carlo technique to calculate effective mean free paths in a wire. Although the numerical results are not so accurate because of the limited computer power available at the time, the Knudsen maximum in the resistivity is found. The results show similar behavior for isotropic and small-angle e-e scattering. The second approach is due to De Gennaro and Rettori [23]. They start from the Boltzmann equation and include e-e scattering by a scattering term due to Callaway [24] in which the electrons are relaxed towards a distribution with a net drift velocity. As pointed out by Gurzhi *et al.* [21], the final results of Ref. [23] are incorrect, because the spatial variation of the drift velocity is neglected.

Our theoretical description starts from a kinetic equation similar to that of Ref. [23]. We have obtained a self-consistent solution of the relevant Boltzmann equation. This is the first theory which provides an analytical expression for the Boltzmann distribution function for *any* set of l_{ee}, l_b, W . It will prove insightful to express the Boltzmann distribution function in terms of an effective mean free path. For the regime $l_{ee} \gg l_b, W$ our solution is equivalent to the results of Movshovitz and Wisner, so that we have provided a formal basis for their method of including e-e scattering events in the electron trajectories. Our approach is indeed able to describe the transition from Knudsen to Poiseuille flow. The transition can be illustrated by the evolution of the electron-flow profiles along the wire.

In the three-dimensional case, which has been addressed in most previous treatments, the e-e scattering rate of electrons in a thermal slice around the Fermi surface is proportional to T^2 , as follows from the well-known phase space argument [2]. For a 2DEG, instead, the e-e scattering rate is proportional to $T^2 \ln T$ [25, 26]. In a study by Laikhtman [27] of relaxation of injected electrons into a zero-temperature 2DEG it is found that small-angle scattering is important. Features of e-e scattering in a 2DEG are also discussed by Gurzhi and coworkers [28, 29]. The e-e scattering term which we use is first proposed by Callaway [24] and is not of a microscopic origin, but takes the main feature of e-e scattering, conservation of momentum, into account. As we will show, an attractive feature of this simplified scattering term is that it allows an exact (numerical) solution of the Boltzmann equation.

We have compared experiment with theory through a three step procedure: First, using the results of the point-contact thermometry we find T_c versus I . Then, using a formula due to Giuliani and Quinn [26] we calculate l_{ee} as a function of T_c . Finally, we determine the wire resistivity for the given l_{ee} from our Boltzmann approach. This has yielded quite a satisfactory agreement for both the Knudsen and the Gurzhi regime. The regime 3) in which phonon scattering due to the heating of the lattice increases the resistivity is outside the range of our theory. From the magnitude of the Knudsen effect we obtain information on the boundary-scattering parameters of the gate-defined wires.

A brief account of this work with an emphasis on the experiments has already been published [30]. Here, we present a more extensive discussion. Particular attention is paid to the derivation of the theoretical model and how its results can be compared with the experiments. The outline of this Chapter is as follows: In Section 7.2 the experiments are presented. Section 7.3 describes the theoretical model formulated in terms of a Boltzmann equation. The method of solution and the theoretical results including flow profiles are studied in Section 7.4. Section 7.5 discusses the comparison between theory and experiment. Finally, we conclude in Section 7.6. Appendix 7A and 7B detail some technical parts of the calculation.

7.2 Experimental observation of Knudsen and Gurzhi transport regimes

The devices are fabricated from two different (Al,Ga)As heterostructures containing a high-mobility 2DEG, grown at Philips Research Laboratories, Redhill, Surrey, UK. The wires used in the experiments are created by electrostatic confinement of the 2DEG using a split-gate technique. On top of the heterostructures, which are mesa-etched in the shape of a Hall bar, a pattern of TiAu gates is defined using electron-beam lithography. The lay-out of the TiAu gates is given schematically in the inset of Fig. 7.1. The wires have a lithographic width $W_{\text{lith}} \simeq 4.0 \mu\text{m}$ (note that due to electrostatic depletion the width W of the wires in the 2DEG is somewhat smaller), and a length L that varies between 20 and 120 μm . A quantum point-contact [12] is incorporated in each wire boundary. Three different types of samples have been used, whose particulars as to L , W , electron density n and mean free path l_b are summarized in Table 7.1. For transport measurements, the samples are kept in a cryostat at temperatures of 1.5 K and above, and at zero magnetic field. For reasons of sensitivity, the differential resistance of point contacts and wires is measured with standard low-frequency lock-in techniques, using a 100 μV ac voltage. All measurements are performed in a four-terminal geometry.

In order to adjust the electron temperature in the wires, a dc heating current $I \equiv I_{15}$ (typically an order of magnitude larger than the ac measuring current) is passed through the wire using Ohmic contacts 1 and 5. Because of power dissipation, the average kinetic energy of the electrons in the wire increases. Due to frequent e-e scattering events, the electron distribution-function in the wire thermalizes rapidly to a heated Fermi function at a temperature T_e , above the lattice temperature T . This increased electron temperature can be measured using the quantum point-contacts in the wire boundaries: since the electrons in the regions outside the wire remain at the same temperature as the lattice, a thermovoltage builds up across both point contacts AB and CD, which can be measured as a transverse voltage $V_{\text{trans}} \equiv V_6 - V_3$. Note that V_{trans} does not contain a contribution from the voltage drop along the wire, since point contacts AB and CD face each other. We thus have

$$V_{\text{trans}} \equiv V_6 - V_3 = (S_{\text{AB}} - S_{\text{CD}})(T_e - T), \quad (7.1)$$

where $S_{\text{AB(CD)}}$ denotes the thermopower of point contact AB(CD).

Like the electrical conductance, the thermopower S of a quantum point-contact exhibits a pronounced quantum size-effect [14, 31]: while the electrical conductance of the point contact varies stepwise with the voltage on the split-gates, the thermopower oscillates. The external gate voltage controls the

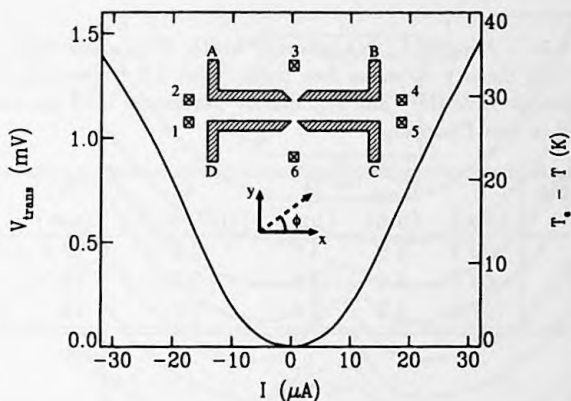


Figure 7.1: Dependence of the thermovoltage $V_{\text{trans}} \equiv V_6 - V_3$ and of the difference between the electron and the lattice temperature $T_e - T$ on the heating current I measured for wire I at $T = 1.5$ K. Point contact AB is adjusted for maximum, CD for zero thermopower. Inset: Schematic layout of the gates (hatched areas) used to define a wire with point-contact voltage probes. The wire width W is typically $4 \mu\text{m}$, the length L varies between 20 and $120 \mu\text{m}$. The crossed boxes denote ohmic contacts. The coordinates used for the theory are indicated.

number of one-dimensional subbands present below the Fermi energy in the point contact. When the Fermi energy inside the point contact falls in between two subbands, the conductance is quantized, and the thermopower $S \simeq 0$. However, when the Fermi energy inside the point contact exactly coincides with the bottom of the N -th subband, the conductance is in between the N -th and the $(N - 1)$ -th plateau, and the thermopower attains a maximum value, which for a step-function transmission probability of the point contact, is given by [31]

$$S = -\frac{k_B}{e} \frac{\ln 2}{N - \frac{1}{2}}, \quad (7.2)$$

if $N > 1$. The quantum oscillations in the thermopower of a quantum point-contact were predicted by Streda [31], and an experimental demonstration of the effect has been reported elsewhere [14]. Here, the effect is utilized to measure the electron temperature in the wire: point contact CD is adjusted on a conductance plateau, thus setting $S_{\text{CD}} \simeq 0$, and adjust point contact AB for maximum thermopower [$G_{\text{AB}} = 1.5 \times (2e^2/h)$, where $S_{\text{AB}} \simeq -40 \mu\text{V/K}$]. The result of such a measurement of V_{trans} as a function of dc heating current I , obtained for a wire of type I, is shown in Fig. 7.1. For the longer wires

Table 7.1: Length L , lithographic width W_{lith} , electrical width W , electron density n , mean free path l_b [at 1.5 K (sample I) and 1.8 K (sample II & III)], and specularity parameter α of the samples discussed in this Chapter.

Sample	L (μm)	W_{lith} (μm)	W (μm)	n (10^{11}cm^{-2})	l_b (μm)	α
I	20.2	3.9	3.5	2.2	12.4	0.6
II	63.7	4.0	3.6	2.7	19.7	0.7
III	127.3	4.0	3.6	2.7	19.7	0.7

a very similar behavior is found. In general, one finds that for $|I| \lesssim 20 \mu\text{A}$, and a lattice temperature $T \lesssim 2 \text{ K}$, the electron temperature T_e in the wire is approximately given by

$$T_e = T + (I/W)^2 \sigma^{-1} C, \quad (7.3)$$

where σ is the conductivity of the wire. The constant $C \simeq 0.05 \text{ m}^2\text{K}/\text{W}$. Evidently, such a quadratic dependence of T_e on I is exactly what one expects to a first approximation for Joule dissipation. For $|I| \gtrsim 20 \mu\text{A}$, the situation is more complicated since at these current levels also the lattice temperature starts to increase.

The hydrodynamic electron-flow effects that are the subject of this article are observed in the differential resistance $dV/dI \equiv dV_{24}/dI_{15}$ of the wires, as a function of dc heating current I . Experimental results obtained for wires I, II, and III for a series of lattice temperatures are given in Figs. 7.2 and 7.3. Also shown are theoretical results that will be discussed in Section 7.5. A strongly non-monotonic behavior of dV/dI is evident for all traces. This non-monotonic behavior in the differential resistance is the focus of this Chapter and we will show that it results from electronic Knudsen and Poiseuille flow.

A first remark we should make here is that in the high-mobility 2DEG quantum corrections to the resistance such as weak localization are not measurable at the temperatures involved. This means that the non-monotonic behavior must result from classical effects. Note further that for the low lattice-temperature results of Figs. 7.2 and 7.3 all three resistance regimes indicated in the Introduction can be observed: 1) Increasing dV/dI due to Knudsen flow, 2) decreasing dV/dI in the Gurzhi regime, and 3) a quasi-parabolically increasing dV/dI due to lattice heating. Only in the last regime, it is found from a nearby thermometer that the lattice temperature of the sample increases, implying that the quasi-quadratic behavior 3) is due to Joule heating

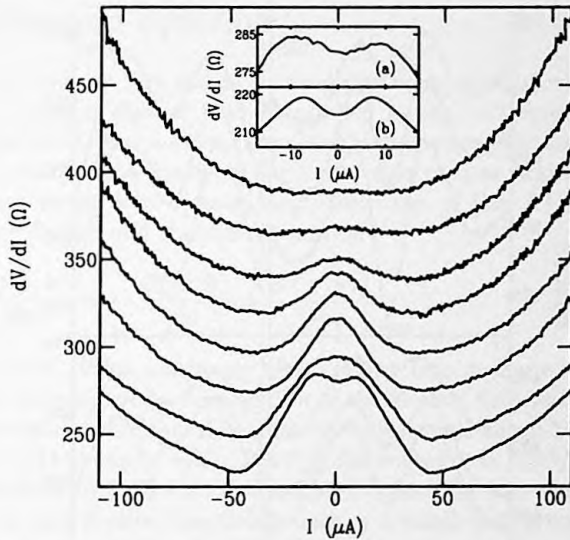


Figure 7.2: Differential resistance dV/dI of wire I as a function of current I for lattice temperatures $T = 24.7, 20.4, 17.3, 13.6, 10.4, 8.7, 4.4,$ and 1.5 K (from top to bottom). The upper panel (a) of the inset is a magnification of the $T = 1.5$ K result. The lower panel (b) displays the result of the theory described in Section 7.5.

of the lattice in combination with the linear increase of electron-phonon scattering [32]. Wire I (cf. Fig. 7.2) exhibits a smaller Knudsen effect (and only at the lowest lattice temperature studied) than wires II and III. As we will demonstrate below, this results from the smaller ratio l_b/W in wire I, compared to wires II and III. If the lattice temperature T is increased one observes in Fig. 7.2 two distinct effects. First, the $I = 0$ resistance increases. This is due to the decrease of l_b by additional electron-phonon scattering. Second, the hydrodynamic effects on the resistance disappear, the Knudsen effect at lower T than the Gurzhi effect. This is caused by the decrease of l_{ee} at $I = 0$ (where $T_e = T$) with increasing lattice temperature. Another point to notice in Fig. 7.3 is that the magnitude of the initial increase of dV/dI (the Knudsen effect) is twice as large for wire III as for wire II. This shows that the effect scales with the length of the wire and does not stem from e.g. the wire entrances.

To see whether the hydrodynamic electron-flow phenomena mentioned in Section 7.1 can indeed be responsible for the anomalous behavior of dV/dI , it is instructive to estimate for wire I the e-e scattering mean free path l_{ee} for a current $I = 15 \mu\text{A}$, i.e. in the regime of decreasing dV/dI . According to Eq. (7.3), $I = 15 \mu\text{A}$ corresponds to an electron temperature $T_e \approx 16$ K (for a

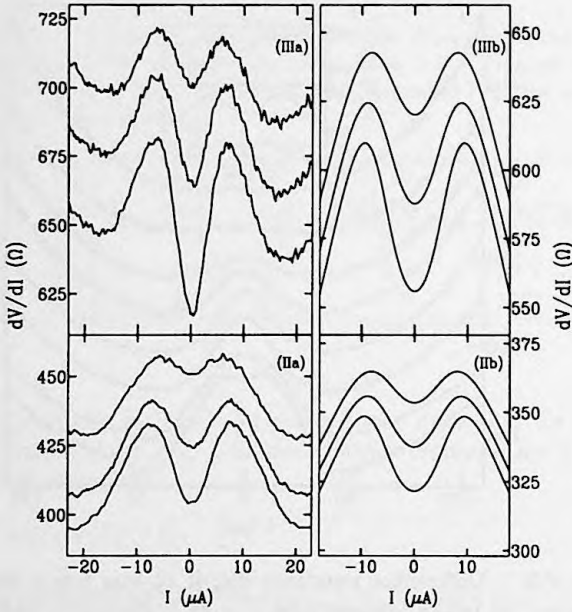


Figure 7.3: Differential resistance dV/dI vs. current I for wire II and III for lattice temperatures of (from top to bottom) $T = 4.5, 3.1,$ and 1.8 K. At higher current levels, dV/dI exhibits a quasi-quadratic increase with current, similar to that in Fig. 7.2. Left panel (IIa) and (IIIa): experimental traces; right panel (IIb) and (IIIb): results of calculations, see Section 7.5.

lattice temperature $T = 1.5$ K). We have $l_{ee} = v_F \tau_{ee}$, where v_F is the Fermi velocity, and τ_{ee} the e-e scattering time, given by [26, 33, 34]

$$\frac{1}{\tau_{ee}} = \frac{E_F}{\hbar} \left(\frac{k_B T_e}{E_F} \right)^2 \left[\ln \left(\frac{E_F}{k_B T_e} \right) + \ln \left(\frac{2q}{k_F} \right) + 1 \right]. \quad (7.4)$$

Here $q = me^2/2\pi\epsilon_r\epsilon_0\hbar^2$ is the Thomas-Fermi screening wave vector. We find $l_{ee} \approx 0.8 \mu\text{m}$, which is much smaller than W . In this limit, the electrons undergo a random-motion due to frequent e-e scattering events, and we assign, at this stage tentatively, the decrease in dV/dI to the Gurzhi effect. For currents below $8 \mu\text{A}$, dV/dI is positive. As $l_{ee} \approx 5 \mu\text{m} \approx W$ for $I = 8 \mu\text{A}$ and $T = 1.5$ K, the positive dV/dI occurs in the right current range for the electronic Knudsen effect. In the following Sections we will formulate our calculations that substantiate the assignment of the anomalous behavior of dV/dI to hydrodynamic electron flow.

7.3 Boltzmann equation

We study the electron flow inside a two-dimensional wire of width W in response to a constant electric field \mathbf{E} , applied in the x -direction, parallel to the wire. The 2DEG has an ideal circular Fermi surface. We look for a time-independent distribution function $f(\mathbf{r}, \mathbf{k})$ for electrons at position $\mathbf{r} = (x, y)$ and with wave vector $\mathbf{k} = k(\cos \varphi, \sin \varphi)$ (see inset of Fig. 7.1), which obeys the stationary Boltzmann transport equation

$$e\mathbf{E} \cdot \frac{\partial f(\mathbf{r}, \mathbf{k})}{\hbar \partial \mathbf{k}} + \mathbf{v} \cdot \frac{\partial f(\mathbf{r}, \mathbf{k})}{\partial \mathbf{r}} = \left. \frac{\partial f(\mathbf{r}, \mathbf{k})}{\partial t} \right|_{\text{scatt}}, \quad (7.5)$$

where the r. h. s. is the scattering term, taking into account both electron-impurity and e-e scattering. Application of the electric field leads to a disturbance of the distribution function from its equilibrium Fermi-Dirac distribution $f_0(\varepsilon) = 1/\{1 + \exp[(\varepsilon - E_F)/k_B T_e]\}$ for energy $\varepsilon = \hbar^2 k^2/2m = mv^2/2$ and with Fermi energy E_F . At not too high fields, the non-equilibrium part of the electron distribution function is only in a small shell around the Fermi surface. Therefore, and using the translational invariance along the x -axis, we write the distribution function as

$$f(\mathbf{r}, \mathbf{k}) = f_0(\varepsilon) + \left(-\frac{\partial f_0}{\partial \varepsilon} \right) \chi(y, \varphi). \quad (7.6)$$

Substitution of Eq. (7.6) into Eq. (7.5) yields in linear response

$$-e\mathbf{E} \cdot \mathbf{v} + \mathbf{v} \cdot \hat{\mathbf{y}} \frac{\partial \chi(y, \varphi)}{\partial y} = \left. \frac{\partial \chi(y, \varphi)}{\partial t} \right|_{\text{scatt}}, \quad (7.7)$$

where $\hat{\mathbf{y}}$ is the unit vector in the y -direction. We neglect the energy dependence of the velocity in the thermal region around the Fermi energy, so that $\mathbf{v} = v_F(\cos \varphi, \sin \varphi)$.

Once the distribution function has been evaluated, the current density can be calculated according to

$$\begin{aligned} \mathbf{j}(y) &= 2 \sum_{\mathbf{k}} f(\mathbf{r}, \mathbf{k}) e \mathbf{v}, \\ &= \int d\varepsilon \mathcal{D}(\varepsilon) \left(-\frac{\partial f_0}{\partial \varepsilon} \right) \int_0^{2\pi} \frac{d\varphi}{2\pi} \chi(y, \varphi) e \mathbf{v}, \\ &= e \mathcal{D} v_F \int_0^{2\pi} \frac{d\varphi}{2\pi} \chi(y, \varphi) \hat{\mathbf{v}}, \end{aligned} \quad (7.8)$$

with the two-dimensional density of states $\mathcal{D}(\varepsilon) = \mathcal{D} = m/\pi\hbar^2$ (assuming a two-fold spin-degeneracy) and with unit vector $\hat{\mathbf{v}} = (\cos \varphi, \sin \varphi)$.

Let us now specify the scattering terms on the r. h. s. of Eq. (7.7). The scattering by bulk impurities is assumed to be elastic and isotropic. This implies for the scattering term

$$\left. \frac{\partial \chi(\mathbf{y}, \varphi)}{\partial t} \right|_b = -\frac{\chi(\mathbf{y}, \varphi)}{\tau_b} + \frac{1}{\tau_b} \int_0^{2\pi} \frac{d\varphi'}{2\pi} \chi(\mathbf{y}, \varphi'), \quad (7.9)$$

where τ_b denotes the electron-impurity scattering time. Note that the second term on the r. h. s. of Eq. (7.9) representing the electrons scattered *into* (\mathbf{y}, φ) is omitted in many treatments of the Boltzmann transport equation. In these cases it is *a priori* assumed that the non-equilibrium density is zero. For completeness, we maintain this term here and show explicitly that it equals zero for our complete Boltzmann equation in Appendix 7A. For the e-e scattering term we follow Refs. [23, 24] (the Callaway ansatz)

$$\left. \frac{\partial \chi(\mathbf{y}, \varphi)}{\partial t} \right|_{ee} = -\frac{\chi(\mathbf{y}, \varphi)}{\tau_{ee}} + \frac{1}{\tau_{ee}} \int_0^{2\pi} \frac{d\varphi'}{2\pi} \chi(\mathbf{y}, \varphi') + \frac{m\mathbf{v} \cdot \mathbf{v}_{\text{drift}}(\mathbf{y})}{\tau_{ee}}, \quad (7.10)$$

with τ_{ee} the e-e scattering time and $\mathbf{v}_{\text{drift}}$ the net drift velocity. The e-e scattering term (7.10) implies that the electrons are relaxed towards a shifted distribution function $f(\mathbf{r}, \mathbf{k}) = f_0(\varepsilon - m\mathbf{v} \cdot \mathbf{v}_{\text{drift}})$. The second term on the r. h. s. of Eq. (7.10) again ensures the conservation of particle density. The drift velocity is related to the current density (7.8) according to $\mathbf{j}(\mathbf{y}) = ne\mathbf{v}_{\text{drift}}$ with the electron density $n = \mathcal{D}E_F$, so that Eq. (7.10) becomes

$$\left. \frac{\partial \chi(\mathbf{y}, \varphi)}{\partial t} \right|_{ee} = -\frac{\chi(\mathbf{y}, \varphi)}{\tau_{ee}} + \frac{1}{\tau_{ee}} \int_0^{2\pi} \frac{d\varphi'}{2\pi} \chi(\mathbf{y}, \varphi') (1 + 2\hat{\mathbf{v}}' \cdot \hat{\mathbf{v}}). \quad (7.11)$$

One readily verifies that this scattering term conserves the total momentum

$$\int_0^{2\pi} d\varphi \left. \frac{\partial \chi(\mathbf{y}, \varphi)}{\partial t} \right|_{ee} \hat{\mathbf{v}} = \mathbf{0}. \quad (7.12)$$

Actually, Eq. (7.11) is the simplest possible scattering term with this property. Since the scattering probability from direction φ to φ' is proportional to $1 + 2\hat{\mathbf{v}}' \cdot \hat{\mathbf{v}} = 1 + 2\cos(\varphi - \varphi')$, small-angle forward scattering ($\varphi - \varphi' \approx 0$) is most probable. The negative values for $\varphi - \varphi' \approx \pi$ correspond to the scattering of a non-equilibrium electron into a non-equilibrium hole in the opposite direction [28, 29].

For the scattering with the boundaries of the wire it is assumed that a fraction p of the incoming electrons is scattered specularly, whereas the remainder is scattered diffusely. In the original theories of size effects [16–18] the specularity coefficient p is taken to be angle independent. A microscopic model by Soffer [19] for the scattering of the incoming waves by the boundary roughness, finds that p depends on the angle of incidence

$$p(\varphi) = \exp[-(\alpha \sin \varphi)^2]. \quad (7.13)$$

This shows that electrons with grazing incidence ($\sin \varphi \rightarrow 0$) approach a unit probability of specular reflection. The parameter $\alpha = 4\pi\delta/\lambda_F$, depends on the ratio between δ , the root-mean-square boundary-roughness, and the Fermi wave vector.

The boundary conditions for the solution of the Boltzmann equation (7.7) are determined by demanding particle conservation. For the $y = 0$ boundary we have

$$\chi(0, \varphi) = p(\varphi)\chi(0, 2\pi - \varphi) + \int_{\pi}^{2\pi} \frac{d\varphi'}{\pi} [1 - p(\varphi')] \chi(0, \varphi'), \quad (7.14a)$$

if $\varphi \in [0, \pi]$, and for the $y = W$ boundary

$$\chi(W, \varphi) = p(\varphi)\chi(W, 2\pi - \varphi) + \int_0^{\pi} \frac{d\varphi'}{\pi} [1 - p(\varphi')] \chi(W, \varphi'), \quad (7.14b)$$

if $\varphi \in [\pi, 2\pi]$. The first term on the r. h. s. represents the specularly reflected electrons, the second term the ones that are diffusely scattered.

To proceed, the non-equilibrium part of the distribution function is written as [18]

$$\chi(y, \varphi) = eE \cos \varphi l_{\text{eff}}(y, \varphi). \quad (7.15)$$

Here, the effective mean free path $l_{\text{eff}}(y, \varphi)$ can be interpreted as the average length an electron at y in the direction φ has covered since the last boundary or impurity collision, as we show below. It is clear that a replacement of $l_{\text{eff}}(y, \varphi)$ in Eq. (7.15) by the bulk mean free path l_b yields the well-known bulk solution of the Boltzmann equation. Let us now introduce mean free paths for bulk-impurity scattering $l_b = v_F \tau_b$, for e-e scattering $l_{ee} = v_F \tau_{ee}$, and for the combination of those two $l^{-1} = l_b^{-1} + l_{ee}^{-1}$. As demonstrated explicitly in Appendix 7A, substitution of Eq. (7.15) into the combined Eqs. (7.7), (7.9), and (7.11) gives

$$\sin \varphi \frac{\partial l_{\text{eff}}(y, \varphi)}{\partial y} + \frac{l_{\text{eff}}(y, \varphi)}{l} = 1 + \frac{\tilde{l}_{\text{eff}}(y)}{l_{ee}}, \quad (7.16)$$

$$\bar{l}_{\text{eff}}(y) = \int_0^{2\pi} \frac{d\varphi}{\pi} \cos^2 \varphi l_{\text{eff}}(y, \varphi). \quad (7.17)$$

The integro-differential equation (7.16) constitutes a major simplification with respect to our starting point. This result is the basis of our further analysis in the following Section. The average effective mean free path $\bar{l}_{\text{eff}}(y)$ is directly proportional to the drift velocity

$$\mathbf{v}_{\text{drift}}(y) = \frac{e\mathbf{E}}{mv_F} \bar{l}_{\text{eff}}(y), \quad (7.18)$$

as follows from Eqs. (7.8), (7.15), and (7.17). The conductivity of the wire, defined according to $\mathbf{j} = \sigma \mathbf{E}$, is given by

$$\sigma = \frac{ne^2}{mv_F} \int_0^W \frac{dy}{W} \bar{l}_{\text{eff}}(y) = \frac{ne^2}{mv_F} L_{\text{eff}}. \quad (7.19)$$

The overall effective mean free path L_{eff} is directly proportional to the conductivity and will be used instead of σ below.

7.4 Theoretical results

As a preliminary application of Eq. (7.16) we briefly treat the case of transport through a bulk conductor. We thus seek a solution of the Boltzmann transport equation independent of the spatial coordinates. As a consequence of the disappearance of the y -dependence in Eq. (7.16) it follows that the effective mean free path l_{eff} is independent of φ as well, so that [from Eq. (7.17)] $\bar{l}_{\text{eff}} = l_{\text{eff}}$. The solution of Eq. (7.16) is then easily found

$$l_{\text{eff}} = \frac{1}{l^{-1} - l_{ee}^{-1}} = l_b. \quad (7.20)$$

Note, that substitution into Eq. (7.15) produces the ordinary bulk solution of the Boltzmann equation in the absence of e-e scattering. This solution is thus shown to be *independent* of the e-e scattering rate. It clearly demonstrates, that momentum-conserving e-e scattering does not influence the bulk conductivity.

Let us now return to the wire, for which e-e scattering can have a prominent influence on the conductivity. As shown in Appendix 7A, it follows from a symmetry argument that $l_{\text{eff}}(y, \varphi) = l_{\text{eff}}(y, \pi - \varphi)$ for all φ . It is then clear from Eq. (7.15) that the second term on the r. h. s. of both Eqs. (7.14a) and (7.14b) vanishes. The solution of Eq. (7.16) in combination with the boundary

conditions (7.14) can be written in the form of an integral equation. For clarity we first treat the case of completely diffusive boundary scattering $p = 0$. We then have for $\varphi \in [0, \pi]$

$$l_{\text{eff}}(y, \varphi) = \int_0^y \frac{dy'}{l \sin \varphi} \frac{y - y'}{\sin \varphi} e^{-(y-y')/l \sin \varphi} + \frac{y}{\sin \varphi} e^{-y/l \sin \varphi} + \int_0^y \frac{dy'}{l_{ee} \sin \varphi} \bar{l}_{\text{eff}}(y') e^{-(y-y')/l \sin \varphi}, \quad (7.21a)$$

and for $\varphi \in [\pi, 2\pi]$

$$l_{\text{eff}}(y, \varphi) = \int_y^W \frac{dy'}{l |\sin \varphi|} \frac{y' - y}{|\sin \varphi|} e^{-(y'-y)/l |\sin \varphi|} + \frac{W - y}{|\sin \varphi|} e^{-(W-y)/l |\sin \varphi|} + \int_y^W \frac{dy'}{l_{ee} |\sin \varphi|} \bar{l}_{\text{eff}}(y') e^{-(y'-y)/l |\sin \varphi|}. \quad (7.21b)$$

Equation (7.21) elucidates the meaning of the effective mean free path $l_{\text{eff}}(y, \varphi)$ as follows: Each electron arriving at y in the direction φ has covered a certain path length since the last diffusive scattering event. The first term on the r. h. s. of Eq. (7.21a) takes into account the length covered from the last scattering event at any y' in between 0 and y . The exponential factor gives the probability that the particle indeed reaches y without any additional scattering, whereas the distance covered is given by $(y - y')/\sin \varphi$. Note, that the scattering event at y' might have been either diffusive impurity scattering or e-e scattering. In the latter case, also the path before the scattering event must be accounted for, which is done by the last term. The second term denotes the contribution of electrons after diffusive boundary scattering. This interpretation of the solution of the Boltzmann equation is originally due to Chambers [18]. The above derivation demonstrates that this approach is still feasible when an e-e scattering term is included in the Boltzmann equation. However, the solution itself is certainly more difficult to obtain, since Eq. (7.21) must be solved self-consistently with Eq. (7.17).

Previously, Movshovitz and Wisner have evaluated the effect of e-e scattering on the resistivity of (three-dimensional) films [10] and wires [9] by calculating effective mean free paths with at most one e-e scattering event per trajectory. This approach (most extensively described in Ref. [10]) yields valid results for the Knudsen regime $l_{ee} \gg W, l_b$. We can treat this regime conveniently within our formalism by solving Eq. (7.21) perturbatively. Only

the result of the first two terms of Eq. (7.21) is substituted into the third term. One can prove that this procedure is precisely equivalent to that of Ref. [10].

In Appendix 7B we discuss a perturbative analysis for the two-dimensional wire with diffusive boundary scattering ($p = 0$). Here, we present the main results. For the limit $l_b \gg W$ the conductivity [see Eq. (7.19)] in the absence of e-e scattering is given by

$$L_{\text{eff}} = \frac{2W}{\pi} \left[\ln(l_b/W) + \ln 2 + \frac{1}{2} - \gamma \right], \quad (7.22)$$

where γ is Euler's constant (see Appendix 7B). In this limit the conductivity is directly proportional to the width, whereas the dependence on the mean free path is only present in the form of a logarithm. The perturbative solution allows us to calculate the first order correction to the conductivity due to e-e scattering. For the situation $l_{ee} \gg l_b \gg W$ we find

$$\Delta L_{\text{eff}} = -\frac{2Wl_b}{\pi l_{ee}}. \quad (7.23)$$

We note that the conductivity *decreases* due to the e-e scattering. This is the Knudsen effect. It is clear from Eqs. (7.22) and (7.23) that the larger l_b/W the more prominent this effect becomes. Previous calculations for this regime have yielded $\Delta L_{\text{eff}} = -\frac{3}{2}Wl_b/l_{ee}$ for a three-dimensional film of thickness W [10] and $\Delta L_{\text{eff}} \sim -(W^2/l_{ee}) \ln(l_{ee}/W)$ for a three-dimensional wire of diameter W [21].

For the opposite limiting regime $l_b \ll W$ the influence of the boundary scattering on the conductivity becomes quite small. From the analysis in Appendix 7B we obtain

$$L_{\text{eff}} = l_b - \frac{4l_b^2}{3\pi W}. \quad (7.24)$$

The diffusive boundary scattering yields a small negative correction to the bulk conductivity. The first order influence of e-e scattering in the regime $l_{ee} \gg W \gg l_b$ is

$$\Delta L_{\text{eff}} = \frac{4l_b^3}{15\pi W l_{ee}}. \quad (7.25)$$

Apparently, in this limit e-e scattering always *increases* the conductivity, which can be understood as follows: Since e-e scattering does not influence the bulk conductivity, it can only change the small negative correction due to the boundary scattering, represented by the second term in Eq. (7.24). Electron-electron scattering decreases this correction, which can be interpreted as the onset of the Gurzhi effect. For comparison, we again mention results for three

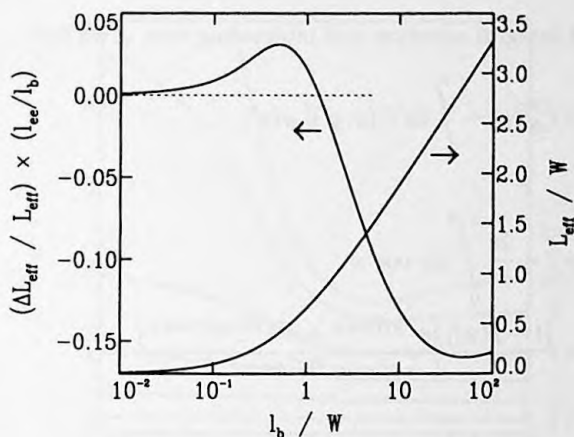


Figure 7.4: The conductivity L_{eff} in the absence of e-e scattering and the first order correction ΔL_{eff} due to e-e scattering against the bulk-impurity mean free path l_b . Results are for a two-dimensional wire with diffusive boundary scattering ($p = 0$) according to Eqs. (7.39) and (7.42), respectively.

dimensions: $\Delta L_{\text{eff}} = \frac{6}{35}(\frac{9}{8} - \ln 2)l_b^4/W^2 l_{ee}$ for a film (this can be calculated from the results given in Ref. [10]) and $\Delta L_{\text{eff}} \sim l_b^3/W l_{ee}$ for a wire [21].

The calculation of the first order correction on the conductivity due to e-e scattering thus displays an opposite behavior in the two limiting regimes. This raises the question how ΔL_{eff} crosses over from a positive value at small l_b/W to a negative value at large l_b/W . One expects that the negative correction to the conductivity appears when $l_b > W$. To substantiate this expectation, we have calculated the correction for the full regime of the ratio l_b/W . Details of this calculation are given in Appendix 7B. The results are presented in Fig. 7.4, which depicts both the conductivity in the absence of e-e scattering as well as the relative first order correction due to e-e scattering as a function of l_b/W . For the conductivity one observes a crossover from bulk-like behavior [Eq. (7.24)] to the logarithmic dependence of Eq. (7.22). The first order correction in the conductivity due to e-e scattering goes from a positive to a negative value. We find that the Knudsen effect is only present for $l_b \gtrsim 1.3W$.

The above results are valid for the regime of very low e-e scattering rate. However, in order to compare with the experiments we must also obtain solutions of Eq. (7.16) for the regime in which l_{ee} becomes comparable with and smaller than l_b, W . In addition, we need to incorporate the boundary condition (7.14) for arbitrary specularity coefficient $p(\varphi)$. By transforming Eq.

(7.16) into an integral equation and integrating over φ we find

$$\tilde{l}_{\text{eff}}(y) = \tilde{l}_{\text{eff}}^{(0)}(y) + \int_0^W dy' G(y, y') \tilde{l}_{\text{eff}}(y'), \quad (7.26)$$

$$\begin{aligned} \tilde{l}_{\text{eff}}^{(0)}(y) = l - \frac{2l}{\pi} \int_0^{\pi/2} d\varphi \cos^2 \varphi \\ \times \frac{[1 - p(\varphi)] [e^{-y/l \sin \varphi} + e^{-(W-y)/l \sin \varphi}]}{1 - p(\varphi) e^{-W/l \sin \varphi}}, \end{aligned} \quad (7.27)$$

$$\begin{aligned} G(y, y') = \frac{2}{\pi l_{ee}} \int_0^{\pi/2} d\varphi \frac{\cos^2 \varphi}{\sin \varphi} \left\{ e^{-|y-y'|/l \sin \varphi} \right. \\ \left. + \frac{p(\varphi) [e^{-(y+y')/l \sin \varphi} + e^{-(2W-y-y')/l \sin \varphi}]}{1 - p(\varphi) e^{-W/l \sin \varphi}} \right\}. \end{aligned} \quad (7.28)$$

These are the key equations which allow the evaluation of the conductivity for all values of l_{ee} , l_b , W , and p . Essentially, the $\tilde{l}_{\text{eff}}^{(0)}$ term is the two-dimensional equivalent of the Fuchs solution [16] of the Boltzmann equation. The second term in Eq. (7.26) is a classical electron propagator-function which takes the correction due to e-e scattering into account. Note, that the perturbative approach as described in Appendix 7B is equivalent to the approximation $\tilde{l}_{\text{eff}} = (1 + G)\tilde{l}_{\text{eff}}^{(0)}$. However, for larger values of l_{ee} Eq. (7.26) must be solved self-consistently according to $(1 - G)\tilde{l}_{\text{eff}} = \tilde{l}_{\text{eff}}^{(0)}$. This can be achieved numerically by discretizing the y -axis, so that Eq. (7.26) becomes a matrix equation. This scheme allows the evaluation of the solution \tilde{l}_{eff} with a precision which is only limited by the available computer power. We have used at least 400 grid points in our calculations to obtain sufficient precision.

In Fig. 7.5 the conductivity for a wire with diffusive boundary scattering ($p = 0$) is plotted against the e-e scattering length for various values of the bulk-impurity mean free path. For a wide wire ($l_b/W = 0.2$) the conductivity remains approximately constant over the full range of l_{ee}/W . The cases $l_b/W = 0.5, 1$ display a monotonous increase of L_{eff} with decreasing l_{ee} , the Gurzhi effect. Only for wires of width smaller than the mean free path ($l_b/W = 2, 5, 10$) can both the Knudsen *and* the Gurzhi regimes be reached: an initial decrease followed by an increase of L_{eff} with decreasing l_{ee} is found from the calculation. The Knudsen minimum in the conductivity is reached at

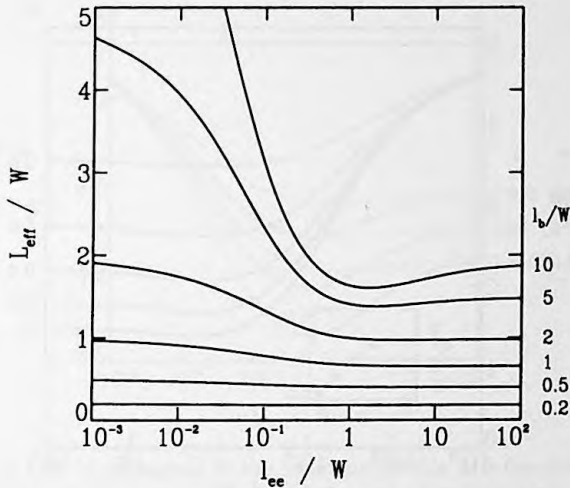


Figure 7.5: The conductivity L_{eff} of a wire with diffusive boundary scattering ($p = 0$) against the e-e scattering mean free path l_{ee} for various bulk-impurity mean free paths l_b .

$l_{ee} \simeq W$. It is clear that both the Knudsen effect and the Gurzhi effect on the conductivity become more prominent for larger ratios l_b/W . We furthermore note that the conductivity saturates to its bulk value ($L_{\text{eff}} \rightarrow l_b$) when the e-e scattering rate becomes high ($l_{ee} \rightarrow 0$), which reflects the vanishing influence of the boundaries in this regime.

Let us now have a closer look at the effect of the boundary scattering. Fig. 7.6 displays the conductivity of a $l_b/W = 5$ wire for various angle-independent specularly coefficients p . The conductivity increases with decreasing diffusive boundary scattering. Besides this, we observe that for all $p < 1$ both the Knudsen and the Gurzhi effect are found. If the boundary scattering is fully specular ($p = 1$), $L_{\text{eff}} = l_b$ regardless of the amount of e-e scattering. Essentially, the situation of specular boundary scattering is equivalent to the bulk case, in which the effects of e-e scattering are absent. It is easily checked that $\tilde{l}_{\text{eff}}(y) = l_b$ solves Eq. (7.26) for $p = 1$. The relative conductivity change at the Knudsen maximum $\Delta L_{\text{eff}}/L_{\text{eff}}$ (with respect to the $l_{ee} = \infty$ value) is depicted in the inset to Fig. 7.6. It decreases when the boundary scattering becomes less diffuse.

As we have remarked above, the modeling of the boundary scattering by a constant specularly coefficient is only approximate. Soffer [19] has shown that a better description is given by the angle-dependent specularly coefficient of Eq. (7.13). Since the hydrodynamic effects in the conductivity are caused

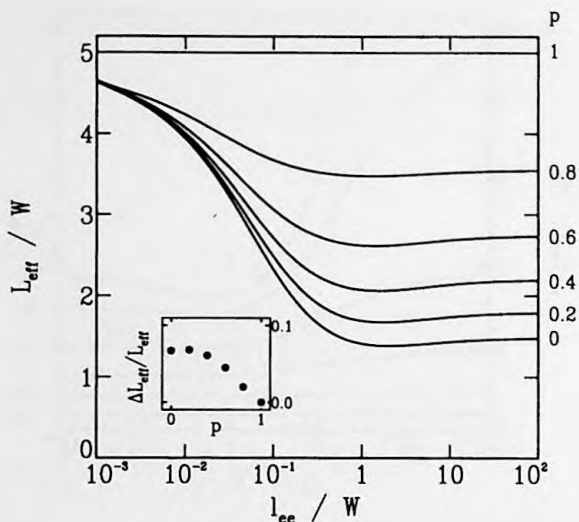


Figure 7.6: The conductivity L_{eff} of a wire with a mean free path $l_b = 5W$ against the e-e scattering mean free path l_{ee} for various specularity coefficients p . The inset shows the relative change in the conductivity at the Knudsen maximum (which corresponds to the *minimum* in the conductivity).

by the interplay between the e-e scattering and the boundary scattering, one may expect that the angle dependence leads to differences in the magnitude of the Knudsen and Gurzhi effects. Results comparing both models of boundary scattering are shown in Fig. 7.7. The parameters in both models are adjusted to yield equal conductivity in the absence of e-e scattering. It is clear from Fig. 7.7 that the angle-dependent scattering leads to a much larger Knudsen effect. The reason is as follows: The conductivity is mainly determined by electrons that move nearly parallel to the wire axis. These electrons hit the boundaries at grazing incidence. In the Soffer model electrons at grazing incidence experience a rather high boundary specularity. However, to have an equal conductivity for both models in the absence of e-e scattering, the boundary scattering of electrons with larger incoming angles must be more diffusive in the Soffer model. It is clear that this enhances the Knudsen effect.

So far, we have focused solely on the conductivity. More insight in the microscopic processes inside the wire can be obtained from the solution $\tilde{l}_{\text{eff}}(y)$. Since it is proportional to the drift velocity according to Eq. (7.18), it represents the flow profile across the wire. Profiles for $l_b = 5.5W$ and $\alpha = 0.7$ and various amounts of e-e scattering are shown in Fig. 7.8. In the absence

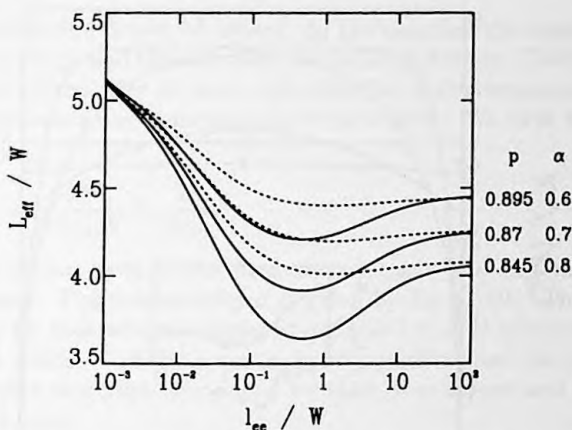


Figure 7.7: Comparison of the conductivity L_{eff} as a function of l_{ee} for constant boundary-scattering coefficients (dotted curves) and for angle-dependent coefficients (solid lines) according to Eq. (7.13). To have approximately equal conductivity in the absence of e-e scattering the comparison is between (top to bottom) $p = 0.895, 0.87, 0.845$ and $\alpha = 0.6, 0.7, 0.8$, respectively. The bulk-impurity mean free path $l_b = 5.5W$.

of e-e scattering the drift velocity is almost constant as a function of y . On increasing the e-e scattering rate, the flow profile over the full cross section of the wire shifts downwards due to the Knudsen effect: Occasional e-e scattering events bend the electrons moving parallel to the wire axis towards the boundaries. This effectively decreases the drift velocity and thus the conductivity. However, for smaller l_{ee} values the flow profile develops a distinct curvature. This indicates that electrons near the boundaries experience more friction due to diffusive boundary scattering than electrons in the middle of the wire. The eventual result of this change in the flow profile is that the conductivity increases with increasing e-e scattering rate, the Gurzhi effect. This behavior becomes more pronounced upon decreasing l_{ee} , and the profile becomes similar to the classical, laminar Poiseuille flow. Ultimately, however, the flow is limited by the bulk-impurity scattering, as shown by the curve in Fig. 7.8 for the smallest value of l_{ee} . The electrons in the middle of the wire have a drift velocity equal to the bulk value, whereas close to the boundaries the drift velocity goes to zero.

In this Section we have demonstrated which flow phenomena may occur in a wire with both diffusive impurity scattering as well as non-resistive e-e scattering. In the next Section we present how the theory can be brought into agreement with the experiments.

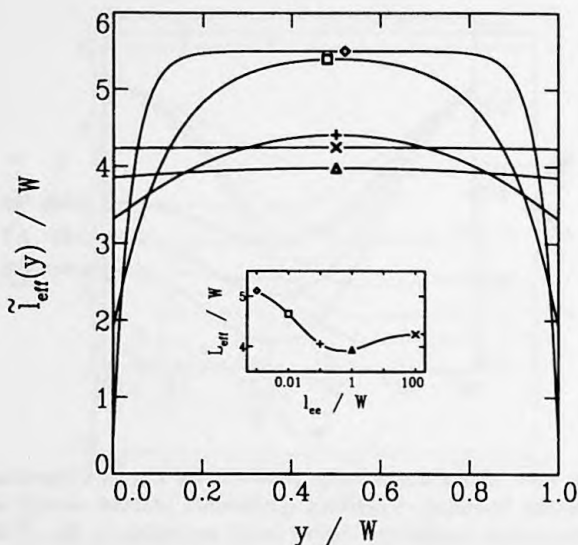


Figure 7.8: Velocity profiles inside the wire show how the flow changes from the Knudsen up to the Gurzhi regime. Depicted are the (normalized) drift velocity $\bar{l}_{\text{eff}}(y)$ as a function of the transverse coordinate y for $l_{ee}/W = 100$ (\times), 1 (Δ), 0.1 (+), 0.01 (\square), and 0.001 (\diamond). The inset shows the conductivity L_{eff} as a function of the e-e scattering length l_{ee} and the symbols that indicate to which value each flow profile corresponds. Results are for the bulk mean free path $l_b = 5.5W$ and for angle-dependent boundary scattering with $\alpha = 0.7$.

7.5 Comparison between experiment and theory

Now that we have found that both the Knudsen and the Gurzhi effect as observed in the experiments, cf. Section 7.2, can at least qualitatively be understood by the theory of the previous Sections, we wish to make a more quantitative comparison. Note, that the experimental traces are dV/dI versus I curves, whereas the theoretical results provide L_{eff} as a function of l_b , l_{ee} , and W .

The resistance R of the sample, as measured in the experiment, is due to two contributions. First, there is the resistance of the wire itself. As shown in Chapter 5, this is equal — to a good approximation — to the sum of the Drude resistance and the Sharvin contact resistance [35]. The second contribution R_0 is due to the unbounded regions in the 2DEG between the Ohmic contacts and the entrance of the wire (see inset to Fig. 7.1). Note, that in an ideal four-probe measurement, the contacts should be so close to the entrance of the wire,

that this contribution would be absent. In the samples, the typical distance between the contacts and the wire is on the order of 200 μm . The actual value of R_0 may vary from wire to wire, and with the lattice temperature. From previous experiments one estimates $R_0 \approx 60 - 90 \Omega$. We thus have for the resistance [36]

$$R = R_0 + \frac{h\pi}{2e^2k_F W} + \frac{L}{W\sigma}, \quad (7.29)$$

in which the second term is the Sharvin resistance [35] and the third the Drude resistance. The conductivity σ is given by Eq. (7.19). The values for L , W , n , and l_b for each wire are displayed in Table 7.1. Due to the electrostatic depletion, the width W of the wires is slightly smaller than the lithographic width of the gate structure. For wire I we take $W = 3.5 \mu\text{m}$ and for wires II and III $W = 3.6 \mu\text{m}$.

The theoretical L_{eff} versus l_{ee} curve can now be transformed into an R versus I curve in a three step procedure. First, we apply Eq. (7.3), which gives the electron temperature T_e against I . Then, l_{ee} is determined as a function of T_e through Eq. (7.4). Finally, the Boltzmann theory provides L_{eff} (and thus σ) for the given l_{ee} , so that the resistance is given by Eq. (7.29). There is a little subtlety here, since the resulting conductivity σ is already used in Eq. (7.3). One could adopt two approaches: The first would be to neglect the dependence of σ here and simply use its $I = 0$ value in Eq. (7.3). The second approach, which we have applied, is to find a self-consistent value of σ and l_{ee} in a numerical procedure. Actually, this only slightly changes the I -axis. From the R versus I curve the differential resistance dV/dI versus I is found. It should be mentioned that we do expect some deviations in the I -axis, because of the approximate nature of Eq. (7.3). Because of the limited validity of Eq. (7.3) we can only treat the regime $|I| < 20 \mu\text{A}$. This is sufficient since we only aim to model the Knudsen and the Gurzhi regimes. The dissipative behavior due to the heating of the lattice, which is observed for higher currents in Figs. 7.2 and 7.3, is not treated in the comparison.

In Fig. 7.9 we apply the above analysis for the differential resistance of wire II at $T = 1.8 \text{ K}$. The experimental curve is a blow-up of the lowest temperature trace in Fig. 7.3. The theoretical curves are for various boundary-scattering parameters and correspond to the plots in Fig. 7.7 (since $l_b = 5.5W$). It should be stressed, that R_0 is not included in the theoretical curves, since its precise value is not known. This will be the case for all the comparisons. Clearly the numerical results for a constant specular coefficient display a far too weak Knudsen and Gurzhi behavior. Both effects can be increased by decreasing p , but this also enhances the $I = 0$ resistance to unreasonable values. The plots in which the boundary scattering is taken to be angle dependent — using Eq. (7.13) — display a much better resemblance

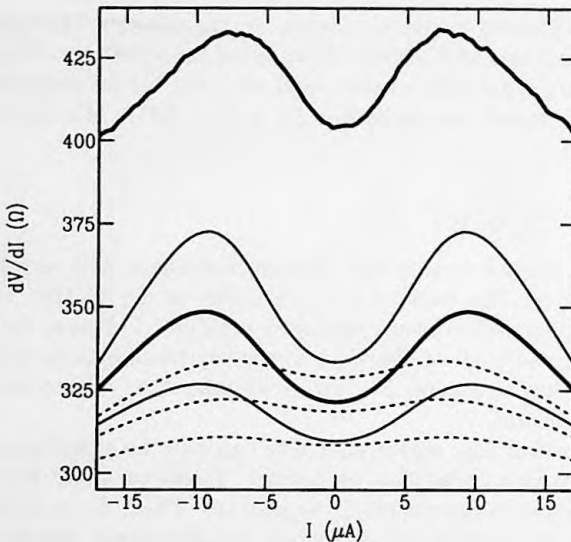


Figure 7.9: Differential resistance dV/dI versus current I for wire II. The top curve is the experimental result at $T = 1.8$ K, as shown for a larger current range in Fig. 7.3. The other curves are theoretical results for various boundary-scattering parameters. The dotted lines are calculated with a constant specularity coefficient $p = 0.845, 0.87, 0.895$ (top to bottom). The solid lines are calculated for angle-dependent boundary scattering, with $\alpha = 0.8, 0.7, 0.6$ (top to bottom). Best agreement with experiment is found for $\alpha = 0.7$ (thick curve).

with the experiment. The experiments thus clearly indicate the validity of Soffer's model [19] for boundary scattering in split-gate defined wires. We find the best agreement with $\alpha = 0.7$. At $I = 0$ the difference between the experimental and the theoretical resistance is 83Ω , which is within the right range of R_0 .

We have applied the same analysis to the $T = 1.5$ K result of wire I. As noted above, the magnitude of the Knudsen effect is much smaller than in wires II and III due to the lower ratio of $l_b/W = 3.5$. This is indeed what is found in the theoretical calculation. The comparison between theory and experiment is given in the inset to Fig. 7.2. We have found that for wire I $\alpha = 0.6$ yields the best agreement.

The values of α that emerge from the comparisons imply that the root-mean-square boundary roughness of the gate-defined wires $\delta \approx 2.5$ nm and that approximately 80% of the boundary scattering is specular. This is consistent with earlier magneto-resistance and electron-focusing experiments in

gate-defined 2DEG systems [12,37]. Note, that in the potassium-wires used for hydrodynamic electron-flow experiments the boundary scattering is much more diffusive, values of $\alpha \approx 25$ are used [9].

Finally, we investigate the resistance behavior when the lattice temperature is increased. The experimental curves for wire II and III for $T = 1.8, 3.5,$ and 4.5 K are given in Fig. 7.3. The change in lattice temperature both influences Eq. (7.3) as well as the bulk mean free path l_b , which also includes some electron-phonon scattering. The difference in the $I = 0$ resistance for the three temperatures are thus caused by changes in l_b and in l_{ee} . Both increase the resistance with increasing lattice temperature. The decrease in l_{ee} causes a part of the Knudsen correction to be already incorporated in the $I = 0$ value of dV/dI . From temperature-dependent mobility measurements one has $l_b = 18.5 \mu\text{m}$ at $T = 3.1$ K and $l_b = 17.1 \mu\text{m}$ at $T = 4.5$ K. Note, that for the theoretical analysis at $T = 3.1, 4.5$ K we push Eq. (7.3) slightly beyond its range of validity. A comparison with theory for $\alpha = 0.7$ is presented in Fig. 7.3. For both wire II and wire III, the theoretical curves are quite similar to the experiments as to shape and amplitude. The decrease in the Knudsen effect with increasing lattice temperature is indeed found. We do observe, however, a difference with the experiment for the additional offset between the individual curves. This is probably caused by a temperature dependence in R_0 .

7.6 Discussion and conclusions

The experiments have provided an unambiguous demonstration of the occurrence of Knudsen and Gurzhi flow regimes in electron transport. The existence of these transport regimes has already been anticipated in the 1960's [2, 4]. Although some aspects of hydrodynamic electron flow have been observed in potassium wires [6-8], it is the high-mobility obtained in (Al,Ga)As heterostructures in combination with nano-lithography techniques that has made the observation of the complete transition from the Knudsen to the Gurzhi flow regime accessible. The current-heating technique appears to be an essential tool, by which the e-e scattering rate can be varied, while keeping the other types of scattering unaltered. Due to the point-contact thermometry we are able to determine the electron temperature inside the wire as a function of the current. Although hydrodynamic electron flow has been predicted many years ago, its actual observation in the two-dimensional wires and the sheer size of the effects is quite astonishing.

We have developed a theory based on the Boltzmann transport equation. The theory is more complex than that for gas-flow because of the presence of bulk-impurity scattering. Most previous theoretical work [4, 9, 10, 21] is only

applicable to certain limiting flow regimes. Our approach is more general, in the sense that it provides the conductivity for the complete flow regime, i.e. for any value of the wire width, the e-e scattering length, and the bulk-impurity mean free path. It should be mentioned that we have made two essential simplifications in our Boltzmann approach. First, we assume isotropic impurity scattering instead of the small-angle scattering known to occur in a 2DEG. Second, we apply a simple e-e scattering term due to Callaway [24], which only takes into account the conservation of the total momentum. At this moment, we do not see a method of solution of the Boltzmann equation with on the one hand more realistic scattering terms, and which is on the other hand applicable to the complete transport regime. However, our method already shows how complex the flow behavior becomes due to the combination of resistive impurity scattering as well as partly diffusive boundary scattering and non-resistive e-e scattering.

A quantitative comparison between experiment and the Boltzmann theory can be made, since the electron temperature and thus the e-e scattering length inside the wire can be inferred from experiment. The obtained agreement is quite good. This proves that in spite of its simplifications our Boltzmann theory contains the essential physical ingredients to describe the experiments. Our results show that the Soffer model [19] for angle-dependent boundary scattering is more appropriate to describe the scattering with the gate-defined wire boundaries than a constant specular coefficient. Apart from the determination of the specular coefficient, our comparison is only based on experimental data and contains no fitting.

Recently, Gurzhi *et al.* have theoretically studied the angle-dependence of e-e scattering in a 2DEG [29]. They state that the resistance decrease observed in the experiments is due to a new hydrodynamic effect: Scattering between electrons with almost opposite momenta results in a one-dimensional diffusion of carriers. This theory is not suitable for a quantitative comparison with the experiments, but predicts qualitatively that the resistance decrease already starts for $l_{ee} \gg W$. However, in the experiments the resistance increases up to the Knudsen maximum, at which we estimate $l_{ee} \approx W$. This fact and the good agreement on the basis of our theory, in which no specific details of the e-e scattering are taken into account, do not support the conclusions of Ref. [29].

It would be of interest to perform further experiments on hydrodynamic electron flow. Promising areas of investigation are the influence of more diffusive boundary scattering, e.g. in wires defined by reactive ion etching or ion exposure, and the application of a magnetic field. The theoretical analysis given here can be adopted in a straightforward manner to describe the transition from Knudsen to Gurzhi flow in three-dimensional systems.

Appendix 7A

We show how Eq. (7.16) can be derived. The combination of the Boltzmann equation (7.7) with the impurity (7.9) and the e-e (7.11) scattering terms yields

$$\begin{aligned}
 -eE v_F \cos \varphi + v_F \sin \varphi \frac{\partial \chi(y, \varphi)}{\partial y} &= -\frac{\chi(y, \varphi)}{\tau} + \frac{1}{\tau} \int_0^{2\pi} \frac{d\varphi'}{2\pi} \chi(y, \varphi') \\
 &+ \frac{1}{\tau_{ee}} \int_0^{2\pi} \frac{d\varphi'}{\pi} \cos(\varphi - \varphi') \chi(y, \varphi'), \quad (7.30)
 \end{aligned}$$

with $\tau^{-1} = \tau_b^{-1} + \tau_{ee}^{-1}$. For the time-independent case the drift velocity has no component in the y -direction

$$\int_0^{2\pi} \frac{d\varphi}{\pi} \sin \varphi \chi(y, \varphi) = 0. \quad (7.31)$$

As a result the $\cos(\varphi - \varphi')$ in the last term in Eq. (7.30) can be replaced by $\cos \varphi \cos \varphi'$. Substitution of the parametrization (7.15) yields

$$\begin{aligned}
 -\cos \varphi + \cos \varphi \sin \varphi \frac{\partial l_{\text{eff}}(y, \varphi)}{\partial y} &= \\
 -\frac{\cos \varphi l_{\text{eff}}(y, \varphi)}{l} + \frac{1}{l} \int_0^{2\pi} \frac{d\varphi'}{2\pi} \cos \varphi' l_{\text{eff}}(y, \varphi') \\
 + \frac{\cos \varphi}{l_{ee}} \int_0^{2\pi} \frac{d\varphi'}{\pi} \cos^2 \varphi' l_{\text{eff}}(y, \varphi'). \quad (7.32)
 \end{aligned}$$

Analysis of Eq. (7.32) shows that $l_{\text{eff}}(y, \varphi)$ and $l_{\text{eff}}(y, \pi - \varphi)$ obey precisely the same equation. In addition the boundary conditions (7.14) are equal. Due to this symmetry we have

$$l_{\text{eff}}(y, \varphi) = l_{\text{eff}}(y, \pi - \varphi). \quad (7.33)$$

In combination with Eq. (7.15) it follows that the non-equilibrium density is zero for all y

$$\int_0^{2\pi} d\varphi \chi(y, \varphi) = eE \int_0^{2\pi} d\varphi \cos \varphi l_{\text{eff}}(y, \varphi) = 0. \quad (7.34)$$

Thus, the second term on the r. h. s. of Eq. (7.32) vanishes. [This equally applies to the second terms on the r. h. s. of Eqs. (7.9), (7.11), and (7.14).] As a result Eq. (7.32) leads to the integro-differential equation (7.16) of the main text.

Appendix 7B

In this Appendix it is shown how some results presented in Section 7.4 can be obtained. We study the conductivity and its first order correction due to e-e scattering for a wire with diffusive boundary scattering ($p = 0$). By multiplication of Eq. (7.21) with $\cos^2\varphi$ and integration over φ one finds

$$\begin{aligned} \bar{l}_{\text{eff}}(y) = l - \frac{2l}{\pi} \int_0^{\pi/2} d\varphi \cos^2\varphi \left[e^{-y/l \sin\varphi} + e^{-(W-y)/l \sin\varphi} \right] \\ + \frac{2}{\pi l_{ee}} \int_0^W dy' \int_0^{\pi/2} d\varphi \frac{\cos^2\varphi}{\sin\varphi} e^{-|y-y'|/l \sin\varphi} \bar{l}_{\text{eff}}(y'). \end{aligned} \quad (7.35)$$

In the limit of very small e-e scattering rate ($l_{ee} \gg l_b, W$) the next step is to solve Eq. (7.35) perturbatively. The first two terms of Eq. (7.35) are substituted into the third term. An additional integration over y then yields the conductivity [cf. Eq. (7.19)]

$$L_{\text{eff}} = l - \frac{4l^2}{\pi W} I(l/W) + \frac{l^2}{l_{ee}} - \frac{8l^3}{\pi l_{ee} W} I(l/W) + \frac{8l^3}{\pi^2 l_{ee} W} K(l/W), \quad (7.36)$$

$$I(\lambda) = \int_0^1 du u \sqrt{1-u^2} \left(1 - e^{-1/\lambda u} \right), \quad (7.37)$$

$$\begin{aligned} K(\lambda) = \int_0^1 du u \sqrt{1-u^2} \int_0^1 dv v \sqrt{1-v^2} \\ \times \left[\frac{1 - e^{-1/\lambda u - 1/\lambda v}}{u+v} + \frac{e^{-1/\lambda u} - e^{-1/\lambda v}}{u-v} \right]. \end{aligned} \quad (7.38)$$

In the absence of e-e scattering ($l_{ee} = \infty$) the conductivity is given by [12]

$$L_{\text{eff}} = l_b - \frac{4l_b^2}{\pi W} I(l_b/W). \quad (7.39)$$

The first order correction due to e-e scattering can be found by subtracting Eq. (7.39) from (7.36) and expanding $l = l_b - l_b^2/l_{ee}$. The result can be evaluated analytically in two limits. For a very wide wire $l_b \ll W$ we use the results

$$\lim_{\lambda \rightarrow 0} I(\lambda) = \frac{1}{3}, \quad (7.40a)$$

$$\lim_{\lambda \rightarrow 0} K(\lambda) = \frac{\pi}{30}, \quad (7.40b)$$

which provide Eqs. (7.24) and (7.25). In the opposite limiting regime of a very narrow wire ($l_b \gg W$) the integrals (7.37) and (7.38) are more complex. We have obtained the following series expansions

$$\lim_{\lambda \rightarrow \infty} I(\lambda) = \frac{\pi}{4\lambda} - \frac{1}{2\lambda^2} (\ln 2\lambda + \frac{1}{2} - \gamma) + \mathcal{O}(\lambda^{-3}), \quad (7.41a)$$

$$\lim_{\lambda \rightarrow \infty} K(\lambda) = \frac{\pi^2}{8\lambda} - \frac{\pi}{2\lambda^2} (\ln 2\lambda + \frac{1}{2} - \gamma) + \mathcal{O}(\lambda^{-3}), \quad (7.41b)$$

where $\gamma \simeq 0.577$ is Euler's constant. These results yield Eqs. (7.22) and (7.23).

The first order correction due to e-e scattering in between these two regimes can be evaluated by subtracting Eq. (7.39) from (7.36). We then have

$$\Delta L_{\text{eff}} = \frac{l_b}{l_{ee}} \left[\frac{8l_b^2}{\pi^2 W} K(l_b/W) - \frac{4l_b}{\pi} J(l_b/W) \right], \quad (7.42)$$

$$J(\lambda) = \int_0^1 du \sqrt{1-u^2} e^{-1/\lambda u}. \quad (7.43)$$

By numerical integration of I , J , and K the plots in Fig. 7.4 are obtained.

References

- [1] M. Knudsen, *Ann. Phys.* **28**, 75 (1909).
- [2] J. M. Ziman, *Electrons and Phonons* (Oxford University Press, Oxford, 1960).
- [3] M. Kaveh and N. Wiser, *Adv. Phys.* **33**, 257 (1984).
- [4] R. N. Gurzhi, *Zh. Eksp. Teor. Fiz.* **44**, 771 (1963) [*Sov. Phys. JETP* **17**, 521 (1963)]; *Zh. Eksp. Teor. Fiz.* **46**, 719 (1964) [*Sov. Phys. JETP* **19**, 490 (1964)]; *Usp. Fiz. Nauk.* **94**, 689 (1968) [*Sov. Phys. Usp.* **11**, 255 (1968)].
- [5] J. Bass, W. P. Pratt, Jr., and P. A. Schroeder, *Rev. Mod. Phys.* **62**, 645 (1990).
- [6] Z.-Z. Yu, M. Haerle, J. W. Zwart, J. Bass, W. P. Pratt, Jr., and P. A. Schroeder, *Phys. Rev. Lett.* **52**, 368 (1984).
- [7] J. Zhao, W. P. Pratt, Jr., H. Sato, P. A. Schroeder, and J. Bass, *Phys. Rev. B* **37**, 8738 (1988).
- [8] Z.-Z. Yu, S. Yin, M. L. Haerle, Y. J. Qian, H. Bidadi, W. P. Pratt, Jr., P. A. Schroeder, and J. Bass, *Phys. Rev. B* **40**, 7601 (1989).
- [9] D. Movshovitz and N. Wiser, *J. Phys. Condens. Matter* **2**, 8053 (1990).
- [10] D. Movshovitz and N. Wiser, *Phys. Rev. B* **41**, 10503 (1990).
- [11] Y.-J. Qian, W. P. Pratt, Jr., P. A. Schroeder, D. Movshovitz, and N. Wiser, *J. Phys. Condens. Matter* **3**, 9459 (1991).
- [12] C. W. J. Beenakker and H. van Houten, *Solid State Phys.* **44**, 1 (1991).
- [13] B. L. Gallagher, T. Galloway, P. Beton, J. P. Oxley, S. P. Beaumont, S. Thoms, and C. D. W. Wilkinson, *Phys. Rev. Lett.* **64**, 2058 (1990).
- [14] L. W. Molenkamp, H. van Houten, C. W. J. Beenakker, R. Eppenga, and C. T. Foxon, *Phys. Rev. Lett.* **65**, 1052 (1990).
- [15] L. W. Molenkamp, Th. Gravier, H. van Houten, O. J. A. Buyk, M. A. A. Mabeoone, and C. T. Foxon, *Phys. Rev. Lett.* **68**, 3765 (1992).
- [16] K. Fuchs, *Proc. Cambridge Philos. Soc.* **34**, 100 (1938).
- [17] R. B. Dingle, *Proc. R. Soc. London Ser. A* **201**, 545 (1950).
- [18] R. G. Chambers, *Proc. R. Soc. London Ser. A* **202**, 378 (1950).
- [19] S. B. Soffer, *J. Appl. Phys.* **38**, 1710 (1967).
- [20] J. R. Sambles, K. C. Elsom, and T. W. Preist, *J. Phys. F* **12**, 1169 (1982).
- [21] R. N. Gurzhi, A. N. Kalinenko, and A. I. Kopeliovich, *Zh. Eksp. Teor. Fiz.* **96**, 1522 (1989) [*Sov. Phys. JETP* **69**, 863 (1989)].
- [22] J. E. Black, *Phys. Rev. B* **21**, 3279 (1980).

- [23] S. De Gennaro and A. Rettori, *J. Phys. F* **14**, L237 (1984); **15**, 2177 (1985).
- [24] J. Callaway, *Phys. Rev.* **113**, 1046 (1959).
- [25] A. V. Chaplik, *Zh. Eksp. Teor. Fiz.* **60**, 1845 (1971) [*Sov. Phys. JETP* **33**, 997 (1971)].
- [26] G. F. Giuliani and J. J. Quinn, *Phys. Rev. B* **26**, 4421 (1982).
- [27] B. Laikhtman, *Phys. Rev. B* **45**, 1259 (1992).
- [28] R. N. Gurzhi, A. N. Kalinenko, and A. I. Kopeliovich, *Phys. Low-Dim. Struct.* **2**, 75 (1994).
- [29] R. N. Gurzhi, A. N. Kalinenko, and A. I. Kopeliovich, *Phys. Rev. Lett.* **74**, 3872 (1995).
- [30] L. W. Molenkamp and M. J. M. de Jong, *Phys. Rev. B* **49**, 5038 (1994).
- [31] P. Streda, *J. Phys. Condens. Matter* **1**, 1025 (1989).
- [32] T. Kawamura and S. Das Sarma, *Phys. Rev. B* **45**, 3612 (1992).
- [33] A. Yacoby, U. Sivan, C. P. Umbach, and J. M. Hong, *Phys. Rev. Lett.* **66**, 1938 (1991).
- [34] L. W. Molenkamp, M. J. P. Brugmans, H. van Houten, and C. T. Foxon, *Semicond. Sci. Technol.* **7**, B228 (1992).
- [35] Yu. V. Sharvin, *Zh. Eksp. Teor. Fiz.* **48**, 984 (1965) [*Sov. Phys. JETP* **21**, 655 (1965)].
- [36] M. J. M. de Jong, *Phys. Rev. B* **49**, 7778 (1994) [Chapter 5].
- [37] T. J. Thornton, M. L. Roukes, A. Scherer, and B. P. Van der Gaag, *Phys. Rev. Lett.* **63**, 2128 (1989).

Summary

This thesis contains a theoretical study of electrical conduction, in particular shot noise, in mesoscopic systems. Mesoscopic electronic devices, typically of very small dimensions and operating at low temperatures, exhibit new phenomena that are either absent or nonobservable in macroscopic conductors. The conductance describes the time-averaged current through the device, while the shot noise refers to the time-dependent fluctuations around the average. The origin of shot noise is the discreteness of the electrical charge. It is a fundamental property of the system, which in contrast to most other noise sources can not be eliminated by decreasing the temperature.

In Chapter 2 the sample-to-sample fluctuations in the shot-noise power of a quasi-one-dimensional, phase-coherent, metallic, diffusive conductor are studied through a scaling equation. The variance of the shot-noise power is shown to be independent of the sample-size and the degree of disorder. The precise numerical value is calculated. Furthermore, a weak-localization effect in the average shot-noise power is found. The effect of inelastic scattering for conductors longer than the phase-coherence length is discussed.

In Chapter 3 the shot-noise power of a normal-metal-superconductor junction is studied for arbitrary normal region. Through a scattering approach, a formula is derived which expresses the shot-noise power in terms of the transmission eigenvalues of the normal region. The noise power divided by the current is enhanced by a factor two with respect to its normal-state value, due to Cooper-pair transport in the superconductor. For a disordered normal region, it is still smaller than the Poisson noise, as a consequence of noiseless open scattering channels.

In Chapter 4 the transport properties of a ferromagnet-superconductor (FS) junction are studied in a scattering formulation. Andreev reflection at the FS interface is strongly affected by the exchange interaction in the ferromagnet. The conductance G_{FS} of a ballistic point contact between F and S can be both larger or smaller than the value G_{FN} with the superconductor in the normal state, depending on the ratio of the exchange and Fermi energies. If the ferromagnet contains a tunnel barrier (I), the conductance G_{FIFS} ex-

hibits resonances which do not vanish in linear response — in contrast to the Tomasch oscillations for non-ferromagnetic materials.

In Chapter 5 the resistance of a conductor is calculated from the ballistic up to the diffusive transport regime through a semi-classical transmission approach. A formula is derived which describes the transition from the Sharvin resistance to the Drude resistance when the mean free path becomes comparable to the wire length. The exact expression differs less than 2.5% from an interpolation formula which simply adds the two resistances. Good agreement with an experiment is obtained.

In Chapter 6 the Boltzmann-Langevin equation is used to relate the shot-noise power of a mesoscopic conductor to classical transmission probabilities at the Fermi level. This semiclassical theory is applied to conduction through a disordered region with impurity scattering. It is shown how the shot noise crosses over from zero in the ballistic regime to one-third of the Poisson noise in the diffusive regime. Furthermore, shot noise in a conductor consisting of n tunnel barriers in series is discussed. For n goes to infinity the shot noise approaches one-third of the Poisson noise, independent of the transparency of the barriers. The analysis of Chapter 6 confirms that the one-third suppression of the shot noise known to occur in diffusive conductors does not require phase coherence. In addition, the effects of electron heating and inelastic scattering on the noise are calculated. This is modeled by putting charge-conserving electron reservoirs between phase-coherent segments of the conductor. The shot noise is slightly enhanced by the electron heating and is fully suppressed by the inelastic scattering.

Chapter 7 deals with the effect of hydrodynamic electron flow on the differential resistance of narrow conductors. A series of experiments is described on electrostatically defined wires in the two-dimensional electron gas in (Al,Ga)As heterostructures. In these experiments current heating is used to induce a controlled increase in the number of electron-electron collisions in the wire. The interplay between boundary scattering and electron-electron scattering leads first to an increase and then to a decrease of the resistance of the wire with increasing current. These effects are the electronic analog of Knudsen and Poiseuille flow in gas transport, respectively. In order to explain these experiments in a quantitative way, the Boltzmann transport equation is used, including impurity, electron-electron, and boundary scattering. A solution is obtained for arbitrary scattering parameters. By calculation of flow profiles inside the wire it is shown how normal flow evolves into Poiseuille flow. The boundary-scattering parameters for the gate-defined wires can be deduced from the magnitude of the Knudsen effect. Good agreement between experiment and theory is obtained.

Samenvatting

Hagelruis en elektrische geleiding in mesoscopische systemen

Dit proefschrift omvat een theoretische studie naar eigenschappen van elektrische geleiding, in het bijzonder hagelruis, in kleine elektronische systemen. Fabrikanten van microelectronica doen grote inspanningen om elektronische circuits te miniaturiseren en te integreren. Hierdoor is het mogelijk om elektronische componenten te produceren met afmetingen van één micrometer en kleiner. Enerzijds zijn deze structuren macroscopisch, daar zij uit vele miljarden atomen bestaan. Anderzijds volstaat de klassieke, macroscopische natuurkunde niet om het fysisch gedrag van deze structuren te beschrijven, vooral bij zeer lage temperaturen. Het blijkt noodzakelijk om tevens theorieën uit de microscopische wereld van atomen en moleculen toe te passen. Deze nieuwe tak van de natuurkunde wordt daarom mesoscopische fysica genoemd. Het afgelopen decennium is de belangstelling voor elektrisch transport door mesoscopische geleiders sterk toegenomen. Deze geleiders vertonen nieuw gedrag dat niet voorkomt, of niet waarneembaar is in macroscopische geleiders.

De geleiding is gedefinieerd als de verhouding tussen de tijdsgemiddelde stroom en de aangelegde spanning. De ruis beschrijft de tijdsafhankelijke fluctuaties rondom de gemiddelde stroom. De grootte van deze fluctuaties wordt weergegeven door het ruisvermogen per frequentiecomponent. Er zijn verschillende soorten ruis, zoals thermische ruis, weerstandsruis en hagelruis. Deze laatste wordt veroorzaakt doordat de elektrische stroom gedragen wordt door elektronen. De stroom is dus niet continu, maar bestaat uit een reeks minuscule pulsjes, die elk overeenkomen met het transport van een enkel elektron. Hagelruis wordt gekenmerkt door een wit ruisspectrum. Het is een fundamentele eigenschap van de geleider en kan in tegenstelling tot overige soorten van ruis niet geëlimineerd worden door de temperatuur te verlagen. Het hagelruisvermogen geeft informatie over de geleidingsprocessen in het systeem die men niet kan verkrijgen door enkel de geleiding te beschouwen. Het klassieke voorbeeld is een vacuümdiode. De hagelruis hiervan is gelijk aan de Poissonruis, twee keer de electronlading maal de tijdsgemiddelde stroom. Dit

geeft aan dat de electronen volledig ongecorrleerd, als in een Poissonproces, van de kathode geëmitteerd worden naar de anode. Als in een geleider de hagelruis kleiner is dan de Poissonruis, duidt dit op fysische processen die de stroom gecorreleerder maken.

In Hoofdstuk 2 wordt het hagelruisvermogen van een fasecoherente, diffuse geleider bestudeerd door middel van een schaalvergelijking. De lengte van een diffuse geleider is veel groter dan de vrije weglengte, de afstand waarop electronen verstrooid worden aan onzuiverheden in het rooster. De hagelruis blijkt één derde van de Poissonruis te zijn. Deze waarde is het gemiddelde over een verzameling van macroscopisch identieke geleiders. Deze geleiders vertonen verschillen op microscopische schaal, omdat de onzuiverheden willekeurig verdeeld zijn. Dit en het golfkarakter van de electronen geeft van geleider tot geleider variaties in de transporteigenschappen. Uit berekening van deze mesoscopische fluctuaties op het hagelruisvermogen blijkt dat deze onafhankelijk zijn van de geleiderafmetingen en de mate van wanorde in de geleider. Tevens is er een effect van "zwakke localisatie," waarneembaar als een kleine afname van het gemiddelde hagelruisvermogen in een magnetisch veld.

Hoofdstuk 3 behandelt het hagelruisvermogen van een junctie tussen een normaal metaal en een supergeleider (een NS junctie). In een supergeleider wordt de stroom weerstandsloos gedragen door paren van electronen, de Cooperparen. Het transport aan het grensvlak tussen metaal en supergeleider vindt plaats middels het Andreevreflectieproces: Een inkomend electron in het normale metaal wordt gereflecteerd als een gat, terwijl er een Cooperpaar de supergeleider ingaat. Als gevolg van het Cooperpaartransport in de supergeleider is het ruisvermogen per eenheid van stroom verdubbeld ten opzichte van het ruisvermogen van een junctie zonder supergeleider. Voor een wanordelijke NS junctie is de hagelruis nog steeds kleiner dan de Poissonruis.

In Hoofdstuk 4 wordt het transport door een ferromagneet-supergeleider (FS) junctie bestudeerd. Een ferromagneet heeft een netto magnetisatie, doordat er zich meer electronen in de spin-op dan in de spin-neer toestand bevinden. De grootte van deze asymmetrie in de bezetting van de spin-toestanden wordt bepaald door de plaats-ruilwisselwerking. Aangezien een Cooperpaar uit zowel een electron met spin-op als met spin-neer bestaat, wordt de Andreevreflectie aan het FS grensvlak sterk beïnvloed door de plaats-ruilwisselwerking in de ferromagneet. De geleiding van een ballistisch punt-contact tussen F en S kan zowel groter als kleiner zijn dan de geleiding waarbij de supergeleider in de normale toestand is. Dit hangt af van de verhouding tussen de plaats-ruilenergie en de Fermi-energie. Als de ferromagneet een tunnelbarrière bevat, vertoont de geleiding resonanties als functie van de afstand tussen de tunnelbarrière en het FS grensvlak.

De berekeningen in Hoofdstukken 2 tot en met 4 zijn gebaseerd op de quantummechanica, waarin met behulp van de Schrödingervergelijking het

golfkarakter van het electron volledig wordt meegenomen. De Hoofdstukken 5 tot en met 7 gaan uit van de semiklassieke Boltzmannvergelijking. Hierin bewegen de electronen volgens de wetten van de klassieke mechanica en voldoen zij tevens aan het uitsluitingsprincipe van Pauli.

In Hoofdstuk 5 wordt de weerstand van een geleider berekend voor willekeurige verhouding tussen de vrije weglengte en de lengte van de geleider. Er wordt een formule afgeleid die de overgang van het ballistische naar het diffuse transportregime beschrijft. De exacte uitdrukking verschilt minder dan 2.5% van een interpolatieformule die de weerstanden in de twee limiterende regimes optelt. Er is goede overeenstemming met experimenten.

Hoofdstuk 6 maakt gebruik van de Boltzmann-Langevinvergelijking om het hagelruisvermogen van een mesoscopische geleider te relateren aan klassieke transmissiekansen van electronen. Deze semiklassieke theorie wordt toegepast op het transport door een wanordelijk gebied met elastische verstrooiing aan onzuiverheden. Er wordt berekend hoe de hagelruis varieert van nul in het ballistische regime, tot één derde van de Poissonruis in het diffuse regime. Tevens wordt de hagelruis bestudeerd in een geleider die bestaat uit n tunnelbarrières in serie. Als n naar oneindig gaat, nadert de hagelruis tot één derde van de Poissonruis, onafhankelijk van de hoogte van de barrières. De analyse in Hoofdstuk 6 bevestigt dat de onderdrukking met één derde, zoals die in diffuse geleiders optreedt, geen fasecoherentie behoeft. Tevens wordt de invloed van electron-electron en inelastische verstrooiing bepaald. Het blijkt dat electron-electron verstrooiing de hagelruis iets doet toenemen, terwijl inelastische verstrooiing de hagelruis volledig doet verdwijnen. Dit laatste effect is de reden dat de hagelruis in een klassieke weerstand afwezig is.

Hoofdstuk 7 behandelt de invloed van hydrodynamische electronenstroming op de weerstand van smalle draden. Er zijn experimenten uitgevoerd in draden die electrostatisch gedefinieerd worden in een tweedimensionaal electronengas in (Al,Ga)As heterostructuren. Bij toename van de stroom neemt het aantal electron-electron botsingen toe. Het samenspel van wandverstrooiing en electron-electron verstrooiing leidt bij toenemende stroom eerst tot een verhoging en vervolgens tot een verlaging van de weerstand van de draad. Deze twee effecten zijn het electronische analogon van respectievelijk Knudsen- en Poiseuillestroming in gastransport. Om de experimenten kwantitatief te verklaren wordt gebruik gemaakt van de Boltzmannvergelijking, die zowel verstrooiing aan onzuiverheden en wanden als van de electronen onderling beschrijft. Berekende stromingsprofielen in de draad demonstreren hoe de normale stroming evolueert in Poiseuillestroming. De theorie stemt goed overeen met het experiment.

List of publications

- M. J. M. de Jong and C. W. J. Beenakker, *Mesoscopic fluctuations in the shot-noise power of metals*, Physical Review B **46**, 13400–13406 (1992) [Chapter 2].
- F. Liefrink, R. W. Stok, J. I. Dijkhuis, M. J. M. de Jong, H. van Houten, and C. T. Foxon, *Reduced shot noise in a quasi-one-dimensional channel*, in *Noise in Physical Systems and 1/f Fluctuations*, edited by P. H. Handel and A. L. Chung (AIP, New York, 1993), 272–275.
- L. W. Molenkamp and M. J. M. de Jong, *Electron-electron-scattering-induced size effects in a two-dimensional wire*, Physical Review B **49**, 5038–5041 (1994).
- M. J. M. de Jong, *Transition from Sharvin to Drude resistance in high-mobility wires*, Physical Review B **49**, 7778–7781 (1994) [Chapter 5].
- L. W. Molenkamp and M. J. M. de Jong, *Observation of Knudsen and Gurzhi transport regimes in a two-dimensional wire*, Solid-State Electronics **37**, 551–553 (1994).
- F. Liefrink, J. I. Dijkhuis, M. J. M. de Jong, L. W. Molenkamp, and H. van Houten, *Experimental study of reduced shot noise in a diffusive mesoscopic conductor*, Physical Review B **49**, 14066–14069 (1994).
- M. J. M. de Jong and C. W. J. Beenakker, *Doubled shot noise in normal-metal-superconductor junctions*, Physical Review B **49**, 16070–16073 (1994) [Chapter 3].
- F. Liefrink, J. I. Dijkhuis, M. J. M. de Jong, L. W. Molenkamp, and H. van Houten, *Experimental study of reduced shot noise in a diffusive mesoscopic conductor*, Superlattices and Microstructures **16**, 253–255 (1994).

- L. W. Molenkamp and M. J. M. de Jong, *The point-contact thermometer and its application in the study of hydrodynamic electron flow*, to appear in *Ultimate Limits in Fabrication and Measurement*, edited by M. E. Welland (Cambridge University Press, Cambridge, 1994).
- M. J. M. de Jong and C. W. J. Beenakker, *Sub-Poissonian shot noise in a diffusive conductor*, in *Coulomb and Interference Effects in Small Electronic Structures*, edited by D. C. Glatli, M. Sanquer, and J. Trần Thanh Vân (Editions Frontières, France, 1994), 427–435 [part of Sub-section 1.1.5].
- Th. G. S. M. Rijks, R. Coehoorn, M. J. M. de Jong, and W. J. M. de Jonge, *Semi-classical calculations of the anisotropic magnetoresistance of NiFe-based thin films, wires, and multilayers*, *Physical Review B* **51**, 283–291 (1995).
- M. J. M. de Jong and C. W. J. Beenakker, *Andreev reflection in ferromagnet–superconductor junctions*, *Physical Review Letters* **74**, 1657–1660 (1995) [Chapter 4].
- L. W. Molenkamp and M. J. M. de Jong, *Hydrodynamic electron flow in a two-dimensional electron gas*, to appear in the proceedings of the XXI-Ith International Conference on the Physics of Semiconductors, edited by D. Lockwood (World Scientific, Singapore, 1995).
- M. J. M. de Jong and L. W. Molenkamp, *Hydrodynamic electron flow in high-mobility wires*, to appear in *Physical Review B* [Chapter 7].
- M. J. M. de Jong and C. W. J. Beenakker, *Semiclassical theory of shot-noise suppression*, to appear in *Physical Review B* [part of Chapter 6].
- H. Birk, M. J. M. de Jong, and C. Schönenberger, *Shot-noise suppression in the single-electron tunneling regime*, submitted.
- J. C. J. Paasschens, M. J. M. de Jong, and C. W. J. Beenakker, *Accuracy of the diffusion equation with extrapolated-boundary condition for transmittance of light through a turbid medium*, submitted.

Curriculum Vitae

van Marc Johan Martijn de Jong

Op 20 augustus 1969 ben ik geboren te Herten. Van 1981 tot 1987 volgde ik middelbaar onderwijs aan het Geert Groote College te Deventer. In mei 1987 voltooidde ik het Gymnasium β . In hetzelfde jaar behaalde ik de derde plaats op de Nederlandse Natuurkunde Olympiade en een bronzen medaille op de Internationale Wiskunde Olympiade te Cuba.

Vervolgens begon ik de studie Technische Natuurkunde aan de Technische Universiteit Delft. In september 1988 slaagde ik voor het Propedeutisch examen, met lof. Mijn afstudeerwerk verrichtte ik aan het Philips Natuurkundig Laboratorium te Eindhoven in de groep van dr. P. J. Kelly. Onder begeleiding van prof. dr. C. W. J. Beenakker, verbonden aan het Instituut-Lorentz van de Rijksuniversiteit Leiden, onderzocht ik theoretisch de mesoscopische fluctuaties in het hagelruisvermogen van diffuse geleiders. In september 1992 slaagde ik voor het Ingenieursexamen, met lof.

Hierna trad ik met financiële steun van Philips in dienst van de Stichting voor Fundamenteel Onderzoek der Materie om als Onderzoeker In Opleiding promotieonderzoek te verrichten bij prof. dr. C. W. J. Beenakker. Mijn dagelijkse werkplek bleef het Philips Natuurkundig Laboratorium, nu in de groep van prof. dr. H. van Houten. De belangrijkste resultaten van dit onderzoek zijn beschreven in dit proefschrift. Ik heb deze resultaten kunnen presenteren bij verscheidene nationale en internationale conferenties, symposia en universiteiten. Tevens nam ik in juli 1994 deel aan de zomerschool in Les Houches, Frankrijk, betreffende mesoscopische quantum physica.

Sinds januari 1995 ben ik in dienst van Philips als wetenschappelijk medewerker.

Acknowledgements

Apart from the members of my thesis committee, I would like to mention explicitly a number of people who have contributed to the realization of this thesis. I am grateful to my colleagues at Philips Research Laboratories, in particular, H. Birk, R. Coehoorn, L. F. Feiner, P. J. Kelly, J. C. J. Paasschens, Th. G. S. M. Rijks, C. M. Schep, C. Schönenberger, and my colleagues at Instituut-Lorentz of Leiden University. In addition, I have enjoyed a fruitful collaboration with the experimental group of J. I. Dijkhuis, F. Liefrink, and M. G. Peters at Utrecht University. I am indebted to R. Landauer at IBM T. J. Watson Research Center for many critical discussions, and to M. H. Devoret at Centre d'Etudes de Saclay and R. C. Liu at Stanford University for hospitality during my stay at their institutes.

Finally, I acknowledge the support of my research by the Philips Research Laboratories and the Dutch Science Foundation NWO/FOM.

Stellingen

behorende bij het proefschrift

Shot Noise and Electrical Conduction in Mesoscopic Systems

van M. J. M. de Jong

1. Het anisotroop magnetoweerstandeffect in een laag van een verdunde magnetische legering heeft een maximum als functie van de laagdikte.
Th. G. S. M. Rijks, R. Coehoorn, M. J. M. de Jong en W. J. M. de Jonge, *Phys. Rev. B* 51, 283 (1995).
2. De analogie tussen Andreevreflectie aan een supergeleider en optische reflectie aan een faseconjugerende spiegel gaat mank, indien meer dan één reflectie optreedt.
3. De lengte-afhankelijkheid van de weerstand van een dunne draad waargenomen door Tarucha *et al.* heeft een klassieke verklaring.
S. Tarucha, T. Saku, Y. Tokura en Y. Hirayama, *Phys. Rev. B* 47, 4064 (1993).
4. Toevoeging van glansmiddelen tijdens de electrochemische groei van magnetische multilagen heeft een desastreus effect op de magnetoweerstand.
5. Reflectie van licht aan een absorberend wanordelijk medium wordt beschreven door het Laguerre ensemble van random-matrix theorie.
6. De Heisenbergkoppeling tussen twee metallische ferromagneten gescheiden door een uiterst smalle, doch zeer hoge barrière is ferromagnetisch en neemt monotoon toe als functie van de plaats-ruil (exchange) energie.
7. De conclusie van Parker dat de stroom in een lichtgevende polymeren diode begrensd wordt door de elektroden is ongerechtvaardigd.
I. D. Parker, *J. Appl. Phys.* 75, 1656 (1995).
8. De Andreevbenadering voor het geleidingsvermogen is nauwkeuriger voor het grensvlak tussen een supergeleider en een ferromagneet dan voor het grensvlak tussen een supergeleider en een normaal metaal.
9. Het gebrek aan communicatie tussen radio-ingenieurs en vaste-stoffysici heeft de ontwikkeling van de theorie van localisatie in één-dimensionale geleiders twintig jaar vertraagd.
10. Pils is ongeschikt als sportdrink.
H. C. Koops, *Chemisch Magazine*, 117 (1995).
11. De discussie of uit milieu-oogpunt het melkpak te prefereren is boven de fles, heeft als logisch eindpunt de terugkeer van de koe in de achtertuin.